# Lecture Notes: Neutrino Physics and Astrophysics*

Antonio Marrone[1,2]

[1] Dipartimento Interateneo di Fisica "Michelangelo Merlin," Via Amendola 173, 70126 Bari, Italy

[1] Istituto Nazionale di Fisica Nucleare, Sezione di Bari, Via Orabona 4, 70126 Bari, Italy

March 30, 2023

# Contents



*Prepared for the School "Theoretical Aspects of Astroparticle Physics, Cosmology and Gravitation - 2023", Mar 20, 2023 - Mar 31, 2023, Galileo Galilei Institute, Arcetri, Firenze.

# 1 Neutrinos in the Standard Model and Beyond

## 1.1 Neutrinos in the Standard Model

In the Standard Model (SM) of Particle Physics, neutrinos are neutral massless particles that can interact only weakly with other particles. The SM is a theory based on the gauge group $SU(3)_c \times SU(2)_L \times U(1)_Y$, but as far as neutrinos are concerned, we can disregard the color group $SU(3)_c$ and focus only on the electroweak subgroup $SU(2)_L \times U(1)_Y$. Here, the subscript $L$ stands for the left-handed chirality or weak isospin $I$, and $Y$ for the hypercharge (wherever no confusion can arise we generally omit group subscripts). As references on the building of the SM, see [1, 2] The two quantum numbers $I$ and $Y$ are related through he Nishijima–Gell-Mann relation $Y = Q - I_3$[1] The *left* nature of the weak interaction implies that the SM building blocks are the left and right-handed fields $\psi_L$ and $\psi_R$, defined through the $\gamma_5$ matrix[2]:

$$\psi_L = \frac{1-\gamma_5}{2}\psi \,, \quad \psi_R = \frac{1+\gamma_5}{2}\psi \,. \tag{1.1}$$

For a brief review of the properties of the Dirac matrices and of the Dirac and Weyl spinors and their relation to the Lorentz group see Appendix A and D.

Even if we know that there are three different families of fundamental particles, both for quarks and leptons, for simplicity, we start by considering only the first family of particles. Therefore, we will consider the two leptons $e$ and $\nu_e$, and the $u$ and $d$ quarks, and precisely their left and right parts. We assume that the left-handed fermions are the basis of the fundamental 2-dimensional irreducible representation of $SU(2)_L$ and transform with the $U$ matrices themselves:

$$\begin{aligned} L &= \begin{pmatrix} \nu_{eL} \\ e_L \end{pmatrix} \,, \quad L \xrightarrow{SU(2)} UL \,. \\ q_L &= \begin{pmatrix} u_L \\ d_L \end{pmatrix} \,, \quad q_L \xrightarrow{SU(2)} Uq_L \,. \end{aligned} \tag{1.2}$$

The fundamental representation is often denoted with $\mathbf{2}$. A generic $U \in SU(2)$ matrix can be expressed in terms of the $SU(2)$ generators, $I_i = \sigma_i/2,\ i = 1,2,3$, the Pauli matrices, as :

$$SU(2) \ni U = e^{-i\boldsymbol{\alpha}(x)\cdot\frac{\boldsymbol{\sigma}}{2}} = e^{-i\boldsymbol{\alpha}(x)\cdot\boldsymbol{I}} \,. \tag{1.3}$$

A generic element of $U(1)$ is simply a phase, and can be written as

$$U(1) \ni U = e^{-i\alpha(x)Y} \,. \tag{1.4}$$

In contrast to (1.2), the right-handed part of the fermion fields, $e_R$, $u_R$, $d_R$, are singlets of $SU(2)$. Concerning neutrinos, the $\nu_{eR}$ is excluded from the SM. We will include it in our discussion from the beginning, in view of the extensions of the model to nonzero neutrino masses. With respect to color, leptons are singlets, while quarks are in the fundamental three-dimensional representation of $SU(3)_c$, denoted by $\mathbf{3}$. We can summarize the transformation properties of the chiral fields into three numbers indicating the color, the weak isospin and the hypercharge $\{c, I, Y\}$ in Table 1.

[1]In many textbook, the relation is written as $Y/2 = Q - I_3$, with a factor two of difference in the hypercharge definition.

[2]Conventions for Dirac matrices are discussed in Appendix 1..

| $SU(2)$ doublets | | $SU(2)$ singlets | | |
|---|---|---|---|---|
| $\{\mathbf{1},\mathbf{2},-1/2\}$ | $\{\mathbf{3},\mathbf{2},+1/6\}$ | $\{\mathbf{1},\mathbf{1},-1\}$ | $\{\mathbf{3},\mathbf{1},+2/3\}$ | $\{\mathbf{3},\mathbf{1},-1/3\}$ |
| $\begin{pmatrix}\nu_{eL}\\ e_L\end{pmatrix}$ | $\begin{pmatrix}u_L\\ d_L\end{pmatrix}$ | $e_R$ | $u_R$ | $d_R$ |
| $\begin{pmatrix}\nu_{\mu L}\\ \mu_L\end{pmatrix}$ | $\begin{pmatrix}s_L\\ c_L\end{pmatrix}$ | $\mu_R$ | $s_R$ | $c_R$ |
| $\begin{pmatrix}\nu_{\tau L}\\ \tau_L\end{pmatrix}$ | $\begin{pmatrix}t_L\\ b_L\end{pmatrix}$ | $\tau_R$ | $t_R$ | $b_R$ |

**Table (1) :** Color, Weak Isospin and hypercharge for the SM building blocks.

Note that the hypercharge $Y$ is chiral, since it distinguishes between the left and the right part of a particle field, while it is the same for fields in the same multiplet of $SU(2)$. It is clear that $\nu_{eR}$, if present in the model, does not interact with other particles, and therefore is sterile, since all its charges are zero. To derive the interaction terms in the lagrangian of the SM, one needs to replace the ordinary derivative with the covariant derivative in the free lagrangian.[3]

$$\partial_\mu \to D_\mu = \partial_\mu + ig\boldsymbol{W}\cdot\boldsymbol{I} + ig' B_\mu Y \ , \tag{1.5}$$

where $g$ and $g'$ are the two coupling constant, one for each symmetry group. Interactions between particle fields can be derived by expanding the kinetic terms where the ordinary derivative is replaced by the covariant one:

$$\mathcal{L}_K = i\overline{L}\not{D}L + i\overline{q_L}\not{D}q_L + \sum_{R\text{ fields}} i\bar{\psi}_R\not{D}\psi_R \ , \tag{1.6}$$

where $\psi_R = e_R, u_R, d_R$ and possibly $\nu_{eR}$. The first two terms of the Lagrangian in (1.6) are scalars of $SU(2)_L$, since $\not{D}L$ transforms with $U$ like $L$, by the very definition of covariant derivative, while $\overline{L}$ transforms with $U^*$ and therefore

$$\overline{L}\not{D}L = L^{*T}\not{D}L \xrightarrow{U} (U^*L^*)^T U(\not{D}L) = L^{*T}U^{*T}U\not{D}L = \overline{L}U^\dagger U\not{D}L = \overline{L}\not{D}L \ . \tag{1.7}$$

The third term of (1.6) is obviously a scalar of $SU(2)$, since all the fields $\psi_R$ have zero weak isospin. In addition to $\mathcal{L}_K$, the full Lagrangian of the SM also includes the free gauge fields and

[3]With a bar over a $SU(2)$, multiplet we denote the transpose of the multiplet, followed by the bar in the sense of Dirac spinors.

the Higgs terms:

$$
\begin{aligned}
&\mathcal{L}_{\text{SM}} = \mathcal{L}_K + \mathcal{L}_{\text{gauge}} + \mathcal{L}_{\text{Higgs}} \,, \\
&\mathcal{L}_{\text{gauge}} = -\frac{1}{4}\boldsymbol{W}_{\mu\nu}\cdot\boldsymbol{W}^{\mu\nu} - \frac{1}{4}B_{\mu\nu}\cdot B^{\mu\nu} \\
&\text{with } \begin{cases} \boldsymbol{W}_{\mu\nu} = \partial_\mu \boldsymbol{W}_\nu - \partial_\nu \boldsymbol{W}_\mu - g\boldsymbol{W}_\mu \times \boldsymbol{W}_\nu \\ B_{\mu\nu} = \partial_\mu B_\nu - \partial_\nu B_\mu \end{cases} \\
&\mathcal{L}_{\text{Higgs}} = (D_\mu \Phi)^\dagger (D^\mu \Phi) - \mu^2 \Phi^\dagger \Phi - \lambda(\Phi^\dagger\Phi)^2 + \mathcal{L}_{\text{Yukawa}} \,.
\end{aligned}
\tag{1.8}
$$

In the last line, $\mathcal{L}_{\text{Yukawa}}$ is defined as

$$
\mathcal{L}_{\text{Yukawa}} = -f_e(\overline{L}\Phi e_R + \overline{e_R}\Phi^\dagger L) - f_u(\overline{q_L}\tilde{\Phi} u_R + \overline{u_R}\tilde{\Phi}^\dagger q_L) - f_d(\overline{q_L}\Phi d_R + \overline{d_R}\Phi^\dagger q_L) \,. \tag{1.9}
$$

The scalar Higgs field in (1.8) and (1.9) is doublet of $SU(2)$.

Besides being a singlet of $SU(2)$, the Lagrangian must have $Y = 0$. Therefore, from the Yukawa terms in (1.9), we see that the Higgs field must have $Y = 1/2$, so it transforms as $\{\mathbf{1}, \mathbf{2}, 1/2\}$. Consequently, the upper field in the Higgs doublet must have charge $Q = Y + I_3 = 1/2 + 1/2 = 1$ while the lower field must be neutral, $Q = Y + I_3 = 1/2 - 1/2 = 0$:

$$
\Phi = \begin{pmatrix} \phi^+ \\ \phi^0 \end{pmatrix} \,. \tag{1.10}
$$

The doublet $\tilde{\Phi}$ in (1.8) is defined as

$$
\tilde{\Phi} = i\sigma_2 \Phi^* = i \begin{pmatrix} 0 & -i \\ i & 0 \end{pmatrix} \Phi * = \begin{pmatrix} 0 & 1 \\ -1 & 0 \end{pmatrix} \Phi^* = \begin{pmatrix} \phi^{0*} \\ -\phi^- \end{pmatrix} \,, \tag{1.11}
$$

and it can be shown to transform exactly as $\Phi$, with the fundamental representation of $SU(2)$. The need for $\tilde{\Phi}$ comes from the fact that the Yukava term for the $u$ quark contains $u_R$ with zero hypercharge, while $Y_u = 2/3$ and $Y_{q_L} = -1/6$. Therefore, to have both a singlet of $SU(2)$ and null hypercharge, we need a doublet of $SU(2)$ with $Y = -(2/3 - 1/6) = -1/2$, that cannot be the Higgs field $\Phi$,that has $Y = 1/2$, but must be constructed with $\Phi^*$ and transform as $\{\mathbf{1}, \mathbf{2}, -1/2\}$.

The Higgs mechanism breaks the symmetry $SU(2)_L \times U(1)_Y$ spontaneously, because of the vacuum expectation value (VEV) of the Higgs:

$$
\langle \Phi \rangle = \frac{1}{\sqrt{2}} \begin{pmatrix} 0 \\ v \end{pmatrix} \tag{1.12}
$$

that minimizes the Higgs potential for a nonzero value $v$. It is always possible to go to the unitary gauge defined by

$$
\Phi = \begin{pmatrix} 0 \\ \frac{1}{\sqrt{2}}(v + H(x)) \end{pmatrix} \,, \tag{1.13}
$$

where $H(x)$ is a real (neutral) field. The expansion of the Lagrangian in the unitary gauge results in the fermion mass terms:

$$
\mathcal{L}_{\text{f.m.}} = -\frac{v}{\sqrt{2}}(f_e \overline{e_L} e_R + f_u \overline{u_L} u_R + f_d \overline{d_L} d_R + \text{h. c.}) = -\frac{v}{\sqrt{2}}(f_e \overline{e} e + f_u \overline{u} u + f_d \overline{d} d) \,. \tag{1.14}
$$

A comparison of mass terms in (1.14) with the usual mass term for a Dirac spinor in the Lagrangian, i.e. $-m\overline{\psi}\psi$, gives the following values for the fermion masses:

$$m_e = \frac{1}{\sqrt{2}} f_e v \,, \quad m_u = \frac{1}{\sqrt{2}} f_u v \,, \quad m_d = \frac{1}{\sqrt{2}} f_d v \,. \tag{1.15}$$

Therefore, we find that the charged lepton and quark masses are proportional to the Higgs VEV $v$ and depend on the unknown Yukawa couplings $f_e$, $f_u$ and $f_d$, one for each particle. No mass is generated for the neutrino, since $\nu_{eR}$ is absent from the start in the Lagrangian, and terms like $\overline{\nu_{eL}}\nu_{eR}$ and $\overline{\nu_{eR}}\nu_{eL}$ cannot be present.

The extension to three families of quarks and lepton is straightforward, but requires a bit of work with the notation. We add a subscript to $L$ and call it $L_m$ with $m = e, \nu, \tau$, to denote the three lepton pairs:

$$L_e = \begin{pmatrix} \nu_{eL} \\ e_L \end{pmatrix} \,, \quad L_\mu = \begin{pmatrix} \nu_{\mu L} \\ \mu_L \end{pmatrix} \,, \quad L_\tau = \begin{pmatrix} \nu_{\tau L} \\ \tau_L \end{pmatrix} \quad , \tag{1.16}$$

and three $SU(2)$ singlets $R_m$ with $m = e, \mu, \tau$

$$R_1 = e_R \quad R_2 = \mu_R \quad R_3 = \tau_R \,. \tag{1.17}$$

Similarly we define the three doublets $q_{Lm}$ with $m = 1, 2, 3$, as

$$q_{L1} = \begin{pmatrix} u_L \\ d_L \end{pmatrix} \,, \quad q_{L2} = \begin{pmatrix} c_L \\ s_L \end{pmatrix} \,, \quad q_{L3} = \begin{pmatrix} t_L \\ b_L \end{pmatrix} \quad , \tag{1.18}$$

and the *up* and *down* quark right parts $u_{Rm}$ and $d_{Rm}$ with $m = 1, 2, 3$:

$$\begin{array}{lll} u_{R1} = u_R \,, & u_{R2} = c_R \,, & u_{R3} = t_R \,, \\ d_{R1} = d_R \,, & d_{R2} = s_R \,, & d_{R3} = b_R \,. \end{array} \tag{1.19}$$

Thanks to these definitions, the kinetic part of the lagrangian can be written as (1.6) by adding generations up (sum on repeated indices is understood):

$$\mathcal{L}_K = i\overline{L_i}\not{D} L_i + i\overline{q_{Li}}\not{D} q_{Li} + \sum_{R \text{ fields}} i\bar{\psi}_R \not{D} \psi_R \,, \tag{1.20}$$

where the last part includes $\psi_R = e_R, \mu_R, \tau_R, u_R, d_R, c_R, s_R, t_R, b_R$ and, eventually, the right-handed components of the neutrino fields. The Yukawa part of the SM lagrangian can be generalized as

$$\begin{aligned} \mathcal{L}_{\text{Yukawa}} \;=\; & -f^\ell_{ij}(\overline{L_i}\Phi R_j + \overline{R_i}\Phi^\dagger L_j) - f^u_{ij}(\overline{q_{Li}}\tilde{\Phi} u_{Rj} + \overline{u_{Ri}}\tilde{\Phi}^\dagger q_{Lj}) + \\ & -f^d_{ij}(\overline{q_{Li}}\Phi d_{Rj} + \overline{d_{Ri}}\Phi^\dagger q_{Lj}) \,. \end{aligned} \tag{1.21}$$

A closer look at (1.21) and a comparison with (1.9) shows that, after the symmetry breaking, $\mathcal{L}_{\text{Yukawa}}$ will have the same structure as (1.14), but now with nondiagonal terms. To simplify the notation for the Yukawa part of the lagrangian, let us define $\ell_L$ and $\ell_R$ as two vectors containing the left and right-handed parts of the charged leptons

$$\ell_L = \begin{pmatrix} e_L \\ \mu_L \\ \tau_L \end{pmatrix} \,, \quad \ell_R = \begin{pmatrix} e_R \\ \mu_R \\ \tau_R \end{pmatrix} \,, \tag{1.22}$$

and, analogously, four vectors containing the left and right-handed parts for the $SU(2)$ up and down quarks:

$$q_L^U = \begin{pmatrix} u_L \\ c_L \\ t_L \end{pmatrix} \ , \quad q_R^U = \begin{pmatrix} u_R \\ c_R \\ t_R \end{pmatrix} \ , \quad q_L^D = \begin{pmatrix} d_L \\ s_L \\ b_L \end{pmatrix} \ , \quad q_R^D = \begin{pmatrix} d_R \\ s_R \\ b_R \end{pmatrix} \quad . \tag{1.23}$$

After symmetry breaking, the mass terms can then be written as

$$\mathcal{L}_{\text{f.m.}} = -\frac{v}{\sqrt{2}}(f_{ij}^{\ell}\overline{\ell_{L}}_i\ell_{Rj} + f_{ij}^{U}\overline{q_L^U}_i q_{R\,j}^U + f_{ij}^{D}\overline{q_L^D}_i q_{R\,j}^D + \text{h. c.}) \ . \tag{1.24}$$

What equation (1.24) tells us is that the flavor (weak interaction) eigenstates are not mass eigenstates, since the three complex matrices $f^\ell$, $f^U$ and $f^D$ need not to be diagonal and experimentally it is found they are not. For this reason, it is often used a prime on $\ell_{L/R}$ and $q_{L/R}$ to distinguish them from the lepton mass eigenstates that will be introduced in the following. Let us start with quarks and with the matrices $f^U$ and $f^D$. They can be diagonalized through a biunitary transformation (see Appendix C), i.e. through two different unitary matrices multiplied to the left and to the right:

$$\begin{aligned} W_L^{U\dagger} f^U W_R^U &= f_{\text{diag}}^U \\ W_L^{D\dagger} f^D W_R^D &= f_{\text{diag}}^D \ , \end{aligned} \tag{1.25}$$

where all the $W_{L/R}^{U/D}$ matrices are unitary and $f_{\text{diag}}^U$ and $f_{\text{diag}}^D$ are diagonal. Let us focus, for instance on the second term of (1.24), written in terms of vectors and matrices:

$$\begin{aligned} &-\frac{v}{\sqrt{2}}\overline{q_L^U} f^U q_R^U = -\frac{v}{\sqrt{2}}\overline{q_L^U}(W_L^U W_L^{U\dagger}) f^U (W_R^U W_R^{U\dagger}) q_R^U = \\ &= (\overline{q_L^U} W_L^U)(W_L^{U\dagger} f^U W_R^U)(W_R^{U\dagger} q_R^U) = \overline{q_{0L}^U} f_{\text{diag}}^U q_{0R}^U \ , \end{aligned} \tag{1.26}$$

where we have introduced the mass eigenstates

$$q_{0L}^U = W_L^{U\dagger} q_L^U \ , \qquad q_{0R}^U = W_R^{U\dagger} q_R^U \quad \Rightarrow \quad q_L^U = W_L^{U\dagger} q_{0L}^U \ , \qquad q_R^U = W_R^{U\dagger} q_{0R}^U \ . \tag{1.27}$$

With an analogous definition we can also introduce the mass eigenstates $q_{0L}^D$ and $q_{0R}^D$:

$$q_{0L}^D = W_L^{D\dagger} q_L^D \ , \qquad q_{0R}^D = W_R^{D\dagger} q_R^D \quad \Rightarrow \quad q_L^D = W_L^{D\dagger} q_{0L}^D \ , \qquad q_R^D = W_R^{D\dagger} q_{0R}^D \ . \tag{1.28}$$

If we denote with $f_m^U$ ($f_m^D$) the eigenvalues of $f_{\text{diag}}^U$ ($f_{\text{diag}}^D$), we can rewrite for the quark part of the Yukawa Lagrangian:

$$\begin{aligned} \mathcal{L}_{\text{Yukawa}}^{\text{quark}} &= -\frac{v}{\sqrt{2}}(f_m^U(\overline{q_{0Lm}^U} q_{0Rm}^U + \overline{q_{0Rm}^U} q_{0Lm}^U) + f_m^D(\overline{q_{0Lm}^D} q_{0Rm}^D + \overline{q_{0Rm}^D} q_{0Lm}^D)) = \\ &= -\frac{v}{\sqrt{2}}(f_m^U \overline{q_0^U}_m q_0^U{}_m + f_m^D \overline{q_0^D}_m q_0^D{}_m) \ , \end{aligned} \tag{1.29}$$

where we have introduced the quark fields $q_0^U = q_{0L}^U + q_{0R}^U$ and $q_0^D = q_{0L}^D + q_{0R}^D$ and we have used the property that for Dirac spinors

$$\overline{\psi}\psi = \overline{\psi_L}\psi_R + \overline{\psi_R}\psi_L \ . \tag{1.30}$$

From (1.29) we can read the quark masses:

$$\begin{aligned} m_n &= \frac{v}{\sqrt{2}} f_n^U \qquad n = u, c, t \\ m_n &= \frac{v}{\sqrt{2}} f_n^D \qquad n = d, s, b \; . \end{aligned} \tag{1.31}$$

The SM quark weak charged current, derived from the covariant derivative (1.5) and the Higgs mechanism, can be rewritten in term of the mass eigenstates

$$\begin{aligned} j^\mu_{\mathrm{q,WC}} &= 2(\overline{u_L}\gamma^\mu d_L + \overline{c_L}\gamma^\mu s_L + \overline{t_L}\gamma^\mu b_L) = 2\overline{q^U_L}\gamma^\mu q^D_L = \\ &= 2\overline{q^U_{0L}} W^{U\dagger}_L \gamma^\mu W^D_L q^D_{0L} = 2\overline{q^U_{0L}} \gamma^\mu W^{U\dagger}_L W^D_L q^D_{0L} \; . \end{aligned} \tag{1.32}$$

In the last passage of (1.32), we used the fact that $\gamma^\mu$ acts on spinor indices and not on weak isospin. We see that the weak current depends on the product $W^{U\dagger}_L W^D_L$ and not separately on the two matrices $W^U_L$ and $W^D_L$. Therefore, we can define a new unitary matrix, the Cabibbo–Kobayashi–Maskawa matrix $U_{CKM} = W^{U\dagger}_L W^D_L$, so that the weak charged current for quarks begins

$$j^\mu_{\mathrm{q,WC}} = 2\overline{q^U_{0L}}\gamma^\mu U_{CKM} q^D_{0L} \; . \tag{1.33}$$

A similar path can be followed for leptons, with the difference that there are no right-handed neutrinos, playing the role of the lower component of quark isodoublets (the down quarks $d, s, b$). Therefore, in the lepton sector, only the matrix $f^\ell$ needs to be diagonalized by means of two unitary matrices $W^\ell_L$ and $W^\ell_R$:

$$W^{\ell\dagger}_L f^\ell W^\ell_R = f^\ell_{\mathrm{diag}} \; . \tag{1.34}$$

As in (1.27), we define the lepton mass eigenstates

$$\ell_{0L} = W^{\ell\dagger}_L \ell_L \qquad\qquad \ell_{0R} = W^{\ell\dagger}_R \ell_R \; . \tag{1.35}$$

If we denote with $f^\ell_m$ are the diagonal elements of $f^\ell_{\mathrm{diag}}$, we can rewrite the charged lepton part of the Yukawa Lagrangian as

$$\mathcal{L}^{\mathrm{lept}}_{\mathrm{Yukawa}} = -f^\ell_m(\overline{\ell_{0Lm}}\ell_{0Rm} + \overline{\ell_{0Rm}}\ell_{0Lm}) = -\frac{v}{\sqrt{2}} f^\ell_m \overline{\ell_{0m}}\ell_{0m} \; , \tag{1.36}$$

from which the charged lepton masses can be read

$$m_n = \frac{v}{\sqrt{2}} f^\ell_n \qquad n = e, \mu, \tau \; . \tag{1.37}$$

Since in the SM neutrinos are strictly massless and degenerate, we are free to redefine

$$\nu_L \to W^{\ell\dagger}_L \nu_L \; (= \nu_{0L}) \; , \tag{1.38}$$

so that neutrino flavor eigenstates are mass eigenstates too. By means of this redefinition, the leptonic charged weak current can be written as:

$$j^\mu_{\ell,\mathrm{WC}} = 2\overline{\nu_L}\gamma^\mu \ell_L = 2\overline{\nu_L}\gamma^\mu W^\ell_L \ell_{0L} = 2\overline{\nu_{0L}}\gamma^\mu \ell_{0L} \to 2\overline{\nu_L}\gamma^\mu \ell_{0L} \; . \tag{1.39}$$

We have defined in equation (1.39) the flavor neutrino eigenstates so that the current couples each neutrino with the corresponding lepton mass eigenstate.

**Neutrinos in the Standard Model**

- In the SM, neutrinos of flavor $m = e, \mu, \tau$ are the $I_3 = 1/2$ upper component of a $SU(2)_L$ doublet
$$L_m = \begin{pmatrix} \nu_{mL} \\ \ell_{mL} \end{pmatrix} ,$$
together with their homologous charged lepton $\ell_m$;
- While every charged lepton has the right-handed part $R_m$, there is no $\nu_{mR}$, so that no mass term $\overline{\nu_{mR}}\nu_{mL} + \overline{\nu_{mL}}\nu_{mR}$ can arise after symmetry breaking;
- The Yukawa sector of the lagrangian contains a term like $\overline{L_i}\Phi R_j$ + h.c., constructed in such a way that $SU(2)_L \times U(1)_Y$ is respected.
- After the symmetry breaking, the Higgs field acquires a $vev$, $\langle\Phi\rangle = 1/\sqrt{2}(0, v)^T$, and one has $\overline{L_i}\Phi R_j \to \sqrt{2}\,\overline{\ell_{iR}}\ell_{jR}$. If there were a neutrino right-handed component, to the doublet $\tilde{\Phi} = i\sigma_2\Phi^*$ that acquires a $vev$ $\langle\tilde{\Phi}\rangle = 1/\sqrt{2}(v, 0)^T$, one would pick up the mass term for the upper $I_3 = 1/2$ component of the doublet $L_i$, i.e. the neutrino, exactly in the same way as for the charged leptons.
- The fact that there are three generations implies that the structure of the mass terms is, in general and as experimentally confirmed, not diagonal. As a consequence, mass and flavor eigenstates do not coincide anymore for quarks, but are related by the unitary matrix $U_{CKM}$ that appears explicit in the weak charged current.
- For strictly massless neutrinos, a suitable redefinition of the fields allows to express the weak charged current as in the case of only one generation, so that each flavor neutrino eigenstate couple to the corresponding lepton mass eigenstate.

## 1.2 Massive Neutrinos

While neutrino masses are absent in the SM by construction, nowadays we know for sure that neutrinos possess mass, because they oscillate and,therefore, it is mandatory to extend the theory so to incorporate this fact. Essentially, there are two possibilities to include neutrino mass in the Lagrangian: the mass can be of Dirac or Majorana type. The first possibility is completely analogous to the charged lepton case, where mass terms are of the kind $m\overline{\psi}\psi = m(\overline{\psi_R}\psi_L + \text{h.c.})$. The second possibility is when the mass term has the form $m(\overline{\psi^c_L}\psi^c_L + \text{ h.c.})$, for a Majorana neutrino. This Majorana term violates lepton number conservation by two units, since, after quantization, corresponds to the annihilation of a neutrino in the initial state and of an antineutrino (that coincides with a neutrino in the Majorana case) in the final state.[4]

[4] An othe way to see this fact is to consider that lepton number conservation corresponds to the transformation $\psi \to e^{i\phi}\psi$ and that $\overline{\psi^c} \to e^{i\phi}\overline{\psi}$ also, so that the mass term does not transorms to itself.

### 1.2.1 Dirac Neutrino Masses

As we have seen, the absence of right-handed neutrinos in the SM makes possible to redefine the neutrino fields so that their mass and flavor eigenstates coincide. However, a Dirac mass for neutrinos can be generated through the Higgs mechanisms if we add $\nu_R$ states to the model. The easiest thing to to is do consider three *sterile* states $\nu_{mR}$ with $m = e, \mu, \tau$, where sterile means that they are singlet of $SU(3)_c \times SU(2)_L$ and have hypercharge $Y = 0$. In other words, the three right-handed sterile neutrinos have absolutely no charge whatsoever and, thus, do not interact at all with the other SM particles. [5] In this model, sometimes called the Minimal Extended Standard Model, the Higgs mechanism generates three neutrino masses in exactly the same way as in (1.21) and in (1.24), that now will read as

$$\begin{aligned}\mathcal{L}_{\text{Yukawa}} = &- f^{\ell}_{ij}(\overline{L_i}\Phi R_j + \overline{R_i}\Phi^{\dagger} L_j) - f^{\nu}_{ij}(\overline{L_i}\tilde{\Phi}\nu_{Rj} + \overline{\nu_{Ri}}\tilde{\Phi}^{\dagger} L_j) + \\ &- f^{u}_{ij}(\overline{q_{Li}}\tilde{\Phi}u_{Ri} + \overline{u_{Ri}}\tilde{\Phi}^{\dagger} q_{Li}) - f^{d}_{ij}(\overline{q_{Li}}\Phi d_{Ri} + \overline{d_{Ri}}\Phi^{\dagger} q_{Li})\,.\end{aligned} \tag{1.40}$$

and

$$\mathcal{L}_{\text{f.m.}} = -\frac{v}{\sqrt{2}}(f^{\ell}_{ij}\overline{\ell_{Li}}\ell_{Rj} + f^{\nu}_{ij}\overline{\nu_{Li}}\nu_{Rj} + f^{U}_{ij}\overline{q^{U}_{L}}_{i}q^{U}_{Rj} + f^{D}_{ij}\overline{q^{D}_{L}}_{i}q^{D}_{Rj} + \text{h. c.})\,. \tag{1.41}$$

The diagonalization of the Yukawa coupling in the lepton sector practically proceeds as for quarks and in the end it is possible to introduce a unitary matrix $U_{\text{PNMS}}$[6] describing the mixing between flavor and mass neutrino eigenstates. In particular, besides the two matrices $W^{\ell}_L$ and $W^{\ell}_R$, we need to introduce two matrices also for neutrinos, $V^{\nu}_L$ and $V^{\nu}_R$ so that

$$\begin{aligned}\nu^0_L &= \begin{pmatrix}\nu^0_{1\,L}\\ \nu^0_{2\,L}\\ \nu^0_{3\,L}\end{pmatrix} = V^{\nu\dagger}_L \begin{pmatrix}\nu_{eL}\\ \nu_{\mu L}\\ \nu_{\tau L}\end{pmatrix}\,,\\ \nu^0_R &= \begin{pmatrix}\nu^0_{1\,R}\\ \nu^0_{2\,R}\\ \nu^0_{3\,R}\end{pmatrix} = V^{\nu\dagger}_R \begin{pmatrix}\nu_{eR}\\ \nu_{\mu R}\\ \nu_{\tau R}\end{pmatrix}\,,\end{aligned} \tag{1.42}$$

where the chiral mass eigenstates vectors $\nu^0_L$ and $\nu^0_R$ have been introduced. With these definitions one can write for the lepton part of the Yukawa Lagrangian

$$\begin{aligned}\mathcal{L}^{\text{lepton}}_{\text{Yukawa}} &= -\frac{v}{\sqrt{2}}\left[\overline{\ell_L}(W^{\ell}_L W^{\ell\,\dagger}_L) f^L (W^{\ell}_R W^{\ell\,\dagger}_R)\ell_R + \overline{\nu_L}(V^{\nu}_L V^{\nu\dagger}_L) f^{\nu} (V^{\nu}_R V^{\nu\dagger}_R)\nu_R + \text{h.c.}\right] = \\ &= -\frac{v}{\sqrt{2}}\left[(\overline{\ell_L}W^{\ell}_L)(W^{\ell\,\dagger}_L f^L W^{\ell}_R)(W^{\ell\,\dagger}_R \ell_R) + (\overline{\nu_L}V^{\nu}_L)(V^{\nu\dagger}_L f^{\nu} V^{\nu}_R)(V^{\nu\dagger}_R \nu_R) + \text{h.c.}\right] = \\ &= -\frac{v}{\sqrt{2}}\left[(\overline{\ell_{0L}} f^L_{\text{diag}} \ell_{0R} + \overline{\nu^0_L} f^{\nu}_{\text{diag}} \nu^0_R) + \text{h.c.}\right]\,,\end{aligned} \tag{1.43}$$

from which one can read the neutrino masses as

$$m_n = \frac{v}{2}(f^{\nu}_{\text{diag}})_{nn}\,. \tag{1.44}$$

[5] The number of sterile neutrinos is completely arbitrary since they do not spoil any symmetry of the theory.
[6] PNMS is an acronym for Pontecorvo, Nakagawa, Maka, and Sakata.

Since all $\nu_R$ charges are zero, the weak current is once again written only in terms of left-handed fields as in (1.39)

$$j^\mu_{\ell,\mathrm{WC}} = 2\overline{\nu_L}\gamma^\mu \ell_L = 2\overline{\nu^0_L} V^{\nu\dagger}_L \gamma^\mu W^\ell_L \ell_{0L} = 2\overline{\nu^0_L} V^{\nu\dagger}_L W^\ell_L \gamma^\mu \ell_{0L} = 2\overline{\nu^0_L} U^\dagger_{\mathrm{PNMS}} \gamma^\mu \ell_{0L} \; , \tag{1.45}$$

where the mixing matrix is

$$U_{\mathrm{PNMS}} \equiv U = W^{\ell\dagger}_L V^\nu_L \; . \tag{1.46}$$

We now redefine the neutrino flavor eigenstates so that they are obtained from the mass eigenstates by multiplying them by the mixing matrix $U$:

$$\nu_L \to W^{\ell\dagger}_L \nu_L = W^{\ell\dagger}_L (V^\nu_L V^{\nu\dagger}_L)\nu_L = U(V^{\nu\dagger}_L \nu_L) = U\nu^0_L \; . \tag{1.47}$$

With this redefinition the weak charged current is

$$j^\mu_{\ell,\mathrm{WC}} = 2\overline{\nu^0_L} U^\dagger \gamma^\mu \ell_{0L} \to 2\overline{\nu_L} U U^\dagger \gamma^\mu \ell_{0L} = \overline{\nu_L}\gamma^\mu \ell_{0L} \tag{1.48}$$

Also in this case, as in (1.39) for massless neutrinos, we have defined the neutrino flavor eigenstates so that each neutrino flavor couples to the corresponding charged lepton only. To unclutter the notation, we will rename from now on the lepton mass eigenstates $\ell_0$ as $\ell$. To summarize, the Yukawa part of the Lagrangian in the SM extended with three sterile right-handed neutrinos after symmetry breaking contains terms of the kind

$$\overline{\ell_L} M_{\mathrm{lept}} \ell_R + \overline{\nu_L} M_\nu \nu_R + \mathrm{h.c.} \; , \tag{1.49}$$

whit nondiagonal complex matrices $M_{\mathrm{lept}}$ and $M_\nu$. Both matrices can be diagonalized through two unitary matrices so that the terms in (1.49) are also diagonalized, at the price of a redefinition of the field, the mass eigenstate fields. The left weak current preserves its form $2\overline{\nu_L}\gamma^\mu \ell_L$ if we use the mixing matrix $U$ to connect flavor and mass eigenstates fields, $\nu_L = U\nu^0_L$, and denote the left-handed lepton mass eigenstates $\ell_{0L}$ as $\ell_L$, to simplify the notation.

### 1.2.2 Majorana Neutrino Masses

In the Weyl representation of the Dirac matrices, the expression of left and right–handled spinors is the most simple (see the Appendix A.2 and B)

$$\begin{aligned} \psi_L &= \frac{1-\gamma_5}{2}\psi = \begin{pmatrix} 0 \\ \chi_L \end{pmatrix} \; , \\ \psi_R &= \frac{1+\gamma_5}{2}\psi = \begin{pmatrix} \chi_R \\ 0 \end{pmatrix} \; , \end{aligned} \tag{1.50}$$

where $\chi_L$ and $\chi_R$ are two-component Weyl spinors. If we remember that charge conjugation for a Dirac spinor is defined by

$$\begin{aligned} C &= i\gamma^2\gamma^0 \; , \\ \psi^c &= C\overline{\psi}^T = i\gamma^2\psi^* \; , \end{aligned} \tag{1.51}$$

we can see that

$$\begin{aligned}\psi_L^c &\equiv (\psi_L)^c = i\begin{pmatrix}0 & \sigma_2\\ -\sigma_2 & 0\end{pmatrix}\begin{pmatrix}0\\ \chi_L^*\end{pmatrix} = \begin{pmatrix}i\sigma^2\chi_L^*\\ 0\end{pmatrix}\\ \psi_R^c &\equiv (\psi_R)^c = i\begin{pmatrix}0 & \sigma_2\\ -\sigma_2 & 0\end{pmatrix}\begin{pmatrix}\chi_R^*\\ 0\end{pmatrix} = \begin{pmatrix}0\\ -i\sigma^2\chi_R^*\end{pmatrix} ,\end{aligned} \tag{1.52}$$

so that $\psi_L^c$ is right-handed and $\psi_R^c$ is left-handed. Note that parity transforms $\psi_L$ into $\psi_R$ and vice versa. Therefore, out of $\psi_L$ only, we can define a Majorana spinor

$$\psi = \psi_L + C\overline{\psi_L}^T = \begin{pmatrix}i\sigma^2\chi_L^*\\ \chi_L ,\end{pmatrix} \tag{1.53}$$

which satisfies

$$\psi^c = i\gamma^2\begin{pmatrix}i\sigma^2\chi_L^*\\ \chi_L\end{pmatrix}^* = i\begin{pmatrix}0 & \sigma_2\\ -\sigma_2 & 0\end{pmatrix}\begin{pmatrix}-i(-\sigma_2)\chi_L\\ \chi_L^*\end{pmatrix} = \begin{pmatrix}i\sigma_2\chi_L^*\\ \chi_L\end{pmatrix} = \psi , \tag{1.54}$$

so that it coincides with its complex conjugate, it is real and has two degrees of freedom. Neutrinos are the only fermions that can be of Majorana type, since they have no electric charge. In case they are massless, the Dirac or Majorana nature of neutrinos can not be ascertained because they satisfy the same Weyl equation: Majorana and Dirac neutrinos would be phenomenologically indistinguishable. They could only be distinguished from effects related to neutrino masses. Since the SM has an intrinsic left symmetry, let us write the lagrangian for a massive left-handed Majorana neutrino. From the Lagrangian for a massive Dirac neutrino, see equation (B.10), we can convince ourselves that the lagrangian for one Majorana neutrino can be written as

$$\mathcal{L}_{\mathcal{M}} = \tfrac{1}{2}(\overline{\nu_L} i\partial\!\!\!/ \nu_L + \overline{\nu_L^c} i\partial\!\!\!/ \nu_L^c) - \tfrac{1}{2}(\overline{\nu_L^c}\nu_L + \overline{\nu_L}\nu_L^c) . \tag{1.55}$$

In the equation (1.55), the structure of the kinetic term is left–$\partial\!\!\!/$–left plus right–$\partial\!\!\!/$–right, the only two terms surviving in $\overline{\nu}\partial\!\!\!/\nu$, while in the mass term only right-left products are non-zero. Let us emphasize again that a Majorana mass term like $\overline{\nu_L^c}\nu_L$ it is not admissible in the SM, since it has $Y = -1$. In fact, $\nu_L$ has $Y = Q - I_3 = 0 - 1/2$ and from the first of (1.52) (see also Appendix B), we see that $\overline{\nu_L^c}$ is also left-handed and has $Y = -1/2$. All in all, $\overline{\nu_L^c}\nu_L$ has $I_3 = 1$ and $Y = -1$ and it does not respect the $SU(2)_L \times U(1)_Y$ symmetry. To derive the equation of motions by varying the lagrangian with respect to the fields, it is useful to express the lagrangian (1.55) in terms of $\nu_L$ alone. To this end we observe that

$$\begin{aligned}\overline{\nu_L^c} &= \overline{(C\overline{\nu_L}^T)} = (C\overline{\nu_L}^T)^\dagger\gamma^0 = (C(\nu_L^\dagger\gamma^0)^T)^\dagger)\gamma^0 = (C\gamma^0\nu_L^*)^\dagger\gamma^0 = i\nu_L^T\gamma^0 i\gamma^2\gamma^0\gamma^0 =\\ &= i\nu_L^T\gamma^0 i\gamma^2 = -\nu_L^T C^\dagger .\end{aligned} \tag{1.56}$$

Thanks to (1.56) and to the properties

$$C^\dagger = C^{-1} = -C = C^T \qquad C\gamma_\mu^T C^\dagger = -\gamma_\mu \qquad C^\dagger\gamma_\mu C = \gamma_\mu^T , \tag{1.57}$$

the Majorana neutrino lagrangian (1.55) can be rewritten as

$$\mathcal{L} = \frac{1}{2}\left[\overline{\nu_L} i\partial\!\!\!/ \nu_L + \nu_L^T i\partial\!\!\!/^T \overline{\nu_L}^T - m(-\nu_L^T C^\dagger\nu_L + \overline{\nu_L} C\overline{\nu_L}^T)\right] . \tag{1.58}$$

To derive the equation of motion, the easier way is to vary the lagrangian terms that depend on $\overline{\nu_L}$. First we note that

$$\begin{aligned}\delta(\overline{\nu_L} C \overline{\nu_T}^T) = \delta\overline{\nu_L}_j C_{jk} \overline{\nu_L}_k + \overline{\nu_L}_j C_{jk} \delta\overline{\nu_L}_k = \delta\overline{\nu_L}_j \overline{\nu_L}_k C_{jk} - \delta\overline{\nu_L}_k \overline{\nu_L}_j C_{jk} = \\ = \delta\overline{\nu_L}_j \overline{\nu_L}_k C_{jk} - \delta\overline{\nu_L}_j \overline{\nu_L}_k C_{kj} = 2\delta\overline{\nu_L}_j \overline{\nu_L}_k C_{jk} \ ,\end{aligned} \tag{1.59}$$

because of the antisymmetry of $C$. Then we have

$$\delta\mathcal{L}(\overline{\nu_L}) = \frac{1}{2}(\delta\overline{\nu_L}_j i\partial\!\!\!/_{jk}\nu_{Lk} + \nu_{Lj} i\delta(\partial\!\!\!/_{kj}\overline{\nu_L}_k) - \frac{m}{2}(2\delta\overline{\nu_L}_j C_{jk}\overline{\nu_L}_k)) \ . \tag{1.60}$$

Consequently

$$\begin{aligned}\frac{\partial\mathcal{L}}{\partial(\partial_\mu\overline{\nu_L}_i)} &= -\frac{i}{2}\nu_{Lj}\gamma^\mu_{ij} \ , \\ \frac{\partial\mathcal{L}}{\partial\overline{\nu_L}_i} &= \frac{i}{2}(\partial\!\!\!/\nu_L)_i - \frac{m}{2}2\overline{\nu_L}_k C_{ik} \ .\end{aligned} \tag{1.61}$$

Therefore, from Lagrange equations we get

$$\frac{\partial\mathcal{L}}{\partial(\partial_\mu\overline{\nu_L}_i)} - \frac{\partial\mathcal{L}}{\partial\overline{\nu_L}_i} = 0 \Rightarrow -\frac{i}{2}(\partial\!\!\!/\nu_L)_i \ - \frac{i}{2}(\partial\!\!\!/\nu_L)_i + mC_{ij}\overline{\nu_L}_i = 0 \ . \tag{1.62}$$

We have obtained the equation for a Majorana spinor

$$i\partial\!\!\!/\nu_L = mC\overline{\nu_L}^T \ , \tag{1.63}$$

i.e. the Weyl equation for a Dirac field with $\psi_R = C\overline{\psi_L}^T$.

## 1.3 Mass terms in the lagrangian: the general case

For the time being, we shall have our discussion for the case of only one fermion generation. We have seen that a Dirac mass term into the SM lagrangian requires the introduction of an additional neutrino field $\nu_R$, besides the left-handed neutrino field $\nu_L$. The $\nu_R$ is a sterile neutrino, transforming as $\{\mathbf{1}, \mathbf{1}, 0\}$, with no charge at all under the SM gauge groups. We then can have a Dirac mass term of the kind

$$\mathcal{L}_D = -m_D(\overline{\nu_R}\nu_L + \overline{\nu_L}\nu_R) \ , \tag{1.64}$$

that comes from the Yukawa sector of the SM lagrangian, once we add a $\nu_R$, and that it respects the symmetry of the theory. Concerning Majorana masses, we can have two more terms, because we can add a Majorana term for both $\nu_R$ and $\nu_L$:

$$\mathcal{L}_M = -\frac{1}{2}m_L\overline{\nu^c_L}\nu_L - \frac{1}{2}m_R\overline{\nu^c_R}\nu_R + h.c. \ . \tag{1.65}$$

While the right-handed neutrino term does not spoil the gauge symmetry, the left-handed term is not admissible in the SM, and must be viewed as an effective low energy term generated by a higher dimensional operator, suppressed by some pover of an unknown high-energy scale, where the new physics is manifested. Let us introduce a left doublet $N$, to write in a compact way the most general mass lagrangian, i.e. the sum of (1.64) and (1.65), and a suitable mass matrix $M$

$$N = \begin{pmatrix} \nu_L \\ \nu_R^c \end{pmatrix} , \qquad M = \begin{pmatrix} m_L & m_D \\ m_D & m_R \end{pmatrix} . \tag{1.66}$$

The most general mass term lagrangian will be written as

$$\begin{aligned} \mathcal{L} &= -\frac{1}{2}\overline{N^c} M N + \text{h.c.} = -\frac{1}{2}\begin{pmatrix} \overline{\nu_L^c} & \overline{\nu_R} \end{pmatrix} \begin{pmatrix} m_L & m_D \\ m_D & m_R \end{pmatrix} \begin{pmatrix} \nu_L \\ \nu_R^c \end{pmatrix} + \text{h.c.} = \\ &= -\frac{1}{2}(m_L \overline{\nu_L^c}\nu_L + m_D \overline{\nu_L^c}\nu_R^c + m_D \overline{\nu_R}\nu_L + m_R \overline{\nu_R}\nu_R^c) + \text{h.c.} = \\ &= \frac{1}{2}(m_L \overline{\nu_L^c}\nu_L + +m_R \overline{\nu_R^c}\nu_R + 2m_D \overline{\nu_R}\nu_L) + \text{h.c.} = \mathcal{L}_M + \mathcal{L}_D , \end{aligned} \tag{1.67}$$

where we have used the fact that

$$\overline{\nu_R}\nu_R^c \quad \xrightarrow{C} \quad \overline{\nu_R^c}\nu_R , \tag{1.68}$$

and that

$$\overline{\nu_L^c}\nu_R^c = (-\nu_L^T C^\dagger) C \overline{\nu_R}^T = -\nu_L^T \overline{\nu_R}^T = -(-\overline{\nu_R}\nu_L)^T = \overline{\nu_R}\nu_L . \tag{1.69}$$

Regardless of the Dirac or Majorana nature of neutrino masses in the most general lagrangian (1.67), from the nondiagonal form of the neutrino mass matrix $M$ we see that $\nu_L$ and $\nu_R$ do not have definite masses. It can be demonstrated that, since $M$ is symmetric and complex, we can go to the basis of the mass eigenstates $n$, through a two dimensional unitary matrix $U$:

$$\begin{aligned} N &= \begin{pmatrix} \nu_L \\ \nu_R^c \end{pmatrix} = U \begin{pmatrix} \nu_{1L} \\ \nu_{2L} \end{pmatrix} = Un , \\ U^T M U &= M_{\text{diag}} = \begin{pmatrix} m_1 & 0 \\ 0 & m_2 \end{pmatrix} . \end{aligned} \tag{1.70}$$

Note that this is not the usual diagonalization through $U^{-1}$, since on the left of $M$ there is $U^T$. Consequently, the lagrangian mass term (1.67) begins

$$\begin{aligned} \mathcal{L} &= -\frac{1}{2}\overline{N^c} M N + \text{h.c.} = -\frac{1}{2}\overline{N^c}(U^T)^{-1} M_{\text{diag}} U^{-1} N + \text{h.c.} = \\ &= -\frac{1}{2}\overline{n^c} M_{\text{diag}} n + \text{h.c.} = -\frac{1}{2}\sum_{i=1}^{2} m_i \overline{\nu_i}\nu_i , \end{aligned} \tag{1.71}$$

where the Majorana states $\nu_i = \nu_{iL} + \nu_{iL}^c$ have been introduced and we have used the fact that $\overline{\nu_{iL}^c}\nu_{iL}^c = \overline{\nu_{iL}}\nu_{iL} = 0$. Thus, we have discovered that, in the most general case of an arbitrary mass matrix $M$, neutrinos are Majorana particles. Going back to the definition of the mass matrix $M$ we note that only two masses among $m_L$, $m_R$ and $m_D$ can be chosen to be real by rephasing the fields $\nu_L$ and $\nu_R$. We choose to take $m_R$ and $m_D$ as real and $m_L$ as complex. Let us try to summarize what we have obtained so far:

- Since the SM is constructed with left-handed fields and we need right-handed neutrino fields to build neutrino mass terms in the lagrangian, we considered the two fields $\nu_R$ and $\nu_R^c$. We know that $\nu_R^c$ transforms like $\nu_L$ and, in the chiral representation of the Dirac matrices, has only lower “left” components;

- We considered the most general lagrangian containing Majorana masses for $\nu_L$ and $\nu_R$ and a Dirac term coupling left and right fields. We regroup these terms in matrix notation as $\overline{N^c}MN$ + h.c.;

- We diagonalize the mass term and discover that the neutrino states with definite masses are Majorana left-handed particles connected to $\nu_L$ and $\nu_R^c$ through a $2\times 2$ unitary mixing matrix $U$. The diagonalization is realized through $U^T MU$ and not $U^{-1}MU$.

- While $\nu_L$ feels the weak interaction, $\nu_R$ is sterile and is a singlet under the SM gauge group.

It is possible, and relatively easy, to generalize the previous discussion to the case of three generations of active neutrinos and $n_s$ right-handed sterile neutrinos. To this end, we introduce the arrays

$$\boldsymbol{N} = \begin{pmatrix} \boldsymbol{\nu}_L \\ \boldsymbol{\nu}_R^c \end{pmatrix} \;, \quad \text{with} \quad \boldsymbol{\nu}_L = \begin{pmatrix} \nu_{eL} \\ \nu_{\mu L} \\ \nu_{\tau L} \end{pmatrix} \quad \text{and} \quad \boldsymbol{\nu}_R^c = \begin{pmatrix} \nu_{1R}^c \\ \nu_{2R}^c \\ \cdots \\ \nu_{n_s R}^c \;, \end{pmatrix} \tag{1.72}$$

and the mass matrix analogous to the mass matrix of (1.66):

$$M_n = \begin{pmatrix} M_L & M_D \\ M_D^T & M_R \end{pmatrix} \;. \tag{1.73}$$

The $M_n$ in (1.73) is a squared symmetric complex matrix with dimension $n = 3 + n_s$, containing three blocks. $M_L$ is a $3 \times 3$ complex symmetric matrix , $M_R$ is a $n_s \times n_s$ complex symmetric matrix and $M_D$ is a $3 \times n_s$ complex matrix. The lagrangian in this general case may be now written as

$$\mathcal{L} = -\frac{1}{2}\overline{\boldsymbol{N}^c} M \boldsymbol{N} + \text{h.c.} \;. \tag{1.74}$$

Thanks to the fact that also in this case $M$ is symmetric and complex, it can be diagonalized through a unitary matrix $U_n$ in the following way:

$$U_n^T M_n U_n = M_{n\text{diag}} = \begin{pmatrix} M_1 & 0 \\ 0 & M_2 \end{pmatrix} \;, \tag{1.75}$$

where $M_1$ is the diagonal mass of the three active neutrino mass eigenstates and $M_2$ the diagonal mass matrix for the $n_s$ sterile neutrinos. In this general case, the neutrino mass eigenstates are Majorana neutrinos, and one can write

$$\mathcal{L} = -\tfrac{1}{2}\overline{\boldsymbol{N}^c} M \boldsymbol{N} + \text{h.c.} = -\tfrac{1}{2}\sum_{i=1}^{n} m_i \overline{\nu_i}\nu_i \;. \tag{1.76}$$

In the right-hand side of (1.76), the first three Majorana neutrino fields correspond to the active neutrino fields $\nu_\alpha = \nu_{\alpha L} + \nu_{\alpha L}^c$ with $\alpha = e, \mu, \tau$, while the indices from 4 to $n$ correspond to the Majorana sterile neutrino fields.

A final remark about the notation is in order. Often the lagrangian mass term

$$\mathcal{L} = -\frac{1}{2}\overline{N^c} M N + \text{h.c.} \;, \tag{1.77}$$

both in one generation or in the general case, is written as

$$\mathcal{L} = -\frac{1}{2}\overline{N^c}MN + \text{h.c.} = -\frac{1}{2}(-N^T C^\dagger)MN + \text{h.c.} = \frac{1}{2}N^T C^\dagger MN + \text{h.c.}\ , \tag{1.78}$$

and sometimes, with an abuse of notation, $C^\dagger$ is omitted.

In equation (1.48), we saw that the weak charged current can be written, because of the neutrino mixing, as

$$j^\mu_{\ell,\text{WC}} = 2\overline{\nu_L}\gamma^\mu \ell_L = 2\overline{\nu^0_L}U^\dagger_{\text{PNMS}}\gamma^\mu \ell_{0L}\ , \tag{1.79}$$

when neutrinos are Dirac particles. It can be demonstrated that, if neutrinos are Majorana particles, the expression for the charged current is still the same, but the mixing matrix $U$ contains two additional phases. These new phases appear because the Majorana mass term is not invariant under a global $U(1)$ gauge transformation. Explicitly, if we consider the phase transformation $\nu_L \to e^{i\phi}\nu_L$ for a Majorana neutrino field, $\overline{\nu^c_L} \to e^{i\phi}\overline{\nu^c_L}$, because we have two complex conjugations. Equivalently, we immediately see that $\nu^T_L C^\dagger \nu_L \to e^{i2\phi}\nu^T_L C^\dagger \nu_L$.

In the general case of three active neutrinos and $n_s$ sterile neutrinos that are all Majorana fields, as we saw in (1.76), the mixing matrix $U$ is a $3 \times (3 + n_s)$ rectangular matrix that can be parametrized in terms of $3 + 3n_s$ mixing angles and $3 + 3n_s$ phases.

## 1.4 Generation of neutrino masses: the See-Saw mechanism

We have discussed the nature of the possible mass terms present in extensions of the SM with massive neutrinos. We wonder what mechanisms can generate these terms. We have seen it that the simplest extension of the SM, in which three sterile right-handed neutrinos are introduced, results in Dirac mass terms, in complete analogy analogous with the charged fermion case, but fails to explain the smallness of the Yukawa couplings needed to generate such small masses. One interesting possibility is that neutrino masses come from a non-renormalizable dimension five lagrangian term, suppressed by a large scale $M$, possibly related to new physics. If we insist on preserving the gauge symmetry, the term $m_L\overline{\nu^c_L}\nu_L$ cannot be present in the Lagrangian, since it violates the hypercharge of one unit and it is a triplet of $SU(2)$. For the same reason, we cannot introduce terms like $\overline{L^c}L$. If we want to have both a $SU(2)$ and a $Y$ singlet, we should use $\overline{L}\tilde{\Phi}$ and $\tilde{\Phi}^T L^c$ (omitting flavor indices), both transforming as right-handed neutrinos. Here, however, we face the problem of renormalizability, since to have a neutrino mass term we must include the product $(\overline{L}\tilde{\Phi})(\tilde{\Phi}^T L^c)$ that has dimension $3/2+1+1+3/2 = 5$ and it not renormalizable. The new term must be divided by a scale $M$ with dimension of a mass, and can be multiplied by a generic dimensionless coefficient $g$ of order 1:

$$\mathcal{L}_{\text{Weinberg}} = -\frac{g}{M}(\overline{L}\tilde{\Phi})(\tilde{\Phi}^T L^c) + \text{h.c.}\ . \tag{1.80}$$

After symmetry breaking we have

$$\frac{g}{M}(\overline{L}\tilde{\Phi})(\tilde{\Phi}^T L^c) \to \frac{1}{\sqrt{2}}\begin{pmatrix}\overline{\nu_L} & \overline{e_L}\end{pmatrix}\begin{pmatrix}0\\ v\end{pmatrix}\frac{1}{\sqrt{2}}\begin{pmatrix}0 & v\end{pmatrix}\begin{pmatrix}\nu^c_L\\ e^c_L\end{pmatrix} = \frac{v^2}{2}\overline{\nu_L}\nu^c_L\ . \tag{1.81}$$

Therefore, we find that

$$\mathcal{L}_{\text{Weinberg}} = -\frac{g}{M}(\overline{L}\tilde{\Phi})(\tilde{\Phi}^T L^c) + \text{h.c.} \to -\frac{gv^2}{2M}(\overline{\nu_L}\nu^c_L + \overline{\nu^c_L}\nu_L)\ . \tag{1.82}$$

Let us note that the Weinberg operator is the only possible dimension five operator that can be written and that it entails violation of the lepton number by two units, since both $\nu_L$ and $\overline{\nu_L^c}$ have lepton number equal to -1. The Weinberg operator can be obtained by starting from a general lagrangian 1.76, where $m_L = 0$, by integrating out the right-handed field $\nu_R$. For instance, consider the following lagrangian:

$$\mathcal{L}_{\mathrm{D+M}} = -y(\overline{\nu_R}\tilde{\Phi}^\dagger L + \overline{L}\tilde{\Phi}\nu_R) - \frac{1}{2}m_R(\overline{\nu_R}^c\nu_R + \overline{\nu_R}\nu_R^c) \ . \tag{1.83}$$

If we derive the equation of motion for $\nu_R$ and suppose that it is very heavy so that the kinetic term can be neglected, we find

$$\frac{\partial\mathcal{L}_{\mathrm{D+M}}}{\partial\nu_R} = -y\overline{L}\tilde{\Phi} - m_R\overline{\nu_R^c} = \partial_\mu\frac{\partial\mathcal{L}_{\mathrm{D+M}}}{\partial(\partial_\mu\nu_R)} \sim 0 \ , \tag{1.84}$$

Thus we have

$$\begin{aligned} \overline{\nu_R^c} &= \frac{y}{m_R}\overline{L}\tilde{\Phi} \ , \\ \nu_R &= -\frac{y}{m_R}\tilde{\Phi}^T L^c \ . \end{aligned} \tag{1.85}$$

Substituting back into (1.83), we have

$$\mathcal{L}_{\mathrm{D+M}} = \frac{y}{2m_R}(\overline{L}\tilde{\Phi}\tilde{\Phi}^T L^c + h.c.) \ , \tag{1.86}$$

which is the Weinberg operator of equation (1.80) If in (1.83) we start from a mass matrix of the form

$$M = \begin{pmatrix} 0 & m_D \\ m_D & m_R \ , \end{pmatrix} \tag{1.87}$$

since the term proportional to $m_L$ would explicitly spoil gauge invariance. The mass eigenvalues are the solutions of

$$\begin{vmatrix} -\lambda & m_D \\ m_D & -\lambda + m_R \end{vmatrix} = -\lambda(m_R - \lambda) - m_D^2 = 0 \Rightarrow \lambda_{1/2} = \frac{m_R \pm \sqrt{m_R^2 + 4m_D^2}}{2} \ . \tag{1.88}$$

There is no reason why $m_R$ should be small, an to the contrary, it could be related to some new very high energy scale. We can make a series expansion in the small quantity $m_D/m_R$ and obtain approximately

$$m_{1/2} = \frac{m_R \pm m_R\sqrt{1 + 4m_D^2/m_R^2}}{2} \sim \frac{m_R \pm m_R(1 + 2m_D^2/m_R^2)}{2} \Rightarrow \begin{cases} m_1 \sim -\dfrac{m_D^2}{m_R} \\ m_2 \sim m_R \ . \end{cases} \tag{1.89}$$

If we define the mass eigenstates through the mixing matrix $U$ as

$$\begin{pmatrix} \nu_L \\ \nu_R^c \end{pmatrix} = \begin{pmatrix} \cos\theta & -\sin\theta \\ \sin\theta & \cos\theta \end{pmatrix} \begin{pmatrix} \nu_1 \\ \nu_2 \end{pmatrix} \quad \text{with} \quad UMU^{-1} = M_{\mathrm{diag}} \ , \tag{1.90}$$

and we impose that off diagonal terms of $M_{\mathrm{diag}}$ are 0, then we easily find $\tan 2\theta = 2m_D/m_R \lesssim 1$. This in turn implies $\cos\theta \sim 1 - m_D^2/m_R^2$ and $\sin\theta \sim m_D/m_R$. Therefore $\nu_L \sim \nu_1$ and $\nu_R^c \sim \nu_2$. If we assume that $m_D$ is at the scale of the electroweak interaction, $m_D \sim 100$ GeV, and $m_R$ at the Grand Unification (GUT) scale, $m_R \sim 10^{14}$ GeV, then the lightest neutrino mass $m_2 \sim 0.1$ eV, in the ballpark of the experimentally expected values. This mechanism is called the see-saw, a tiny active neutrino mass obtained from a sterile neutrino mass at the GUT scale.

**Neutrinos masses and their origin**

- Neutrino masses can be included in the model in two ways:

$$\begin{aligned}&\text{Dirac terms} \sim \overline{\nu_L}\nu_R + \text{h.c.}\ ,\\&\text{Majorana terms} \sim \overline{\nu_L^c}\nu_c + \overline{\nu_R^c}\nu_R + \text{h.c.}\ .\end{aligned}$$

- If we define a left isodoublet $N = (\nu_L, \nu_R^c)$ the most general case with Majorana and Dirac mass terms at the same time can be summed up in the lagrangian

$$\mathcal{L} = -\frac{1}{2}\overline{N^c}MN + \text{h.c.} \ \text{ with } \quad M = \begin{pmatrix} m_L & m_D \\ m_D & m_R \end{pmatrix}\ . \tag{1.91}$$

- The see-saw mechanism provides an intriguing way to explain the smallness of the active neutrino masses. By starting from a lagrangian with Dirac and Majorana terms with $m_L = 0$, after integrating away the massive right-handed sterile neutrino field, a small mass of the order $m_D^2/m_R$ is generated for the active neutrino.


**Figure (1.1) :** SM Feynman vertices for CC and NC neutrino interactions.

## 1.5 Neutrino Interactions

Neutrinos interact with other particles only through the weak force, thus exchanging $W^\pm$ and $Z$ vector bosons. In section 1 we have explicitly written some of the terms of the SM lagrangian involving neutrinos. Neutrino interactions are governed by the charged (CC) and neutral (NC) lagrangian terms:

$$\begin{aligned} \mathcal{L}_{\rm CC} &= -\frac{g}{2\sqrt{2}}(j^\mu_{\ell,{\rm WC}} W_\mu + j^\mu_{\ell,{\rm WC}}{}^\dagger W^\dagger_\mu) \ , \\ \mathcal{L}_{\rm NC} &= -\frac{g}{2\cos\theta_W} j^\mu_{\ell,{\rm NC}} Z_\mu \end{aligned} \tag{1.92}$$

where the charged and neutral current are

$$\begin{aligned} j^\mu_{\ell,{\rm WC}} &= 2\overline{\nu_L}\gamma^\mu \ell_L = 2\sum_{\alpha=e,\mu,\tau} \overline{\nu_{\alpha L}}\gamma^\mu \ell_{\alpha L} = \sum_{\alpha=e,\mu,\tau} \overline{\nu_\alpha}\gamma^\mu(1-\gamma_5)\ell_\alpha \ , \\ j^\mu_{\ell,{\rm NC}} &= \overline{\nu_L}\gamma^\mu \nu_L = \sum_{\alpha=e,\mu,\tau} \overline{\nu_{\alpha L}}\gamma^\mu \nu_{\alpha L} = \frac{1}{2}\sum_{\alpha=e,\mu,\tau} \overline{\nu_\alpha}\gamma^\mu(1-\gamma_5)\nu_\alpha \ , \end{aligned} \tag{1.93}$$

The vertices corresponding to the interaction terms of equations (1.92) are shown in Figure 1.1. In the SM the electron, muon and tau lepton numbers are conserved, so that to a lepton on the left (initial state) corresponds a neutrino on the right (final state) and vice versa, while to an antilepton will correspond in the other state an antineutrino. Equivalently, the couples neutrino-antilepton or antineutrino-lepton can be found in the initial or in the final state. Since ordinary matter is composed of electrons, neutrons and protons, we will briefly review the neutrino interactions with these particles.

### 1.5.1 Neutrino-electron scattering

Let us consider the elastic scattering processes $\nu_\alpha + e^- \to \nu_\alpha + e^-$ and $\overline{\nu}_\alpha + e^- \to \overline{\nu}_\alpha + e^-$, in which the initial and final state coincide. For $\nu_\mu$ and $\nu_\tau$ neutrinos the scattering can proceed only through the $Z$, while for a $\nu_e$ there is a possibility to exchange a $W$, so that the neutrino goes into an electron and vice versa. At low energies, as compared to the $Z$ and $W$ masses, $E \ll 100$ GeV, the momentum of the virtual vector boson can be neglected in the denominator of the propagator and the process can be described by an effective four-fermion Fermi interaction. Let us start with the $\nu_e e^-$ scattering that contains both CC and NC diagrams, as shown in Figure 1.95. The two

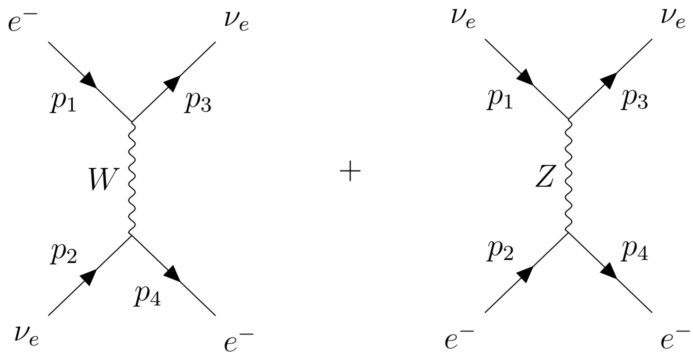


(1.95)

**Figure (1.2) :** Feynman diagrams for the scattering of neutrinos on electrons. On the left the CC diagrams, on the right the NC channel.

lagrangian terms for these two diagrams are

$$\begin{aligned}\mathcal{L}(\nu_e e^- \to \nu_e e^-) = &- \frac{G_F}{\sqrt{2}} \{[\overline{\nu_e}\gamma^\mu(1-\gamma_5)e]\,[\overline{e}\gamma_\mu(1-\gamma_5)\nu_e] + \\ &+ [\overline{\nu_e}\gamma^\mu(1-\gamma_5)\nu_e]\,\left[\overline{e}\gamma_\mu(g_V^\ell - g_A^\ell\gamma_5)e\right]\} = \\ &= - \frac{G_F}{\sqrt{2}} [\overline{\nu_e}\gamma^\mu(1-\gamma_5)\nu_e]\;\left[\overline{e}\gamma_\mu((1+g_V^\ell) - (1+g_A^\ell)\gamma_5)e\right]\;,\end{aligned} \tag{1.94}$$

where $g_V^\ell = -1/2 + 2\sin^2\theta_W$ and $g_A^\ell = -1/2$. In Figure (1.3), we se that there is a hierarchy between the cross sections, that, for the integrated cross sections, can be approximately summarized as

$$\sigma_{\nu_e} : \sigma_{\overline{\nu}_e} : \sigma_{\nu_{\mu,\tau}} : \sigma_{\overline{\nu}_{\mu,\tau}} = 1 : 0.42 : 0.16 : 0.14\,. \tag{1.96}$$

The difference in the neutrino-antineutrino cross-section is a consequence of the $V - A$ structure of the weak interaction while the difference between $\nu_e e^-$ and $\nu_{\mu,\tau} e^-$ scattering is due to the additional charged current diagram of the Figure 1.95. As we will see in the section 1.5.4, on dimensional ground, the total cross section must be proportional to the center-of-mass system (CMS) squared total energy, $\sigma \sim G_F^2 s$. It is useful to introduce the inelasticity parameter $y$ so defined

$$1 - y = -\frac{u}{s} = \frac{1}{2}(1+\cos\theta)\,, \tag{1.97}$$

where $u$ and $s$ are the Mandelstam variables[7] and $\theta$ is the scattering angle of the electron in the center-of-mass frame reference. In the following, we will use the CMS and assume the high-energy limit, neglecting the electron mass. With an explicit calculation, it can be shown that the following results hold true for the differential cross-section $\nu_x\, e^-$:

- The differential cross-section for the neutral current scattering is

$$\frac{d\sigma^{NC}}{dy}(\nu_x e^- \to \nu_x e^-) = \frac{G_F^2 s}{4\pi}\left[(g_V^e + g_A^e)^2 + (g_V^e + g_A^e)^2(1-y)^2\right]\,. \tag{1.98}$$

[7]Given a scattering of two particles with momenta $p_1$ and $p_2$ into two particles of momenta $p_3$ and $p_4$, the Mandelstam variable $s, t, u$ are defined in the followin way: $s = (p_1 + p_2)2$, $t = (p_1 - p_3)^2$ and $u = (p_1 - p_4)$, where $p_1$ and $p_3$ refer to the "most similar" particles in the initial and final state.

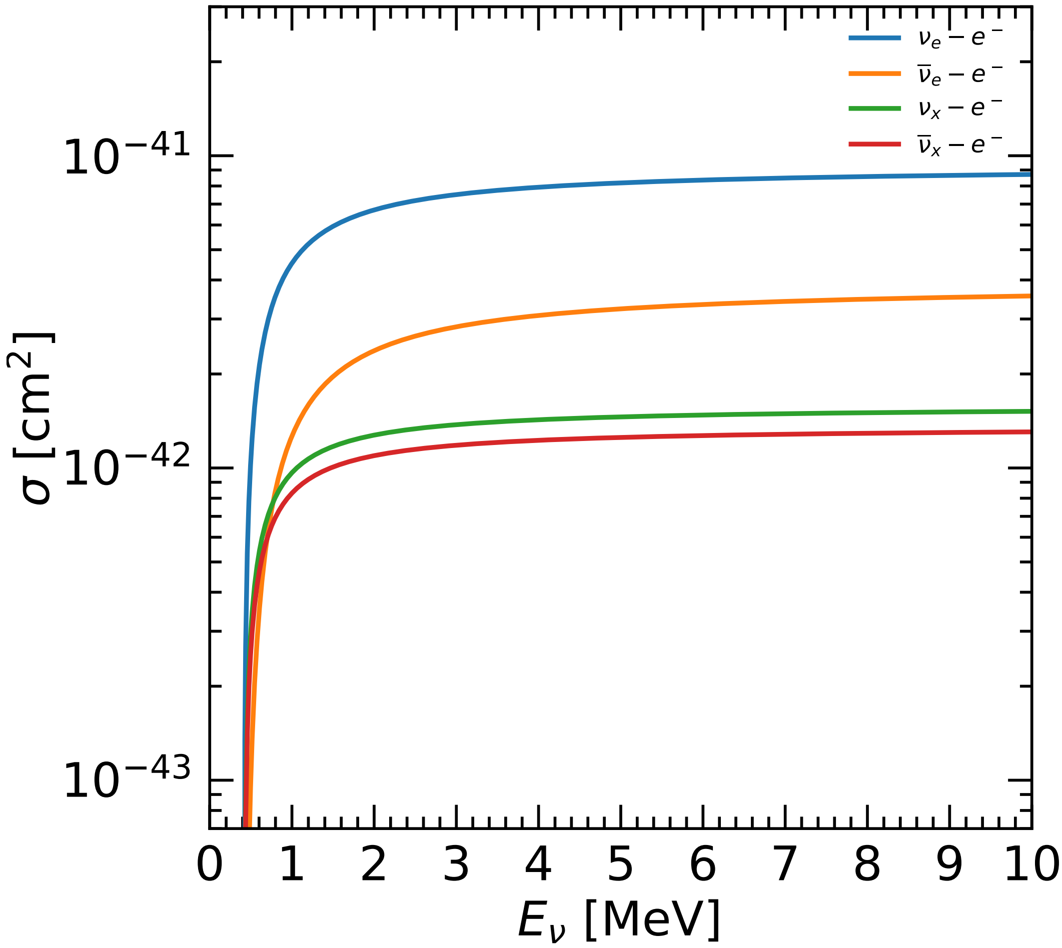


**Figure (1.3) :** Neutrino-lepton cross sections.

The factor in parentheses is equal to $(-1 + 2\sin^2\theta_W)^2 + (2\sin^2\theta_W)^2(1-y)^2$. Since $g_L^e = (g_V^e + g_A^e)/2$ and $g_L^e = (g_V^e - g_A^e)/2$, we see that in (1.98), the $\nu$ scattering on the left and right components of the electron add incoherently. However, the right part is suppressed by the factor $(1-y)^2$ that, when integrated over, gives a factor $1/3$. Numerically, $(-1 + 2\sin^2\theta_W)^2 + (2\sin^2\theta_W)^2/3 \sim 0.37$. The presence of the term $1-y = (1+\cos\theta)/2$ is related to the left-handed nature of the neutrino and the conservation of the angular momentum, as can be seen in Figure 1.4.

- The differential cross-section for the charged current scattering is

$$\frac{d\sigma^{CC}}{dy}(\nu_e e^- \to \nu_e e^-) = \frac{G_F^2 s}{4\pi} \,. \tag{1.99}$$

In this case, only $\nu_e$ can interact with electrons and the cross-section is isotropic. This is a consequence of the fact that only the left part of the electron is interacting with the neutrino, and the angular momentum is conserved, whatever the angle of the final electron.

- For the $\nu_e$ scattering, both the CC and NC diagrams contribute, and they must be taken into account at the same time The result of the calculation is

$$\frac{d\sigma^{CC+NC}}{dy}(\nu_e e^- \to \nu_e e^-) = \frac{G_F^2 s}{4\pi}\left[(g_V^e + g_A^e + 2)^2 + (g_V^e - g_A^e)^2(1-y)^2\right] \,, \tag{1.100}$$

so that the result is the same as the NC one, with the substitutions $g_V^e \to g_V^e + 1$ and $g_A^e \to g_A^e + 1$. Plugging into the cross sections the numbers, one obtains the suppression of a factor $\sim 0.16$ between the cross section $\nu_{\mu,\tau}e^- \to \nu_{\mu,\tau}e^-$ and $\nu_e e^- \to \nu_e e^-$.

- For the antineutrinos, the cross-section is suppressed with respect to the neutrino one. The crossing symmetry in the evaluation of a Feynman diagram, allows one to trade an incoming (outgoing) particle for an outgoing (incoming) antiparticle. Looking, for instance, at the right diagram of Figure 1.95, we see that this amounts to the change $p_1 \leftrightarrow -p_3$ and, therefore, to $s \leftrightarrow u$ in the matrix element. By exploiting the fact that the matrix element is proportional to $s^2$, we have the substitution

$$\frac{d\sigma^{CC}}{dy}(\nu_e e^- \to \nu_e e^-) = \frac{G_F^2 s^2}{4\pi s} \to \frac{d\sigma^{CC}}{dy}(\overline{\nu}_e e^- \to \overline{\nu}_e e^-) = \frac{G_F^2 u^2}{4\pi s} = \frac{G_F^2 s^2(1-y)^2}{4\pi} \,. \tag{1.101}$$

When the formula (1.101) is integrated over $y$, we find a suppression of 1/3 of the antineutrino cross-section. Strictly speaking, 1/3 is the suppression factor for energies larger than $m_e$ but smaller than the electroweak scale.

### 1.5.2 Neutrino-nucleon scattering

From the point of view of the neutrino detection, it also very important to know the neutrino-nucleon cross-section. In general, we have to consider both CC and NC interactions of neutrinos and antineutrinos hitting free nucleons or nucleons bounded in nuclei. This very last case is of fundamental importance for long-baseline oscillation neutrino experiments. Because of lepton flavor conservation, CC neutrino interaction will produce a negative charged lepton in the final state, while antineutrino interactions, instead, will produce positively charged leptons. To produce the lepton in the final state, neutrinos must posses energy above a threshold which, in the laboratory system, is

$$E_\nu > E_{\text{th}} = \frac{m_\ell^2 + 2Mm_\ell}{2M} \,. \tag{1.103}$$

For $\nu_e$, $E_{\text{th}} \sim 0$, while for $\nu_\mu$ and $\nu_\tau$ we found, respectively, $E_{\text{th}} \sim 0.11$ GeV and $\sim 3.5$ .eV. Equation (1.103) simply expresses the requirement $s = (E_\nu + M)^2 \gtrsim (m_\ell + M)^2$, where the right

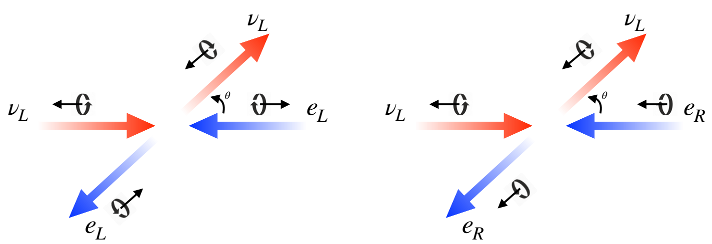


**Figure (1.4) :** The conservation of angular momentum in the $\nu e^-$ scattering suppresses backward scattering for right-handed electrons.

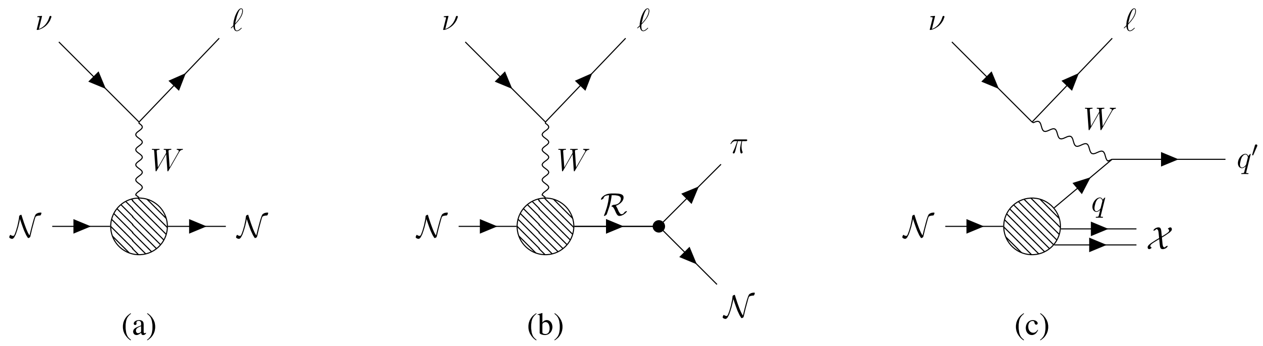


(1.102)

**Figure (1.5) :** Feynman diagrams for the scattering of neutrinos on electrons.

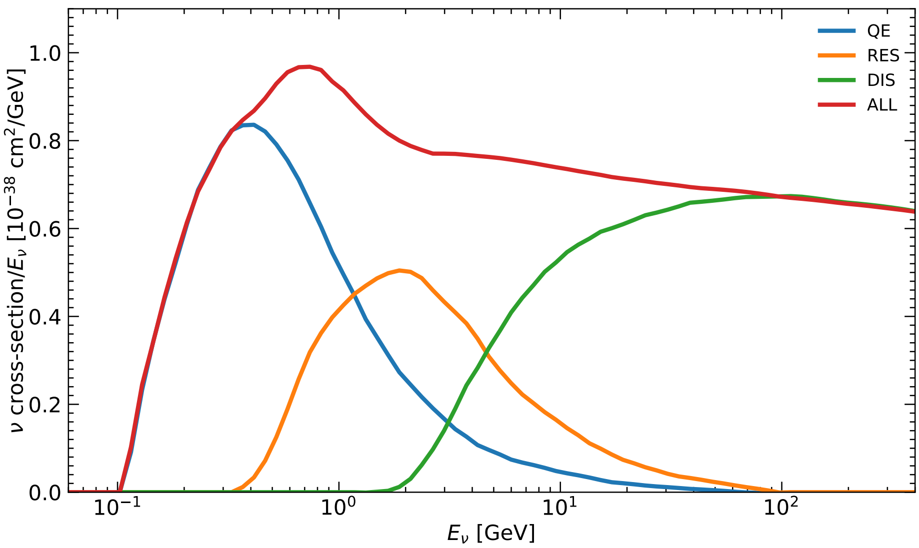


**Figure (1.6) :** Neutrino-Nucleon cross-section for Quasi-elastic (QE), Resonant (RES) and Deep Inhelastic Scattering (DIS) interactions..

side is the energy squared, in the case of negligible kinetic energy of the lepton and the nucleon in the final state. In the diagram (a) of Figure (1.5) one considers the quasi-elastic scattering neutrino-nucleon processes $\nu_e + n \to e^- + p$ and $\overline{\nu}_e + p \to e^+ + n$, also dubbed as inverse neutrino beta decay.

The name quasi-elastic comes from the fact that, by ignoring the proton-neutron mass difference and the electron mass, the process can be considered "elastic". In this case, the neutrino probe does not break up the nucleon. The relevant energies of the incoming neutrino are ranging from a few hundreds of MeV to a few G.V. With the increasing of the neutrino energy, the nucleon can be excited to a resonance, diagram (b) of Figure 1.5, for instance the $\Delta$, afterwords decaying in a pion and a nucleon. Also in this case, the energy of the neutrino ($\sim 1 - 10$ GeV) is not enough to break up the nucleon. Above around 10 GeV, diagram (c) of Figure 1.5, the neutrino starts to see the internal structure of the nucleon and the scattering breaks up it, producing a bunch of hadronic debris. The behavior of the $\nu\mathcal{N}$ cross-section is shown in Figure 1.6.

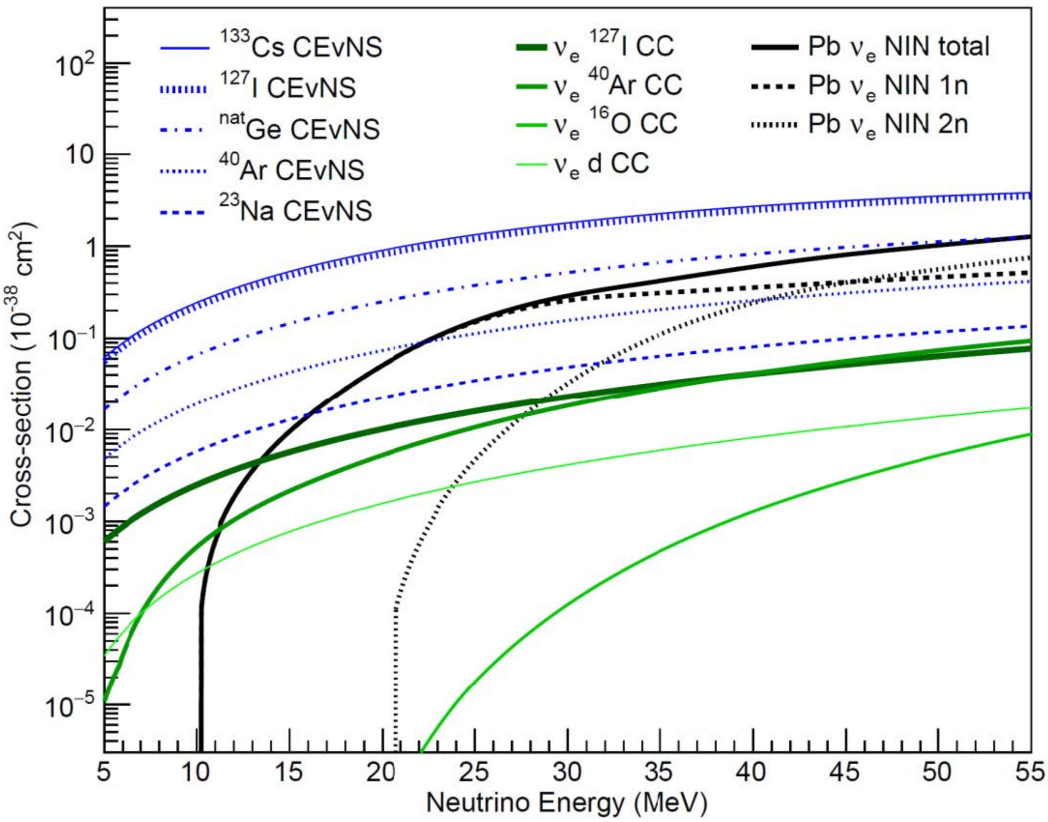


**Figure (1.7) :** Coherent neutrino scattering cross sections (from "New results from COHERENT", Daniel Pershey, Plenary Talk at Neutrino 2022).

### 1.5.3 Coherent Neutrino Scattering

Coherent neutrino scattering refers to a process in which a neutrino scatters off an entire atomic nucleus as a whole, rather than interacting with individual nucleons within the nucleus. More precisely, the Coherent Elastic Neutrino Nucleus Scattering (CE$\nu$NS) is the NC scattering of a neutrino with a nucleus, in which the nucleus is not excited but receives a small kick in the collision. The weak interaction can become "coherent" when the energy of the neutrino is very low and the size of the target nucleus is relatively large. In this situation, the entire nucleus can act as a single coherent target for the neutrino in the reaction $\nu + A \to \nu + A$. Coherent neutrino scattering is a relatively new field of research, with experiments designed to detect this process being conducted in recent years. It has the potential to provide new insights into the properties of neutrinos and the structure of atomic nuclei. The cross section is

$$\sigma_{\rm coh} \simeq \frac{G_F^2 M}{2\pi}\frac{Q_W^2}{4}F^2(q^2)\left(2 - \frac{MT}{E_\nu^2}\right) . \tag{1.104}$$

where $E_\nu$ is the energy of the incoming neutrino, $M$ is the mass of the target nucleus, $Q_W$ is the weak charge of the target nucleus, $F(q^2)$ is the nuclear form factor ($F = 1$ for full coherence), and $q^2$ is the momentum transfer squared. The weak charge of the nucleus, $Q_W = N-(1-4\sin^2\theta_W)Z$, depends on the neutron number $N$, so that $\sigma_{\rm coh} \sim N^2$, a large enhancement that makes it possible to measure this cross section. For instance, in Figure (1.7), you can see an enhancement of the total cross section of about 1 or 2 order of magnitude between the blue curves, for the coherent interactions, and the green and black ones for other interactions.

### 1.5.4 Neutrino Absorption

As you can see in Figures (1.6) and (1.7), the order of magnitude of the neutrino cross sections in matter is of the order of $10^{-38}$ cm$^2$. Actually, this result can be obtained with a simple order of magnitude estimation. On dimensional ground,

$$\sigma \sim G_F^2 s \,, \tag{1.105}$$

since the matrix element is proportional to the Fermi constant $G_F$, that has dimension of inverse energy squared, and $s$ is the energy available for the reaction. If we evaluate in the target rest system the total energy, we get

$$s = [(M,0) + (E, E\vec{u})]^2 = M^2 + 2ME \sim 2ME \,, \tag{1.106}$$

where $M$ is the target mass, $E$ the neutrino energy, and we assume $ME \gg M^2$. Therefore, we have

$$\begin{aligned} \sigma \sim G_F^2 s \sim \frac{G_F^2}{\text{GeV}^{-4}} \text{GeV}^{-4} \left(\frac{ME}{\text{GeV}^2}\right) \text{GeV}^2 = 10^{-10} \left(\frac{ME}{\text{GeV}^2}\right) \frac{(197 \text{ MeV fm})^2}{\text{GeV}^2} \sim \\ \sim 10^{-10} \left(\frac{ME}{\text{GeV}^2}\right) 10^4\, 10^{-6}\, 10^{-26} \text{ cm}^2 \sim 10^{-38} \left(\frac{ME}{\text{GeV}^2}\right) \text{cm}^2 \,. \end{aligned} \tag{1.107}$$

The neutrino mean free path can be estimated as

$$\ell \sim \frac{1}{n\sigma} \,, \tag{1.108}$$

where $n$ is the target number density. In ordinary matter, $n \sim N_A \sim 10^{24}$ cm$^{-3}$, so that $n\sigma \sim 10^{-14}$ cm$^{-1}$. Therefore, a neutrino of energy of $\sim 1$ GeV has a mean free path of the order of $10^9$ km. The mean free path is of the order of the Earth diameter when the neutrino energy is $\sim 10^5$ GeV. Inside a forming neutron star, the number density can be as high as $10^{12} N_A$ cm$^{-3}$, so that MeV neutrinos will have a mean free path of the order of one kilometer or so.

# 2 Neutrino Oscillations

As we saw in the previous section, neutrino mass and flavor eigenstates do not coincide. The immediate consequence of this fact is the phenomenon of the neutrino oscillations: when neutrinos are produced, they are flavor eigenstates, the eigenstates of the weak interaction; when they propagate in vacuum, the states with definite momenta are the mass eigenstates. These two bases are related to each other by the mixing matrix $U$: if $U$ is not trivial, the mass eigenstates will develop different phases during their propagation and, at the detection point, their superposition will no longer be equal to the initial one. Thus, there will be a non-zero probability of detecting a neutrino with flavor different from the initial one.

## 2.1 Neutrino Oscillations in vacuum

A generic unitary $3 \times 3$ matrix can be parametrized by means of 3 mixing angles $(\theta_{12}, \theta_{13}, \theta_{23})$ and one phase $\delta$, (see C.2). The standard parametrization for $U$ is

$$\begin{aligned} U &= R_{23}(\theta_{23}) \varGamma_\delta R_{13}(\theta_{13}) \varGamma_\delta^\dagger R_{12}(\theta_{12}) = \\ &= \begin{pmatrix} c_{12}c_{13} & s_{12}c_{13} & s_{13}e^{-i\delta} \\ -s_{12}c_{23} - c_{12}s_{23}s_{13}e^{i\delta} & c_{12}c_{23} - s_{12}s_{23}s_{13}e^{i\delta} & s_{23}c_{13} \\ s_{12}s_{23} - c_{12}c_{23}s_{13}e^{i\delta} & -c_{12}s_{23} - s_{12}c_{23}s_{13}e^{i\delta} & c_{23}c_{13} \end{pmatrix} , \end{aligned} \tag{2.1}$$

where $c_{ij} = \cos\theta_{ij}$ and $s_{ij} = \sin\theta_{ij}$ and

$$\begin{aligned} R_{23}(\theta_{23}) &= \begin{pmatrix} 1 & 0 & 0 \\ 0 & \cos\theta_{23} & \sin\theta_{23} \\ 0 & -\sin\theta_{23} & \cos\theta_{23} \end{pmatrix} , \\ R_{13}(\theta_{13}, \delta) &= \begin{pmatrix} \cos\theta_{13} & 0 & \sin\theta_{13}e^{-i\delta} \\ 0 & 1 & 0 \\ -\sin\theta_{13}e^{i\delta} & 0 & \cos\theta_{13} \end{pmatrix} , \\ R_{12}(\theta_{12}) &= \begin{pmatrix} \cos\theta_{12} & \sin\theta_{12} & 0 \\ -\sin\theta_{12} & \cos\theta_{12} & 0 \\ 0 & 0 & 1 \end{pmatrix} , \\ \varGamma_\delta &= \mathrm{diag}(0, 0, e^{i\delta}) . \end{aligned} \tag{2.2}$$

The three $R_{23}$, $R_{13}$ and $R_{12}$ matrices are ordinary 3-dimensional rotations. As we will see, $\varGamma_\delta$ is related to CP-violating transitions. Note that this is just one of the possible ways to parameterize the mixing matrix. The rotation matrices are defined in such a way that the mixing angles are real, and defined in the intervals $[0, \pi/2]$. The CP-violating phase may vary in the range $\delta \in [0, 2\pi]$. Let us consider the mixing of the three known active neutrino states $|\nu_\alpha\rangle$, with $\alpha = e, \mu, \tau$. Flavor neutrino states are a superposition of mass eigenstates, weighted by the $U^*$ matrix

$$|\nu_\alpha\rangle = \sum_{i=1}^{3} U^*_{\alpha i} |\nu_i\rangle , \tag{2.3}$$

and, conversely, multiplying by $U_{\alpha j}$ and summing over $\alpha$

$$\sum_\alpha U_{\alpha j} |\nu_\alpha\rangle = \sum_{i,\alpha} U_{\alpha j} U^\dagger_{i\alpha} |\nu_i\rangle = \sum_i \delta_{ij} |\nu_i\rangle = |\nu_j\rangle . \tag{2.4}$$

The presence of $U^*$ in equation (2.3) is due to the fact that a neutrino in the initial states corresponds to the filed $\overline{\nu}$. However, if you consider a generic states $|\nu\rangle$ as a superposition of the flavor or the mass eigenstates in terms of its components $\nu^\alpha$ or $\nu^i$, respectively:

$$
\begin{aligned}
|\nu\rangle &= \sum_{i=1}^{3} (|\nu_i\rangle \langle\nu_i|)\,|\nu\rangle = \sum_{i=1}^{3} \langle\nu_i|\nu\rangle\,|\nu_i\rangle = \sum_{i=1}^{3} \nu^i\,|\nu_i\rangle \ , \\
|\nu\rangle &= \sum_{\alpha=e,\mu,\tau} (|\nu_\alpha\rangle \langle\nu_\alpha|)\,|\nu\rangle = \sum_{\alpha=e,\mu,\tau} \langle\nu_\alpha|\nu\rangle\,|\nu_\alpha\rangle = \sum_{\alpha=e,\mu,\tau} \nu^\alpha\,|\nu_\alpha\rangle
\end{aligned}
\tag{2.5}
$$

.

The components transform with $U$, like the fields. In fact

$$
\begin{aligned}
&|\nu\rangle = \sum_{\alpha=e,\mu,\tau} \nu^\alpha\,|\nu_\alpha\rangle = \sum_{\alpha=e,\mu,\tau} \nu^\alpha \sum_{i=1}^{3} U^*_{\alpha i}\,|\nu_i\rangle = \sum_{j=1}^{3} \nu^j\,|\nu_j\rangle \Rightarrow \\
&\nu^i = \sum_{\alpha=e,\mu,\tau} U^*_{\alpha i}\nu^\alpha \ , \quad \nu^\alpha = \sum_{i=1}^{3} U_{\alpha i}\nu^i \ .
\end{aligned}
\tag{2.6}
$$

We want to describe a process in which neutrino of flavor $\alpha$ is produced at time $t = 0$, and it is detected at time $t$ as a neutrino of flavor $\beta$. We suppose that the neutrino is ultrarelativistic. This means that for each neutrino $\nu_i$, the energy $E_i$ can be approximated as

$$
E_i = \sqrt{p_i^2 + m_i^2} = p_i\sqrt{1 + m_i^2/p_i^2} \sim p_i(1 + m_i^2/2p_i^2) \sim p + m_i^2/2E \ , \tag{2.7}
$$

where, in the last equality, we assume $p_i \sim E_i \sim p \sim E$ for all mass eigenstates, neglecting a quantity proportional to the tiny squared mass $m_i^2$. Moreover, to the same order we replace the time $t$ with the neutrino path $L$. The amplitude for the $\nu_\alpha \to \nu_\beta$ transition to happen is $\langle\nu_\beta|\nu_\alpha(t)\rangle$ and the probability is

$$
\begin{aligned}
P(\nu_\alpha \to \nu_\beta) &= |\langle\nu_\beta|\nu_\alpha(L)\rangle|^2 = \left|\sum_{ij} U_{\beta j} U^*_{\alpha i}\,\langle\nu_j|\nu_i(L)\rangle\right|^2 = \left|\sum_{ij} U_{\beta j} U^*_{\alpha i}\,\langle\nu_j|e^{-iE_iL}\nu_i\rangle\right|^2 = \\
&= \left|\sum_{ij} U_{\beta j} U^*_{\alpha i} e^{-ip_iL(1+m_i^2)/2E_i^2}\delta_{ij}\right|^2 = \left|\sum_{i} U_{\beta i} U^*_{\alpha i} e^{-ipL(1+m_i^2L)/2E}\right|^2 = \\
&= \left|e^{-ipL}\sum_{i} U_{\beta i} U^*_{\alpha i} e^{-iLm_i^2/2E}\right|^2 = \sum_{ij} U_{\beta i} U^*_{\alpha i} e^{-iLm_i^2/2E} U^*_{\beta j} U_{\alpha j} e^{iLm_j^2/2E} = \\
&= \sum_{ij} U^*_{\alpha i} U_{\beta i} U_{\alpha j} U^*_{\beta j} e^{-iL(m_i^2-m_j^2)/2E} = \sum_{ij} U^*_{\alpha i} U_{\beta i} U_{\alpha j} U^*_{\beta j} e^{-iL\Delta m_{ij}^2/2E} \ ,
\end{aligned}
\tag{2.8}
$$

where we have introduced the squared-mass differences $\Delta m_{ij}^2 = m_i^2 - m_j^2$. This is the general formula for the neutrino oscillation in three generations in vacuum. This formula can be written in three different ways:

$$\begin{aligned} P(\nu_\alpha \to \nu_\beta) &= \sum_{ij} U^*_{\alpha i} U_{\beta i} U_{\alpha j} U^*_{\beta j} e^{-iL\Delta m^2_{ij}/2E} \\ &= \sum_i |U_{\alpha i}|^2 |U_{\beta i}|^2 + 2\sum_{i>j} U^*_{\alpha i} U_{\beta i} U_{\alpha j} U^*_{\beta j} e^{-iL\Delta m^2_{ij}/2E} \\ &= \delta_{\alpha\beta} - 2\sum_{i>j} \mathrm{Re}(U^*_{\alpha i} U_{\beta i} U_{\alpha j} U^*_{\beta j}) \left(1 - \cos\frac{\Delta m^2_{ij} L}{2E}\right) + \\ &\quad + 2\sum_{i>j} \mathrm{Im}(U^*_{\alpha i} U_{\beta i} U_{\alpha j} U^*_{\beta j}) \sin\frac{\Delta m^2_{ij} L}{2E} \ . \end{aligned} \tag{2.9}$$

The second expression for $P_{\alpha\beta}(L, E)$ comes simply from separating in the double sum the cases $i = j$ from $i \neq j$, and from the observation of the symmetry in $i$ and $j$ of the product of the four mixing matrix elements. The third formula of (2.9) can be easily demonstrated by squaring the unitary condition

$$\sum_i U_{\alpha i} U^*_{\beta i} = \delta_{\alpha\beta} \ , \tag{2.10}$$

from which we get

$$\begin{aligned} &\left(\sum_i U_{\alpha i} U^*_{\beta i}\right)^2 = \sum_i U_{\alpha i} U^*_{\beta i} \sum_k U_{\alpha k} U^*_{\beta k} = \sum_{i=k} U_{\alpha i} U^*_{\beta i} U_{\alpha k} U^*_{\beta k} + 2\sum_{i>k} U_{\alpha i} U^*_{\beta i} U_{\alpha k} U^*_{\beta k} = \\ &= \sum_{i=k} |U_{\alpha i}|^2 |U_{\beta i}|^2 + 2\sum_{i>k} \mathrm{Re}\left(U_{\alpha i} U^*_{\beta i} U_{\alpha k} U^*_{\beta k}\right) \ . \end{aligned} \tag{2.11}$$

Going back to equations (2.9), we see that the neutrino vacuum oscillation probability depends on the squared-mass differences, on the $\nu$ path length, and on the $\nu$ energy. The mixing matrix elements $U_{\alpha i}$ are new parameters for the model that will extend the SM, so to include neutrino masses. If the generic $U_{\alpha i}$ is rephased as $e^{i\theta_\alpha} U_{\alpha i} e^{i\theta_i}$, then the product $U^*_{\alpha i} U_{\beta i} U_{\alpha j} U^*_{\beta j}$ will turn into itself:

$$U^*_{\alpha i} U_{\beta i} U_{\alpha j} U^*_{\beta j} \to e^{-i\theta_\alpha} U^*_{\alpha i} e^{-i\theta_i} e^{i\theta_\beta} U_{\beta i} e^{i\theta_i} e^{i\theta_\alpha} U_{\alpha j} e^{i\theta_j} e^{-i\theta_\beta} U^*_{\beta j} e^{-i\theta_j} = U^*_{\alpha i} U_{\beta i} U_{\alpha j} U^*_{\beta j} \ . \tag{2.12}$$

Thanks to this invariance property, it is possible to rephase charged lepton and neutrino fields. In the case of Majorana neutrinos, the mixing matrix $U$ of equation (2.1) will contain two additional phases

$$U_{\mathrm{Majorana}} = U\ \mathrm{Diag}(1, e^{i\phi_1}, e^{i\phi_2}) \ , \tag{2.13}$$

but the oscillation probability (2.9) will not depend on $\phi_1$ and $\phi_2$. The vacuum oscillation probability for antineutrinos can be obtained from (2.9), with the substitution $U \to U^*$. The vacuum oscillation probability is CPT-invariant, $P(\nu_\alpha \to \nu_\beta) = P(\overline{\nu_\beta} \to \overline{\nu_\alpha})$, while the CP-violating term can be written as

$$\begin{aligned} P(\nu_\alpha \to \nu_\beta) - P(\overline{\nu_\alpha} \to \overline{\nu_\beta}) &= 4\sum_{i>j} \mathrm{Im}(U^*_{\alpha i} U_{\beta i} U_{\alpha j} U^*_{\beta j}) \sin^2\frac{\Delta m^2_{ij} L}{2E} = , \\ &= 4\sum_{i>j} J^{ij}_{\alpha\beta} \sin\frac{\Delta m^2_{ij} L}{2E} \ , \end{aligned} \tag{2.14}$$

where

$$J^{ij}_{\alpha\beta} = U^*_{\alpha i} U_{\beta i} U_{\alpha j} U^*_{\beta j} \; , \tag{2.15}$$

is called the Jarlskog invariant that vanishes for $\delta = 0, \pi$, while is maximal for $\delta = \pi/2, 3\pi/2$.

The derivation of the oscillation probability was not rigorous, but a complete treatment in quantum field theory gives the same results. However, a few remarks are in order: First of all, the formula (2.9) is valid if the different contributions of mass eigenstates at the production and detection point can be ignored, as it is in all real experiments. Moreover, the removal of the equal momentum assumption, i.e. the fact that we assumed all neutrinos to have the same momentum $p$, does not alter the final result. Finally, also a rigorous treatment, without the assumption $t = L$, does not change the final result. Oscillations are a quantum process that requires coherence. Thanks to their very weak interactions, neutrinos can maintain coherence over very long distances. Moreover, both at the creation and detection points, the mass eigenstates wave packets must not be distinguishable and a coherent flavor superposition must be possible. Consider, for instance, the case where the neutrino momentum is measured with very high precision so that the uncertainty on the neutrino mass is smaller than the mass gap between two neutrinos:

$$\delta m^2 = \frac{\partial m^2}{\partial p} \delta p = 2p\delta p \ll \Delta m^2 \; . \tag{2.16}$$

From the Heisenberg principle we derive the error on the position determination

$$\delta x \gtrsim \frac{1}{\delta p} \sim \frac{2E}{\Delta m^2} \sim \frac{L_0}{2\pi} \; , \tag{2.17}$$

where $L_0$ is the oscillation length (see (2.22)). Therefore the uncertainty on $x$ is of the order of the oscillation length, and oscillations will be destroyed: the flavor eigenstates becomes an incoherent sum of mass eigenstates. Another possibility that will destroy the oscillation pattern is realized when the separation between the neutrino wave packets becomes so large that the two packets no longer overlap and their interference is not possible anymore. Summarizing, the wave packet formalism allows one to see that oscillations are possible if the momentum is not too well determined, so that there can be a transition from one mass eigenstate to the other, and the two wave packets are not separated with respect to their size.

### 2.1.1 Neutrino Oscillations in vacuum: two generations

To understand the behavior of the oscillation probability it is better to study the formula for two neutrino generations. In this case, the mixing matrix only depends on one mixing angle, and there is no phase. $U$ is simply a rotation matrix in the plane by an angle $\theta$:

$$U = \begin{pmatrix} \cos\theta & \sin\theta \\ -\sin\theta & \cos\theta \end{pmatrix} \; . \tag{2.18}$$

If we call the two flavor $e$ and $\mu$, then we have

$$\begin{aligned} P(\nu_e \to \nu_\mu) &= -2U_{e2}U_{\mu 2}U_{e1}U_{\mu 1}\left(1 - \cos\frac{\Delta m^2_{12} L}{2E}\right) = 2\sin^2\theta\cos^2\theta \cdot 2\sin^2\frac{\Delta m^2 L}{4E} = \\ &= \sin^2 2\theta \sin^2\frac{\Delta m^2 L}{4E} \; . \end{aligned} \tag{2.19}$$

where we have denoted with $\Delta m^2$ the squared-mass difference $\Delta m^2_{21} = m_2^2 - m_1^2$. First of all, let us calculate the numerical factor hidden in equation (2.19):

$$\begin{aligned}\frac{\Delta m^2 L}{4E} &= \frac{\Delta m^2}{\text{eV}^2}\ \text{eV}^2 \frac{L}{\text{km}}\ \text{km} \frac{1}{4\frac{E}{\text{GeV}}\text{GeV}} = \\ &= \frac{\left(\frac{\Delta m^2}{\text{eV}^2}\right)\left(\frac{L}{\text{km}}\right)}{\left(\frac{E}{\text{GeV}}\right)} \frac{\text{eV m}}{4\ 10^6} \frac{1}{197\ \text{MeV fm}} = 1.27\, \frac{\left(\frac{\Delta m^2}{\text{eV}^2}\right)\left(\frac{L}{\text{km}}\right)}{\left(\frac{E}{\text{GeV}}\right)} = \\ &= 1.27\, \frac{\left(\frac{\Delta m^2}{\text{eV}^2}\right)\left(\frac{L}{\text{m}}\right)}{\left(\frac{E}{\text{MeV}}\right)}\ .\end{aligned} \tag{2.20}$$

Therefore, we can rewrite (2.19) as

$$\begin{aligned}P_{e\mu} &= \sin^2 2\theta\ \sin^2 \frac{\Delta m^2 L}{4E} = \\ &= \sin^2 2\theta\ \sin^2 \left[1.27\, \frac{\left(\frac{\Delta m^2}{\text{eV}^2}\right)\left(\frac{L}{\text{km}}\right)}{\left(\frac{E}{\text{GeV}}\right)}\right]\ .\end{aligned} \tag{2.21}$$

When we speak of neutrino oscillations, we mean oscillations in space, depending on the traveled distance $L$, or oscillations in the energy $E$, when the distance is fixed. In the first case, the oscillation length is

$$L_0 = \pi \frac{4E}{\Delta m^2} = \frac{\pi}{1.27} \frac{\left(\frac{E}{\text{GeV}}\right)}{\left(\frac{\Delta m^2}{\text{eV}^2}\right)}\ . \tag{2.22}$$

Let's make two examples that are relevant for atmospheric and solar neutrinos that we will discuss later. In the first case, we can consider $E \sim 1$ GeV, $\Delta m^2 \sim 2.5 \times 10^{-3}$ eV$^2$ and we obtain $L_0 \sim 990$ km. In the second case, the one relevant for solar neutrinos, with energy $E \sim 1$ MeV, $\Delta m^2 \sim 7.5 \times 10^{-5}$, the oscillation length is $L_0 \sim 32$ km. The oscillation probability (2.21) is invariant under the transformations $\theta \to \theta - \pi/4$ and $\Delta m^2 \to -\Delta m^2$. The amplitude of the oscillations is $\sin^2 2\theta$. If we mediate the probability over many oscillation cycles, then we get a factor one half from the sine squared:

$$P_{e\mu}^{\text{ave}} = \frac{1}{2} \sin^2 2\theta\ . \tag{2.23}$$

If the distance traveled by a neutrino is very large, then the neutrino flavor state will be an incoherent sum of mass eigenstate and viceversa. Therefore, $P_{ee} = P_{e1}P_{1e} + P_{e2}P_{2e} = \cos^2\theta\cos^2\theta + \sin^2\theta\sin^2\theta = \cos^4\theta + \sin^4\theta = (\cos^2\theta + \sin^2\theta)^2 - 2\sin^2\theta\cos^2\theta = 1 - 1/2\sin^2 2\theta$, where we have denoted with $P_{i\alpha}$ and $P_{i\alpha}$ the probability of detecting $\nu_\alpha$ as a $\nu_i$ and viceversa. Similarly, , $P_{e\mu} = P_{e1}P_{1\mu} + P_{e2}P_{2\mu} = \cos^2\theta\sin^2\theta + \sin^2\theta\cos^2\theta = 2\cos^2\theta\sin^2\theta = 1 - P_{ee}$. Thus, we see that the probabilities for averaged oscillations and for complete decoherence are equal, for two neutrino generations.

**Vacuum Neutrino Oscillations**

- In the three-generation neutrino framework, the mixing matrix $U$ depends on three mixing angle $(\theta_{12}, \theta_{13}, \theta_{23})$ and one phase $\delta$, and can be parametrized by means of three rotation matrices as $U = R_{23}(\theta_{23})\mathit{\Gamma}_\delta R_{13}(\theta_{13})\mathit{\Gamma}_\delta^\dagger R_{12}(\theta_{12})$ and $\mathit{\Gamma}_\delta = \mathrm{diag}(1, 1, e^{i\delta})$
- In the three-generation neutrino framework, the mixing matrix $U$ depends on three mixing angle $(\theta_{12}, \theta_{13}, \theta_{23})$ and one phase $\delta$, and can be parametrized by means of three rotation matrices as $U = R_{23}(\theta_{23})\mathit{\Gamma}_\delta R_{13}(\theta_{13})\mathit{\Gamma}_\delta^\dagger R_{12}(\theta_{12})$;
- $U$ is the matrix connecting flavor and mass eigenstates through $|\nu_\alpha\rangle = \sum_{i=1}^{3} U^*_{\alpha i} |\nu_i\rangle$;
- The vacuum oscillation probability can be written as

$$P(\nu_\alpha \to \nu_\beta) = \sum_{ij} U^*_{\alpha i} U_{\beta i} U_{\alpha j} U^*_{\beta j} e^{-iL\Delta m^2_{ij}/2E} \; ; \tag{2.24}$$

- If neutrinos are Majorana particles then $U_{\mathrm{Majorana}} = U \; \mathrm{diag}(1, e^{i\phi_1}, e^{i\phi_2})$, but the oscillation probability formula does not change;
- In the case of two neutrino generations

$$P_{e\mu} = \sin^2 2\theta \; \sin^2 \frac{\Delta m^2 L}{4E} = \sin^2 2\theta \; \sin^2 \left[ 1.27 \, \frac{\left(\frac{\Delta m^2}{\mathrm{eV}^2}\right)\left(\frac{L}{\mathrm{km}}\right)}{\left(\frac{E}{\mathrm{GeV}}\right)} \right] \tag{2.25}$$

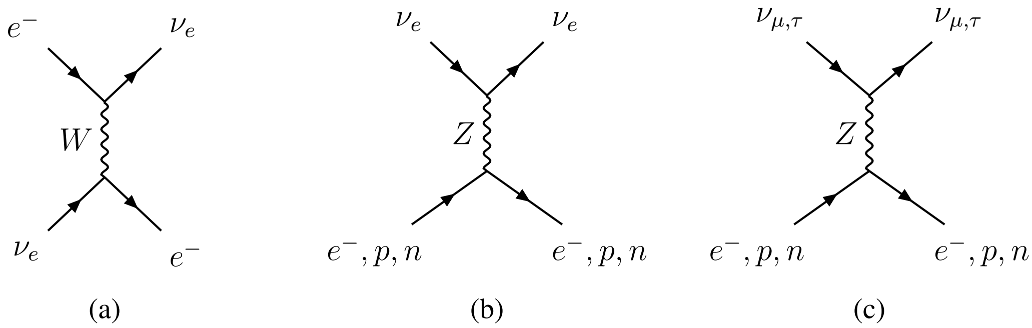


**Figure (2.1) :** Feynman diagrams for the scattering of neutrinos in matter.

## 2.2 Neutrino Oscillations in Matter

As we have seen in Section 1.5, when neutrinos propagate through matter, for instance through the Earth, they interact with electrons and nucleons. Their interaction can be mediated by the $W$ and the $Z$ boson, as shown in Figure (2.1). When neutrinos interact with electrons, both charged and neutral current interactions are possible. Moreover, the scattering can be incoherent or coherent. A simple estimate shows that in most cases incoherent scattering is very small and can be neglected. From the four-fermion interaction, we expect the incoherent cross section to be proportional to the Fermi constant $G_F$ squared. As we saw in section (1.5.4), we expect $\sigma \sim G_F^2 s$, where $s$ is the center-of-mass energy squared. If we assume, for instance, that a nucleon of mass $M = 1$ GeV, at rest in the laboratory frame, scatters a neutrino of energy $E$, then $\sigma \sim 3.9 \times 10^{-38} \mathrm{cm}^2 (E/\mathrm{GeV})$. If we multiply a cross-section of the order of $10^{-38}$ cm$^2$ by the target number density $n$, for instance of the Earth, $n \sim 3.3$ gr cm$^{-3}$, then we get the mean free path

$$L \sim \frac{1}{N_A n \sigma} \sim \frac{10^{14}}{E/\mathrm{GeV}}\ \mathrm{cm}\ , \tag{2.26}$$

where we assumed there are $\sim N_A$ scattering centers of mass $M = 1$ GeV per gram.

The smallness of the weak cross-section can be compensated by coherent scattering when neutrinos propagate in matter, the so-called "coherent forward elastic scattering". Here forward elastic scattering means that the momentum of neutrinos is unchanged and that there is a change of the phases in the wave function. When the scattering is happening coherently on all the particles of the medium, the net effect is an enhancement of the cross-section by a factor $n$, so that this process can result in a sizable effect. To calculate the effective hamiltonian for this process, let us start from the charged current interaction term in the Fermi theory:

$$\mathcal{H}_{cc} = \frac{G_F}{\sqrt{2}} \left[\overline{\nu_e}\gamma_\mu(1-\gamma_5)e\right] \left[\overline{e}\gamma^\mu(1-\gamma_5)e\right]\ , \tag{2.27}$$

which is the tree level contribution in the low-energy case, when the momentum is much lower than the $W$ or $Z$ boson mass. After rearranging the fields through a Fierz transformation, we get

$$\mathcal{H}_{cc} = \frac{G_F}{\sqrt{2}} \left[\overline{e}\gamma_\mu(1-\gamma_5)e\right] \left[\overline{\nu_e}\gamma^\mu(1-\gamma_5)\nu_e\right]\ . \tag{2.28}$$

We need to make an average of this interaction hamiltonian over the medium, i.e. the part depending on electron fields. To do so, we consider the rest frame of the medium and a distribution function $f(E,T)$ which counts the density of electrons with given energy $E$, momentum $p$ and temperature $T$, normalized so that

$$\int d^3p\, f(E,T) = N_e V \ , \tag{2.29}$$

where $N_e$ is the number of electrons contained in the volume $V$. To calculate the average over the medium, we have to integrate over momenta, and sum up over spin, the matrix element of $\mathcal{H}_{cc}$ between the states of the electron $|e(p,s)\rangle$:

$$\begin{aligned} |e\rangle &= |e(p,s)\rangle = \frac{1}{2EV} b^\dagger(p,s)\,|0\rangle \ , \\ \langle \mathcal{H}_{cc}\rangle &= \frac{G_F}{\sqrt{2}} \overline{\nu_e}\gamma_\mu(1-\gamma_5)\nu_e \int d^3p \frac{1}{2}\sum_{\text{spin}} \langle e|\,\overline{e}\gamma^\mu(1-\gamma_5)e\,|e\rangle \ . \end{aligned} \tag{2.30}$$

When the field $e$ and $\overline{e}$ hit the state $|e\rangle$ on the left or $\langle e|$ on the right, they give the spinors $u$ or $\overline{u}$ times a normalization constant depending on the convention adopted.[8] The sum over the spin of the spinor product $u\overline{u}$ gives

$$\sum_{\text{spins}} u_e(p,s)\overline{u}_e(p,s) = \not{p} + m_e \ , \tag{2.31}$$

and the result is

$$\begin{aligned} &\frac{1}{2}\sum_{\text{spin}} \langle e|\,\overline{e}\gamma^\mu(1-\gamma_5)e\,|e\rangle = \frac{1}{4EV}\mathrm{Tr}[(\not{p}+m_e)\gamma^\mu(1-\gamma_5)] = \\ &= \frac{1}{4EV}\mathrm{Tr}(\not{p}\gamma^\mu - m_e\gamma^\mu\gamma_5) = \frac{1}{4EV}\mathrm{Tr}(\not{p}\gamma^\mu) = \frac{p^\mu}{EV} \ . \end{aligned} \tag{2.32}$$

Going back to the hamiltonian we have

$$\begin{aligned} \langle \mathcal{H}_{cc}\rangle &= \frac{G_F}{\sqrt{2}\,V}\int d^3p f(E,T)\overline{\nu_e}\gamma_\mu(1-\gamma_5)\nu_e\,\frac{p^\mu}{E} = \frac{G_F}{\sqrt{2}\,V}\int d^3p f(E,T)\overline{\nu_e}\gamma^0\,2\,\nu_{eL}\,\frac{p^0}{E} = \\ &= \sqrt{2}G_F N_e\,\overline{\nu_L}\gamma^0\nu_{eL} = V_{CC}\,\overline{\nu_{eL}}\gamma^0\nu_{eL} \ , \end{aligned} \tag{2.33}$$

where the potential $V_{CC} = \sqrt{2}G_F N_e$ has been introduced and the vector part depending on $\vec{p}$ of the integral is zero, because the integrand function is odd. It can be shown that formula (2.33) changes the potential energy of the neutrino by the amount $V_{CC}$.

In a similar way, one can show that, for the neutral current scattering over a fermion $f$, the result is $V_{NC}^f = \sqrt{2}G_F N_f g_V^f$, since in the expression (2.28) for the hamiltonian, the part relative to the fermion will change according to the substitution $1-\gamma^5 \to g_V^f - g_A^f\gamma^5$. Taking into account

[8] Here we follow the convention of [3].

that $g_V^f = I_3 - Q\sin^2\theta_W$, we have explicitly

$$\begin{aligned} g_V^e &= -\frac{1}{2} + \sin^2\theta_W \ , \\ g_V^u &= +\frac{1}{2} + \frac{2}{3}\sin^2\theta_W \ , \\ g_V^d &= -\frac{1}{2} - \frac{1}{3}\sin^2\theta_W \ , \\ g_V^p &= +\frac{1}{2} + \sin^2\theta_W \ , \\ g_V^n &= -\frac{1}{2} \ . \end{aligned} \tag{2.34}$$

Since matter is usually neutral, the neutral-current potential is

$$V_{NC} = -\frac{1}{2}\sqrt{2}G_F N_n \ . \tag{2.35}$$

With this result, the general matter potential can now be written as

$$\boxed{V_\alpha = V_{CC}\delta_{\alpha e} + V_{NC} = \sqrt{2}G_F\left(N_e\delta_{\alpha e} - \tfrac{1}{2}N_n\right)} \ . \tag{2.36}$$

Now, the task is to derive the flavor evolution equation in the presence of the matter potential (2.36). The evolution of a given flavor state $|\nu_\alpha(t)\rangle$ is governed by the full hamiltonian containing the vacuum term $\mathcal{H}_0$ and the matter term $\mathcal{H}_I = V_\alpha$. The meaning of the $\alpha$ subscript is that at $t = 0$ we impose $|\nu(0)\rangle = \nu_\alpha$. The evolution equation is

$$i\frac{d}{dt}|\nu_\alpha(t)\rangle = \mathcal{H}|\nu_\alpha(t)\rangle = (\mathcal{H}_0 + \mathcal{H}_I)|\nu_\alpha(t)\rangle \ . \tag{2.37}$$

The free hamiltonian is diagonal in the mass basis $(\nu_1, \nu_2, \nu_3)^T$, so that $\mathcal{H}_0|\nu_i\rangle = E_i|\nu_i\rangle$ or, in matrix notation,

$$\mathcal{H}_0^{\mathrm{d}} = \begin{pmatrix} E_1 & 0 & 0 \\ 0 & E_2 & 0 \\ 0 & 0 & E_3 \end{pmatrix} \ , \tag{2.38}$$

while the interaction term is diagonal in the flavor basis

$$\mathcal{H}_I|\nu_\alpha\rangle = V_\alpha|\nu_\alpha\rangle \ . \tag{2.39}$$

To find the oscillation probabilities we will proceed in a way similar to that of the vacuum oscillations. The probability amplitude $\mathcal{A}_{\alpha\beta}(t)$ of finding the state in the flavor $\beta$ at the time $t$ is

$$\mathcal{A}_{\alpha\beta}(t) = \langle\beta|\nu_\alpha(t)\rangle \ . \tag{2.40}$$

These amplitudes are none other than the components of equations (2.5). By projecting equation (2.37) on $\langle\beta|$ we have

$$\begin{aligned} i\frac{d}{dt}\mathcal{A}_{\alpha\beta}(t) &= \langle\beta|\mathcal{H}|\nu_\alpha(t)\rangle = \langle\beta|\mathcal{H}_0|\nu_\alpha(t)\rangle + \langle\beta|\mathcal{H}_I|\nu_\alpha(t)\rangle = \\ &= \sum_\gamma \langle\beta|\mathcal{H}_0|\gamma\rangle\langle\gamma|\nu_\alpha(t)\rangle + \sum_\gamma \langle\beta|\mathcal{H}_I|\gamma\rangle\langle\gamma|\nu_\alpha(t)\rangle = \\ &= (\mathcal{H}_0)_{\beta\gamma}\mathcal{A}_{\gamma\alpha}(t) + (\mathcal{H}_I)_{\beta\gamma}\mathcal{A}_{\gamma\alpha}(t) \ . \end{aligned} \tag{2.41}$$

The matrix elements of $\mathcal{H}$ in (2.41) are calculated in the flavor basis, and, as anticipated before, only $\mathcal{H}_I$ is diagonal in that basis

$$\langle\beta|\mathcal{H}_I|\gamma\rangle = V_\gamma \langle\beta|\gamma\rangle = V_\gamma \delta_{\beta\gamma} \, . \tag{2.42}$$

For the free hamiltonian part, by taking into account that from (2.3) we get $\langle j|\alpha\rangle = U^*_{\alpha \mathrm{j}}$, we can evaluate the matrix element as

$$(\mathcal{H}_0)_{\beta\gamma} = \langle\beta|\mathcal{H}_0|\gamma\rangle = \sum_{ij} \langle\beta|i\rangle \langle i|\mathcal{H}_0|j\rangle \langle j|\gamma\rangle = \sum_{ij} U_{\beta i}\mathcal{H}^{\mathrm{d}}_{ij}U^*_{\gamma j} = (U\mathcal{H}^{\mathrm{d}}U^\dagger)_{\beta\gamma} \, . \tag{2.43}$$

Before proceeding, we observe that also in this case, as in (2.7), for ultrarelativistic neutrinos we can use the approximation $E_i \sim p + m_i^2/2E$, and in matrix notation

$$\begin{aligned}\mathcal{H}^{\mathrm{d}}_0 = \begin{pmatrix} E_1 & 0 & 0 \\ 0 & E_2 & 0 \\ 0 & 0 & E_3 \end{pmatrix} \sim \begin{pmatrix} p + \dfrac{m_1^2}{2E} & 0 & 0 \\ 0 & p + \dfrac{m_2^2}{2E} & 0 \\ 0 & 0 & p + \dfrac{m_3^2}{2E} \end{pmatrix} = \\ = \left(p + \frac{m_1^2}{2E}\right) I + \begin{pmatrix} 0 & 0 & 0 \\ 0 & \dfrac{\Delta m^2_{21}}{2E} & 0 \\ 0 & 0 & \dfrac{\Delta m^2_{31}}{2E} \end{pmatrix} \, .\end{aligned} \tag{2.44}$$

We can write the matter potential in matrix notation, in the flavor basis, with an explicit possible dependence on the position $x$

$$\begin{aligned} V = \begin{pmatrix} V_e & 0 & 0 \\ 0 & V_\mu & 0 \\ 0 & 0 & V_\tau \end{pmatrix} = V_{NC}(x) I + \begin{pmatrix} V_{CC}(x) & 0 & 0 \\ 0 & 0 & 0 \\ 0 & 0 & 0 \end{pmatrix} = \\ = V_{NC}(x) I + \begin{pmatrix} \sqrt{2}G_F N_e(x) & 0 & 0 \\ 0 & 0 & 0 \\ 0 & 0 & 0 \end{pmatrix} \, . \end{aligned} \tag{2.45}$$

If we introduce the vector

$$\mathcal{A}_\alpha = \begin{pmatrix} \mathcal{A}_{\alpha e} & \mathcal{A}_{\alpha\mu} & \mathcal{A}_{\alpha\tau} \end{pmatrix} \, , \tag{2.46}$$

and replace $t$ with $x$, we can rewrite equation (2.41) as

$$\begin{aligned} i\frac{d}{dx}\mathcal{A}_\alpha(x) = (U\mathcal{H}^{\mathrm{d}}U^\dagger + V)\mathcal{A}_\alpha(x) = \left(p + \frac{m_1^2}{2E} + V_{NC}\right)\mathcal{A}_\alpha(x) + \\ + \begin{pmatrix} \sqrt{2}G_F N_e(x) & 0 & 0 \\ 0 & \dfrac{\Delta m^2_{21}}{2E} & 0 \\ 0 & 0 & \dfrac{\Delta m^2_{31}}{2E} \end{pmatrix} \mathcal{A}_\alpha \, . \end{aligned} \tag{2.47}$$

We can easily convince ourselves that the first term of (2.47) is irrelevant to the oscillations, since the redefinition

$$\mathcal{A}_\alpha(x) \to \mathcal{A}'_\alpha(x) = \mathcal{A}_\alpha(x)\, e^{-i\left(p+\frac{m_1^2}{2E}\right)x - i\int_0^x V_{NC}(x')dx'} \,, \tag{2.48}$$

will make it disappear from the right-hand side of (2.47). In fact, with this substitution we have

$$\begin{aligned} i\frac{d}{dx}\mathcal{A}'_\alpha = {} & i\left(\frac{d}{dt}\mathcal{A}_\alpha\right) e^{-i\left(p+\frac{m_1^2}{2E}\right)x - i\int_0^x V_{NC}(x')dx'} + \\ & + \mathcal{A}_\alpha\left(p+\frac{m_1^2}{2E}+V_{NC}(x)\right) e^{-i\left(p+\frac{m_1^2}{2E}\right)x - i\int_0^x V_{NC}(x')dx'} \,, \end{aligned} \tag{2.49}$$

and, by using equation (2.47), we find that the evolution equation for $\mathcal{A}'_\alpha$ does not contain anymore the term proportional to the identity matrix. From now on, we will refer to $\mathcal{A}'_\alpha$, without the prime and the transformation (2.48) will be implicit. Finally, if we introduce the two matrices

$$M = \begin{pmatrix} 0 & 0 & 0 \\ 0 & \Delta m^2_{21} & 0 \\ 0 & 0 & \Delta m^2_{31} \end{pmatrix} \,, \qquad A = \begin{pmatrix} 2\sqrt{2}G_F E N_e(x) & 0 & 0 \\ 0 & 0 & 0 \\ 0 & 0 & 0 \end{pmatrix} \,. \tag{2.50}$$

The evolution equation is then written as

$$i\frac{d}{dx}\mathcal{A}_\alpha(x) = \frac{1}{2E}(UMU^\dagger + A)\mathcal{A}_\alpha(x) = \mathcal{H}_\mathrm{f}\mathcal{A}_\alpha(x) \,, \tag{2.51}$$

where, to describe neutrino oscillations in matter, the hamiltonian $\mathcal{H}_\mathrm{f}$ in the flavor basis has been introduced

$$\mathcal{H}_\mathrm{f} = \frac{1}{2E}(UMU^\dagger + A) \,. \tag{2.52}$$

The explicit form of $\mathcal{H}_\mathrm{f}$, confirms once again that the neutrino oscillations depend on the squared-mass differences and not on absolute masses. When the matter potential depends on $x$, in general, the full solution of equation (2.52) must be computed numerically. Analytical solutions exist in a few cases, for analytical matter profiles, and, in particular, for constant matter density.

### 2.2.1 Two-flavor neutrino oscillations in matter: constant density

Let us consider the mixing of two neutrinos, $\nu_e$ and $\nu_\mu$, for constant density matter, $N_e(x) = N_e$. We define $A_{CC} = 2\sqrt{2}G_F E N_e$, so that the flavor evolution equation is

$$\begin{aligned} i\frac{d}{dx}\begin{pmatrix}\mathcal{A}_{ee}\\ \mathcal{A}_{e\mu}\end{pmatrix} &= \frac{1}{2E}\left[\begin{pmatrix}\cos\theta & \sin\theta \\ -\sin\theta & \cos\theta\end{pmatrix}\begin{pmatrix}0 & 0 \\ 0 & \Delta m^2\end{pmatrix}\begin{pmatrix}\cos\theta & -\sin\theta \\ \sin\theta & \cos\theta\end{pmatrix} + \begin{pmatrix}A_{CC} & 0 \\ 0 & 0\end{pmatrix}\right]\begin{pmatrix}\mathcal{A}_{ee}\\ \mathcal{A}_{e\mu}\end{pmatrix} = \\ &= \frac{1}{2E}\begin{pmatrix}\Delta m^2\sin^2\theta + A_{CC} & \sin\theta\cos\theta\Delta m^2 \\ \sin\theta\cos\theta\Delta m^2 & \Delta m^2\cos^2\theta\end{pmatrix}\begin{pmatrix}\mathcal{A}_{ee}\\ \mathcal{A}_{e\mu}\end{pmatrix} = \\ &= \frac{1}{2E}\begin{pmatrix}\Delta m^2(\frac{1}{2}-\cos 2\theta) + A_{CC} & \frac{1}{2}\sin 2\theta\Delta m^2 \\ \frac{1}{2}\sin 2\theta\Delta m^2 & \Delta m^2(\frac{1}{2}+\cos 2\theta)\end{pmatrix}\begin{pmatrix}\mathcal{A}_{ee}\\ \mathcal{A}_{e\mu}\end{pmatrix} = \\ &= \frac{\Delta m^2 + A_{CC}}{4E}\begin{pmatrix}\mathcal{A}_{ee}\\ \mathcal{A}_{e\mu}\end{pmatrix} + \frac{1}{4E}\begin{pmatrix}-\Delta m^2\cos 2\theta + A_{CC} & \Delta m^2\sin 2\theta \\ \Delta m^2\sin 2\theta & \Delta m^2\cos 2\theta - A_{CC}\end{pmatrix}\begin{pmatrix}\mathcal{A}_{ee}\\ \mathcal{A}_{e\mu}\end{pmatrix} \,. \end{aligned} \tag{2.53}$$

As we have done before, we disregard the first term on the right-hand side of (2.53), that is irrelevant for the oscillations, and we finally rewrite

$$i\frac{d}{dx}\begin{pmatrix}\mathcal{A}_{ee}\\ \mathcal{A}_{e\mu}\end{pmatrix} = \mathcal{H}_{\rm f}\begin{pmatrix}\mathcal{A}_{ee}\\ \mathcal{A}_{e\mu}\end{pmatrix} ,$$
$$\mathcal{H}_{\rm f} = \frac{1}{4E}\begin{pmatrix}-\Delta m^2\cos 2\theta + A_{CC} & \Delta m^2 \sin 2\theta \\ \Delta m^2\sin 2\theta & \Delta m^2\cos 2\theta - A_{CC}\end{pmatrix} . \tag{2.54}$$

The matter hamiltonian in the flavor basis can be diagonalized through an orthogonal (unitary) transformation, since it is real and symmetric:

$$U_{\rm m} = \begin{pmatrix}\cos\theta_{\rm m} & \sin\theta_{\rm m}\\ -\sin\theta_{\rm m} & \cos\theta_{\rm m}\end{pmatrix} ,$$
$$U_{\rm m}\mathcal{H}_{\rm f}U_{\rm m}^T = \frac{1}{4E}\begin{pmatrix}-\Delta m^2_{\rm m} & 0\\ 0 & \Delta m^2_{\rm m}\end{pmatrix} = \mathcal{H}_{\rm d} . \tag{2.55}$$

with

$$\Delta m^2_{\rm m} = \sqrt{(\Delta m^2\cos 2\theta - A_{CC})^2 + (\Delta m^2 \sin 2\theta)^2} ,$$
$$\tan 2\theta_{\rm m} = \frac{\tan 2\theta}{1-\dfrac{A_{CC}}{\Delta m^2\cos 2\theta}} . \tag{2.56}$$

In particular we have

$$\sin 2\theta_{\rm m} = \frac{\sin 2\theta}{\sqrt{\left(\cos 2\theta - A_{CC}/\Delta m^2\right)^2 + \sin^2 2\theta}} ,$$
$$\cos 2\theta_{\rm m} = \frac{\cos 2\theta - A_{CC}/\Delta m^2}{\sqrt{\left(\cos 2\theta - A_{CC}/\Delta m^2\right)^2 + \sin^2 2\theta}} , \tag{2.57}$$

What we have obtained implies that the neutrino propagation in a medium with constant electron density can be studied exactly as the vacuum case, provided we use the matter mixing angle $\theta_{\rm m}$ and the matter squared-mass difference $\theta_{\rm m}$. In fact, the evolution equation for the oscillation amplitudes is

$$i\frac{d}{dx}\begin{pmatrix}\mathcal{A}_{ee}\\ \mathcal{A}_{e\mu}\end{pmatrix} = U_{\rm m}\mathcal{H}_{\rm d}U_{\rm m}^T\begin{pmatrix}\mathcal{A}_{ee}\\ \mathcal{A}_{e\mu}\end{pmatrix} \Rightarrow i\frac{d}{dx}U_{\rm m}^T\begin{pmatrix}\mathcal{A}_{ee}\\ \mathcal{A}_{e\mu}\end{pmatrix} = \mathcal{H}_{\rm d}U_{\rm m}^T\begin{pmatrix}\mathcal{A}_{ee}\\ \mathcal{A}_{e\mu}\end{pmatrix} \Rightarrow$$
$$i\frac{d}{dx}\begin{pmatrix}\mathcal{A}^{\rm m}_{ee}\\ \mathcal{A}^{\rm m}_{e\mu}\end{pmatrix} = \mathcal{H}_{\rm d}\begin{pmatrix}\mathcal{A}^{\rm m}_{ee}\\ \mathcal{A}^{\rm m}_{e\mu}\end{pmatrix} = \frac{1}{4E}\begin{pmatrix}-\Delta m^2_{\rm m} & 0\\ 0 & \Delta m^2_{\rm m}\end{pmatrix}\begin{pmatrix}\mathcal{A}^{\rm m}_{ee}\\ \mathcal{A}^{\rm m}_{e\mu}\end{pmatrix} . \tag{2.58}$$

were $(\mathcal{A}^{\rm m}_{ee}, \mathcal{A}^{\rm m}_{e\mu})$ are the oscillation amplitudes for the matter eigenstates, defined by the rotation $|\nu_\alpha\rangle = (U_{\rm m})_{\alpha i}\,|i\rangle$. Since $\mathcal{H}_{\rm d}$ is diagonal, the time evolution of $(\mathcal{A}^{\rm m}_{ee}, \mathcal{A}^{\rm m}_{e\mu})$ is simple:

$$\mathcal{A}^{\rm m}_{ee}(x) = \mathcal{A}^{\rm m}_{ee}(0)e^{i\frac{\Delta m^2_{\rm m}x}{4E}}$$
$$\mathcal{A}^{\rm m}_{e\mu}(x) = \mathcal{A}^{\rm m}_{ee}(0)e^{-i\frac{\Delta m^2_{\rm m}x}{4E}} \tag{2.59}$$

Flavor and mass amplitudes are related through the rotation $U_{\rm m}$ and thus

$$\begin{pmatrix}\mathcal{A}_{ee}(x)\\ \mathcal{A}_{e\mu}(x)\end{pmatrix} = \begin{pmatrix}\cos\theta_{\rm m} & \sin\theta_{\rm m}\\ -\sin\theta_{\rm m} & \cos\theta_{\rm m}\end{pmatrix}\begin{pmatrix}\mathcal{A}^{\rm m}_{ee}(x)\\ \mathcal{A}^{\rm m}_{e\mu}(x)\ .\end{pmatrix} \tag{2.60}$$

If, for instance, the initial state is an electron neutrino, i.e. $(\mathcal{A}_{ee}(0), \mathcal{A}_{e\mu}(0)) = (1, 0)$, for the matter initial amplitudes we will have $(\mathcal{A}^{\rm m}_{ee}(0), \mathcal{A}^{\rm m}_{e\mu}(0)) = (\cos\theta_{\rm m}, \sin\theta_{\rm m})$, Therefore, for $\mathcal{A}_{ee}(x)$ we obtain

$$\begin{aligned}\mathcal{A}_{ee}(x) &= \cos\theta_{\rm m}\mathcal{A}^{\rm m}_{ee}(x) + \sin\theta_{\rm m}\mathcal{A}^{\rm m}_{e\mu}(x) =\\ &= \cos\theta_{\rm m}\mathcal{A}^{\rm m}_{ee}(0)e^{i\frac{\Delta m^2_{\rm m}x}{4E}} + \sin\theta_{\rm m}\mathcal{A}^{\rm m}_{e\mu}(0)e^{-i\frac{\Delta m^2_{\rm m}x}{4E}} =\\ &= \cos^2\theta_{\rm m}e^{i\frac{\Delta m^2_{\rm m}x}{4E}} + \sin^2\theta_{\rm m}e^{-i\frac{\Delta m^2_{\rm m}x}{4E}}\ .\end{aligned} \tag{2.61}$$

For the probability the result is

$$\begin{aligned}P_{ee} = |\mathcal{A}_{ee}(x)|^2 &= \left(\cos^2\theta_{\rm m}e^{i\frac{\Delta m^2_{\rm m}x}{4E}} + \sin^2\theta_{\rm m}e^{-i\frac{\Delta m^2_{\rm m}x}{4E}}\right)\cdot\\ &\left(\cos^2\theta_{\rm m}e^{-i\frac{\Delta m^2_{\rm m}x}{4E}} + \sin^2\theta_{\rm m}e^{i\frac{\Delta m^2_{\rm m}x}{4E}}\right) =\\ &= \cos^4\theta_{\rm m} + \sin^4\theta_{\rm m} + \sin^2\theta_{\rm m}\cos^2\theta_{\rm m}\left(e^{i\frac{\Delta m^2_{\rm m}x}{2E}} + e^{-i\frac{\Delta m^2_{\rm m}x}{2E}}\right) =\\ &= \cos^4\theta_{\rm m} + \sin^4\theta_{\rm m} + 2\cos\frac{\Delta m^2_{\rm m}x}{2E}\sin^2\theta_{\rm m}\cos^2\theta_{\rm m} =\\ &= 1 - 2\sin^2\theta_{\rm m}\cos^2\theta_{\rm m} + 2\cos\frac{\Delta m^2_{\rm m}x}{2E}\sin^2\theta_{\rm m}\cos^2\theta_{\rm m} =\\ &= 1 - 2\sin^2\theta_{\rm m}\cos^2\theta_{\rm m}\left(1-\cos\frac{\Delta m^2_{\rm m}x}{4E}\right) = 1 - \sin^2 2\theta_{\rm m}\sin^2\frac{\Delta m^2_{\rm m}x}{4E}\ .\end{aligned} \tag{2.62}$$

From an explicit calculation or, more simply, from the probability conservation we obtain

$$P_{e\mu} = 1 - P_{ee} = \sin^2 2\theta_{\rm m}\sin^2\frac{\Delta m^2_{\rm m}x}{4E}\ . \tag{2.63}$$

Going back to (2.56), we see that

$$\theta_{\rm m} \to \pm\frac{\pi}{4} \quad \text{when} \quad \frac{A_{CC}}{\Delta m^2\cos 2\theta} \to \mp 1\ . \tag{2.64}$$

When $\theta_{\rm m} \to \pm\pi/4$, we say that the mixing is maximal, because the amplitude of the oscillations is maximal ($\sin 2\theta_{\rm m} = 1$), even if the vacuum mixing angle is small. This resonance phenomenon is called the Mikheyev–Smirnov–Wolfenstein (MSW) effect. Note that for neutrinos ($A_{CC} > 0$) the resonance can happen for $\theta < \pi/4$, while for antineutrinos ($A_{CC} < 0$) the vacuum mixing must be in the second octant, $\theta > \pi/4$. Note also that when the resonance condition $A_{CC} = \Delta m^2 \cos 2\theta$ is satisfied, the diagonal elements of the $\mathcal{H}_{\rm f}$ are equal to zero, in accordance with the fact that the oscillation probability amplitude is maximal. Finally, at the resonance, the matter mass squared difference is minimal.

As we will see, matter effects give rise to many interesting consequences for neutrino oscillations, but before we proceed, it is better to take a step back a to summarize in simple terms what we have done.

### 2.2.2 Two-flavor neutrino oscillations in matter: varying density

Let us rewrite equations (2.54) and (2.56), that we have derived to study the neutrino propagation in constant matter density

$$\begin{aligned}
\mathcal{H}_{\rm f} &= \frac{1}{4E}\begin{pmatrix} -\Delta m^2 \cos 2\theta + A_{CC} & \Delta m^2 \sin 2\theta \\ \Delta m^2 \sin 2\theta & \Delta m^2 \cos 2\theta - A_{CC} \end{pmatrix} \\
\Delta m^2_{\rm m} &= \sqrt{(\Delta m^2 \cos 2\theta - A_{CC})^2 + (\Delta m^2 \sin 2\theta)^2}\,, \\
\tan^2 2\theta_{\rm m} &= \frac{\tan 2\theta}{1 - \dfrac{A_{CC}}{\Delta m^2 \cos 2\theta}}\,.
\end{aligned} \tag{2.65}$$

The flavor hamiltonian is connected to the matter mass diagonal hamiltonian through the rotation $U_{\rm m}$:

$$\begin{aligned}
& U_{\rm m}\mathcal{H}_{\rm f}U_{\rm m}^T = \frac{1}{4E}\begin{pmatrix} -\Delta m^2_{\rm m} & 0 \\ 0 & \Delta m^2_{\rm m} \end{pmatrix} = \mathcal{H}_{\rm d} \Rightarrow \mathcal{H}_{\rm f} = U_{\rm m}^T \mathcal{H}_{\rm d} U_{\rm m} = \\
& = \frac{1}{4E}\begin{pmatrix} \cos\theta_{\rm n} & -\sin\theta_{\rm n} \\ \sin\theta_{\rm m} & \cos\theta_{\rm m} \end{pmatrix}\begin{pmatrix} -\Delta m^2_{\rm m} & 0 \\ 0 & \Delta m^2_{\rm m} \end{pmatrix}\begin{pmatrix} \cos\theta_{\rm n} & \sin\theta_{\rm n} \\ -\sin\theta_{\rm m} & \cos\theta_{\rm m} \end{pmatrix} = \\
& = \begin{pmatrix} -\Delta m^2_{\rm m}\cos 2\theta_{\rm n} & \Delta m^2_{\rm m}\sin 2\theta_{\rm n} \\ \Delta m^2_{\rm m}\sin 2\theta_{\rm m} & \Delta m^2_{\rm m}\cos 2\theta_{\rm m} \end{pmatrix}\,.
\end{aligned} \tag{2.66}$$

On one side, it is always possible to numerically solve equation (2.51) with the hamiltonian (2.66), when $A_{CC}$ depends on $x$. On the other side, we can study the evolution of the mass eigenstates in matter by changing basis in equation (2.51) as we have done before, but by taking into account, this time, that also the matrix elements of $U_{\rm m}$ depends on $x$:

$$\begin{aligned}
& i\frac{d}{dx}\begin{pmatrix} \mathcal{A}_{ee} \\ \mathcal{A}_{e\mu} \end{pmatrix} = U_{\rm m}\mathcal{H}_{\rm d}U_{\rm m}^T \begin{pmatrix} \mathcal{A}_{ee} \\ \mathcal{A}_{e\mu} \end{pmatrix} \Rightarrow i\frac{d}{dx}\left[U_{\rm m}\begin{pmatrix} \mathcal{A}^{\rm m}_{ee} \\ \mathcal{A}^{\rm m}_{e\mu} \end{pmatrix}\right] = U_{\rm m}\mathcal{H}_{\rm d}\begin{pmatrix} \mathcal{A}^{\rm m}_{ee} \\ \mathcal{A}^{\rm m}_{e\mu} \end{pmatrix} \Rightarrow \\
& i\frac{dU_{\rm m}}{dx}\begin{pmatrix} \mathcal{A}^{\rm m}_{ee} \\ \mathcal{A}^{\rm m}_{e\mu} \end{pmatrix} + U_{\rm m} i\frac{d}{dx}\begin{pmatrix} \mathcal{A}^{\rm m}_{ee} \\ \mathcal{A}^{\rm m}_{e\mu} \end{pmatrix} = U_{\rm m}\mathcal{H}_{\rm d}\begin{pmatrix} \mathcal{A}^{\rm m}_{ee} \\ \mathcal{A}^{\rm m}_{e\mu} \end{pmatrix}\,.
\end{aligned} \tag{2.67}$$

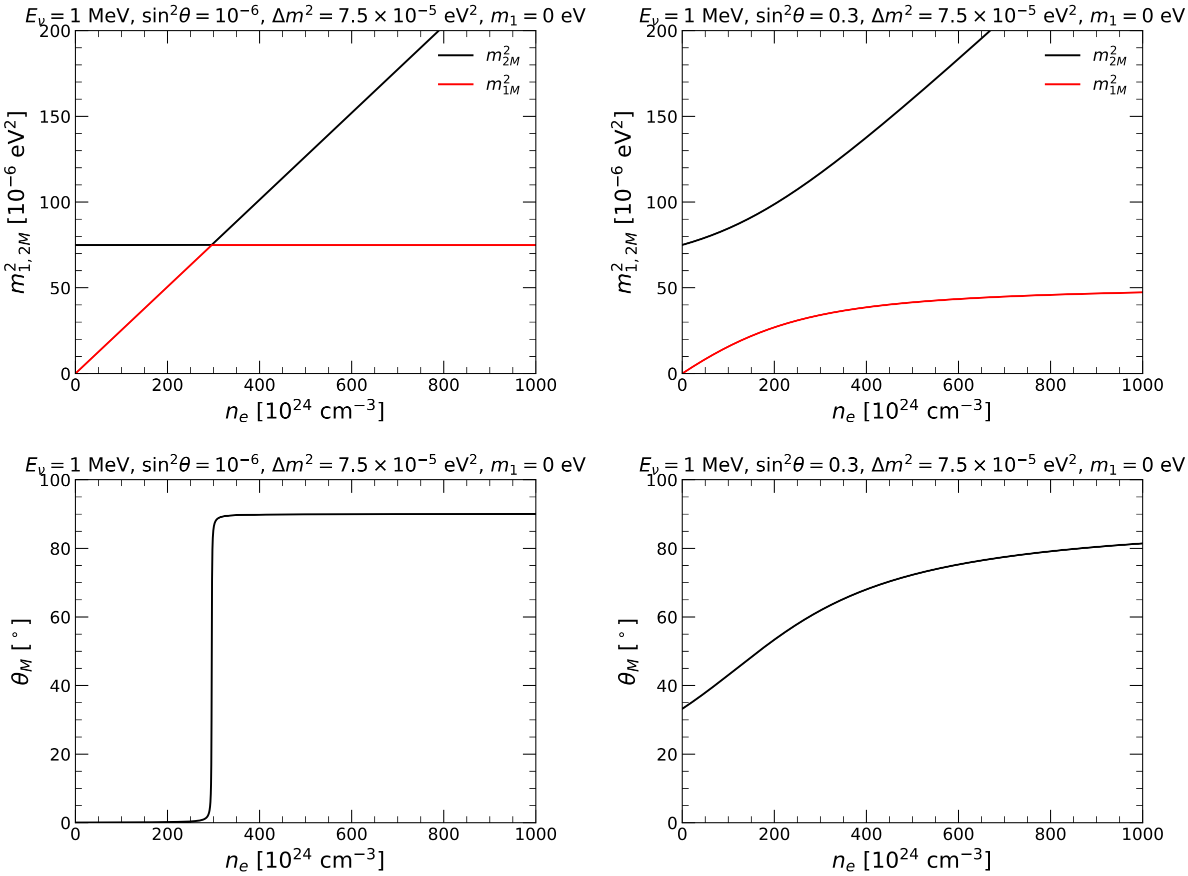


**Figure (2.2) :** Effective mixing angle (bottom) and mass eigenstates (up) in matter, as a function of the electron density $n_e$

Multiplying both sides of the equation (2.67) by $U_{\rm m}^T$, we have

$$
\begin{aligned}
&i\frac{d}{dx}\begin{pmatrix}\mathcal{A}^{\rm m}_{ee}\\ \mathcal{A}^{\rm m}_{e\mu}\end{pmatrix} = \mathcal{H}_{\rm d}\begin{pmatrix}\mathcal{A}^{\rm m}_{ee}\\ \mathcal{A}^{\rm m}_{e\mu}\end{pmatrix} - iU_{\rm m}^T\frac{dU_{\rm m}}{dx}\begin{pmatrix}\mathcal{A}^{\rm m}_{ee}\\ \mathcal{A}^{\rm m}_{e\mu}\end{pmatrix} = \\
&= \left[\frac{1}{4E}\begin{pmatrix}-\Delta m^2_{\rm m} & 0\\ 0 & \Delta m^2_{\rm m}\end{pmatrix} - i\begin{pmatrix}0 & d\theta_{\rm m}/dx\\ d\theta_{\rm m}/dx & 0\end{pmatrix}\right]\begin{pmatrix}\mathcal{A}^{\rm m}_{ee}\\ \mathcal{A}^{\rm m}_{e\mu}\end{pmatrix} \; .
\end{aligned} \tag{2.68}
$$

Finally, we can write

$$
\boxed{i\frac{d}{dx}\begin{pmatrix}\mathcal{A}^{\rm m}_{ee}\\ \mathcal{A}^{\rm m}_{e\mu}\end{pmatrix} = \frac{1}{4E}\begin{pmatrix}-\Delta m^2_{\rm m} & -4iEd\theta_{\rm m}/dx\\ -4iEd\theta_{\rm m}/dx & \Delta m^2_{\rm m}\end{pmatrix}\begin{pmatrix}\mathcal{A}^{\rm m}_{ee}\\ \mathcal{A}^{\rm m}_{e\mu}\end{pmatrix} \; .} \tag{2.69}
$$

If the electron density depends on $x$ the off diagonal terms in (2.69) must be taken into account. Explicitly, we find by a direct calculation

$$\frac{d\theta_{\rm m}}{dx} = \frac{\Delta m^2 \sin 2\theta A'_{CC(x)}}{(\Delta m^2)^2 + A_{CC}(x)^2 - 2\Delta m^2 A_{CC}(x)\cos 2\theta} \ . \tag{2.70}$$

With the help of the formula

$$\sin 2\theta \Delta m^2 = \sin 2\theta_{\rm m} \Delta m^2_{\rm m} \ , \tag{2.71}$$

equation (2.70) can also be written as

$$\frac{d\theta_{\rm m}}{dx} = \frac{1}{2}\frac{\sin 2\theta_{\rm m}}{\Delta m^2_{\rm m}}\frac{dA_{CC}}{dx} \ . \tag{2.72}$$

The off-diagonal terms of (2.69) will induce oscillations between the neutrino matter eigenstates, $\nu_{1\rm m} \leftrightarrow \nu_{2\rm m}$. However, if the adiabaticity parameter $\gamma$, the ratio of off-diagonal to diagonal terms is small,

$$\gamma = \frac{\Delta m^2_{\rm m}}{4Ed|\theta_{\rm m}/dx}| \ll 1 \ , \tag{2.73}$$

then, during the propagation in matter, $\nu_{1m}$ and $\nu_{2m}$ evolve separately, adiabatically. This is, for instance, the case of solar neutrinos. Figure 2.2 shows an example of the adiabatic evolution of mass eigenstates and of the matter effective mixing angle, when the electron density changes. Nonadiabatic transitions can happen only around the resonance with a probability $P_c$ that depends on the matter potential profile, and can be calculated, for instance, with the Landau-Zener formula:

$$P_c = 1 - \exp\left(-\frac{\pi\Delta^2}{E}\right) \ , \tag{2.74}$$

where $\Delta$ is the energy difference between the two mass eigenstates at the resonance and $E$ is the neutrino energy. In the case of solar neutrinos, when the neutrino energy $E \gtrsim$ few MeV we know that the evolution is adiabatic. The two-generation oscillations, neglecting $\theta_{13}$, depend on $(\theta_{12}, \delta m^2)$. Neutrinos are produced inside the Sun, where the density is very high and $A_{CC}/\delta m^2 \gtrsim 1$, so that from (2.57) we get $\theta_{\rm m12} \simeq \pi/2$, and the initial neutrino state $\nu_e^{\rm in} = \nu_{\rm m2}$. The adiabatic evolution implies that, when neutrinos reaches the surface of the Sun, the final state is still a $\nu_2$, but now in vacuum. The probability $P(\nu_e \to \nu_e) = \sin^2\theta_{12}$ is the probability of "finding" a $\nu_e$ in a $\nu_2$. When $E \lesssim$ few MeV, from (2.57) one has $\theta_{\rm m12} \simeq \theta_{12}$, at the production point and $\nu_e^{\rm in} = \cos\theta_{12}\nu_{\rm m1} + \sin\theta_{12}\nu_{\rm m2}$. Afterwards, the mass eigenstates evolve adiabatically, and at the Sun surface $\theta_{\rm m12} = \theta_{12}$. Since the oscillation length is much smaller than the path, we can assume kinematic decoherence by averaging out the interference terms, so that when leaving the sum the probability of having a $\nu_1$ is $\cos^2\theta_{12}$, the probability of having a $\nu_2$ is $\sin^2\theta_{12}$. By taking into account the probability of finding a $\nu_e$ in the mass eigenstates, one has $P(\nu_e \to \nu_e) = \cos^4\theta_{12} + \sin^4\theta_{12} = 1 - 1/2\sin^2\theta_{12}$.

**Neutrino Oscillations in Matter**

- We saw that the neutrino coherent forward scattering on matter particle, for instance electrons, of density $N_e(x)$, will generate an additional potential $V_\alpha$, to be added to the free hamiltonian of a propagating $\nu_\alpha$;
- For neutrino scattering on ordinary matter, the only term that matters is $V_e = \sqrt{2}G_F N_e(x)$;
- We have written the flavor evolution equation for the oscillation amplitudes and found that their evolution is governed by the vacuum hamiltonian $UMU^\dagger/2E$, plus a flavor diagonal term for the $ee$ matrix element that $A_{CC}/2E = V_e$;
- We have considered later the simplest case of constant density matter $N_e(x) = N_e$ in two flavors, and we have diagonalized the hamiltonian through a rotation (unitary) matrix

$$U_{\rm m} = \begin{pmatrix} \cos\theta_{\rm n} & \sin\theta_{\rm n} \\ -\sin\theta_{\rm m} & \cos\theta_{\rm m} \end{pmatrix}$$

  that connects the flavor and the matter "mass" states;
- The same oscillation formula as before will hold, if one replaces the vacuum mixing angle and squared-mass difference with the matter ones.
- When the matter density changes slowly along the path, the evolution is adiabatic and the instantaneous mass eigenstates changes slowly with the matter potential, and crossing probability among them is negligible, except at the resonance.

# 3 Neutrino Phenomenology

As we have seen in sections 1 and 2, the parameters governing neutrino physics are the three masses $(m_1, m_2, m_3)$, the three mixing angles $(\theta_{12}, \theta_{13}, \theta_{23})$, one phase $\delta$ responsible for possible CP violations, and two more phases $(\phi_1, \phi_2)$, if neutrinos are Majorana particles.

## 3.1 Neutrino oscillations Parameters

Neutrino oscillations depend on the squared-mass differences $\Delta m_{ij} = m_i^2 - m_j^2$, and not on the absolute masses, and are unaffected by the Majorana phases. Therefore, the parameter space that can be investigated with oscillation experiments is six-dimensional, $(\theta_{12}, \theta_{13}, \theta_{23}, \Delta m_{21}^2, \Delta m_{32}^2, \delta)$. There is an ambiguity on the order of the neutrino masses. By convention, we assume $\Delta m_{21}^2 = m_2^2 - m_1^2 > 0$ and we refer to it as $\delta m^2$, without the 12 subscript. Two possibilities remain, however,

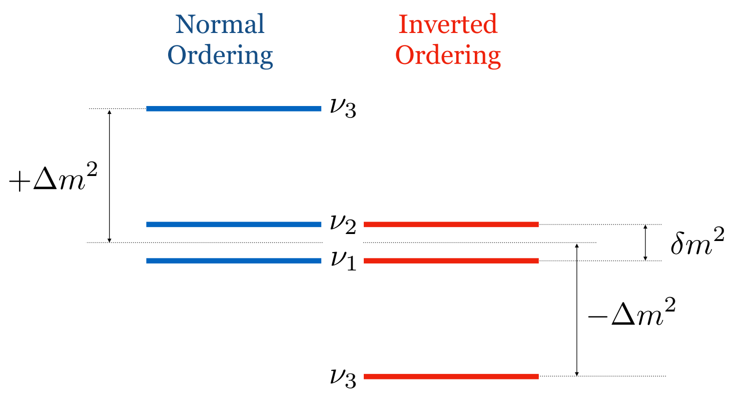


**Figure (3.1) :** Neutrino mass ordering, normal and inverted.

$m_3 > m_2 > m_1$ and $m_3 < m_1 < m_2$, as shown in Figure (3.1). We call Normal Ordering (NO) the case in which the $(m_1, m_2)$ doublet is lighter than $m_3$, Inverted Order (IO), the opposite one. We also adopt a new definition for the squared-mass differences, to avoid the potential confusion arising from the fact that, in NO, the largest positive mass difference is $\Delta m_{31}^2$, while, in IO, is $-\Delta m_{32}^2$. We define the "large" squared-mass difference

$$\Delta m^2 = m_3^2 - \frac{m_1^2 + m_2^2}{2} \; . \tag{3.1}$$

To go from NO to IO, with equal $\Delta m_{32}^2$ in NO and $\Delta m_{13}^2$ in IO, it is enough to change $\Delta m^2$ with $-\Delta m^2$. Commonly, $\Delta m^2$ and $\delta m^2$ are referred to as the "atmospheric" and "solar" squared-mass difference, respectively.

Oscillation experiments are not sensitive to the absolute mass scale of the neutrino spectrum, i.e. to $m_1$ in NO, and to $m_3$ in IO. There are, nevertheless, experiments sensitive to this absolute scale: they will be discussed in section 4. There are observables depending on the sum of neutrino masses, also in cosmology and astrophysics.

## 3.2 Neutrino Sources

Neutrinos are produced by a variety of sources, as the Sun in the nuclear reactions, supernova explosions, cosmic ray interactions with the nuclei in the atmosphere, and man-made sources, such as nuclear reactors and particle accelerators. The neutrino energy spectrum at Earth is summarized in Figure (3.2) It is remarkable that the neutrino energy spans a huge range of orders of magnitude, from $10^{-6}$ to $10^{20}$ eV, with a flux ranging from $10^{-36}$ to $10^{15}$ eV$^{-1}$ cm$^{-2}$ sec$^{-1}$. We can briefly summarize the different spectrum components with increasing energies:

- *Relic neutrinos from thr Early Universe (CNB, Cosmic Neutrino Background).* These neutrinos are a remnant echo of the Universe about 1 sec after the Big Bang, and, in the hypothesis of massless neutrinos, have a density today of $\sim$ 112 cm$^{-3}$ $\nu_\alpha + \overline{\nu}_\alpha$ for each flavor $\alpha$. They have a blackbody spectrum at $T = 1.945$ K, corresponding to energy of 0.168 meV. If we assume NO $(m_1 < m_2 < m_3)$ and $m_1 = 0$, then $m_2 = \sqrt{\delta m^2} \sim 8.6$ meV and $m_3 \sim \sqrt{\Delta m^2} \sim 50$ meV. The high number density of relic neutrinos implies that, even if at least two of them are nonrelativistic, the neutrino flux is very high, as Figure (3.2) shows. The flux is of the order of $10^{10} - 10^{14}$ eV$^{-1}$ cm$^{-2}$ sec$^{-1}$ (flux $\phi \sim n \times v$), depending on the details of the neutrino mass spectrum.

- *Big-Bang Nucleosynthesis neutrinos.* During the first few minutes after Big Bang, neutrinos are produced from neutron and $^3H$ decays, with an energy $\sim 10 - 100$ meV. Their flux is the dominant one in a small window between the CNB and the flux of solar neutrinos.

- *Solar Neutrinos*. These neutrinos are produced in the hydrogen fusion through the $pp$ chain and the CNO cycle. Neutrino energies vary from $\sim 0.1$ to $\sim 20$ MeV. The flux of solar neutrinos at Earth is $\Phi \sim 6.5\ 10^{10}$ cm$^{-2}$ sec$^{-1}$ with a number density of $\sim 2.2$ cm$^{-3}$. There is also a thermal component of the solar neutrino spectrum in the keV range, produced by plasmon decay (plasma oscillations leading to $\gamma \to \nu + \overline{\nu}$), Compton processes ($\gamma + e^- \to e^- + \nu + \overline{\nu}$) and electron bremsstrahlung ($e^- + Ze \to e^- + Ze + \nu + \overline{\nu}$).

- *Geoneutrinos*. Some radioactive isotopes in the Earth crust and mantle, $^{238}$U, $^{232}$Th and $^{40}$K produce a flux of antineutrinos $\overline{\nu}_e$ with energies of few MeV, in the same energy range as solar neutrinos. Although smaller than the solar one ($\Phi_{\overline{\nu}_e} \sim 2 \times 10^{-6}$ cm$^{-2}$ sec$^{-1}$, depending on the position on earth's surface), this flux has been measured and gives geological information on the Earth interior.

- *Reactor Neutrinos*. Nuclear reactors all over the world produce a flux of antineutrinos $\overline{\nu}_e$ from the beta decays of the fission products of $^{235}$U, $^{239}$Pu, $^{238}$U, and $^{241}$Pu. The energy range is $\sim 0 - 10$ MeV, and while the global flux at Earth is just a few percent of the geoneutrino one, near the reactor core, it is largely dominating even at distances of tens of kilometers.

- *Accelerator Neutrinos*. Accelerator neutrinos with energies $\sim 1$ GeV are produced by the decay of pions, kaons and muons. Even if they do not constitute a significant global flux, it is worth mentioning them here, among the terrestrial, man-made sources.

- *Supernova Neutrinos*. Supernova (SN) explosions emit, in a few seconds, a huge flux of MeV neutrinos. However, the integral of all the collapsed and collapsing starts, about 2 per second in the visible Universe, generates an expected flux of the order of $10^{-1}$ cm$^{-2}$ sec$^{-1}$ MeV$^{-1}$.

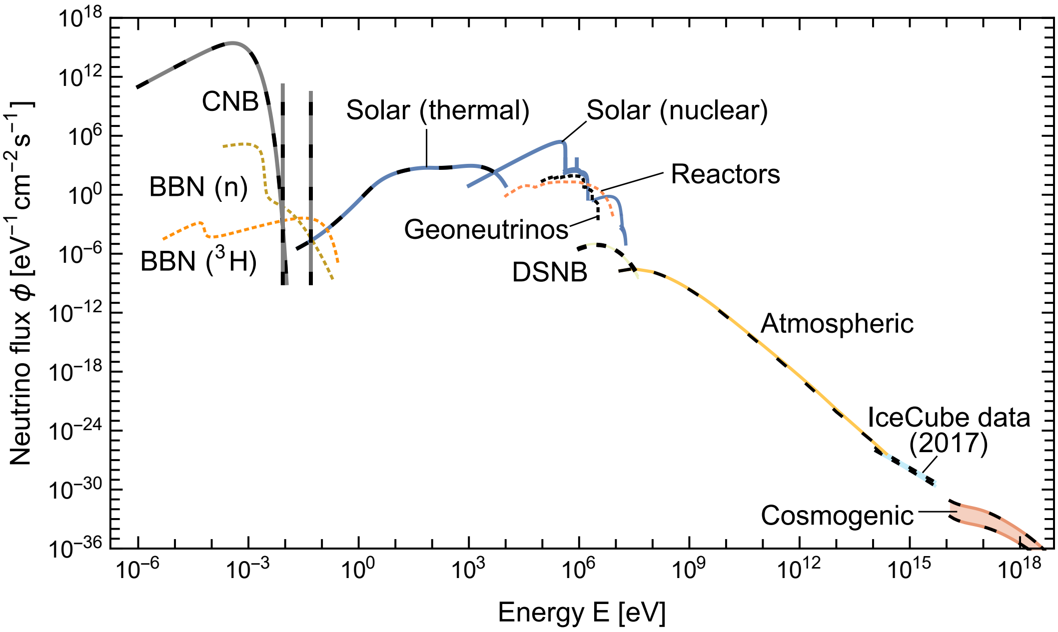


**Figure (3.2) :** Grand Unified Neutrino Spectrum (GUNS) at Earth, integrated over directions and summed over flavors. Solid lines are for neutrinos, dashed or dotted lines for antineutrinos. The CNB spectrum corresponds to the masses $(m_1 = 0, m_2 = 8.6, m_3 = 50)$ meV, resulting in a blackbody spectrum plus two monochromatic lines of nonrelativistic neutrinos with energies corresponding to neutrinos with masses $m_2$ and $m_3$. Figure from [4].

- *Atmospheric Neutrinos*. The interaction of the cosmic rays with the atmosphere nuclei produces atmospheric neutrinos. They come mostly from the decays of the pions and muons that are produced in the cosmic ray interactions. Atmospheric neutrino fluxes span a vast energy range, like the cosmic rays that generate them: the energy goes from $\sim 200$ MeV to $10^{20}$ eV,

- *Extraterrestrial High-Energy Neutrinos.* At energies from about TeV to PeV, neutrinos are produced in the source (for instance star-forming galaxies, gamma ray bursts or active galactic nuclei) or around it, or during cosmic ray propagation towards the Earth.

The impressive differentiation in the energies, processes and flux intensities of the neutrino sources implies, in turn, diversification on the detection side, concerning the technologies and physics involved. The study of the different GUNS components of Figure (3.2) is important, both from the point of view of the neutrino physics and the study of the source properties. Typically, we can simplify the problem in a production-propagation-detection scheme. Neutrino oscillations certainly play a crucial role in the propagation from the source to the detector. The purpose of the experiment is to extract the neutrino parameters, masses and mixing, from the data. On the other hand, the physics of the source is not always sufficiently well known, and the properties of the source and the neutrino parameters are to be determined at the same time from data, if possible. The length scale of the neutrino path and the energy set the relevant parameters that can be extracted from the experimental data at hand.

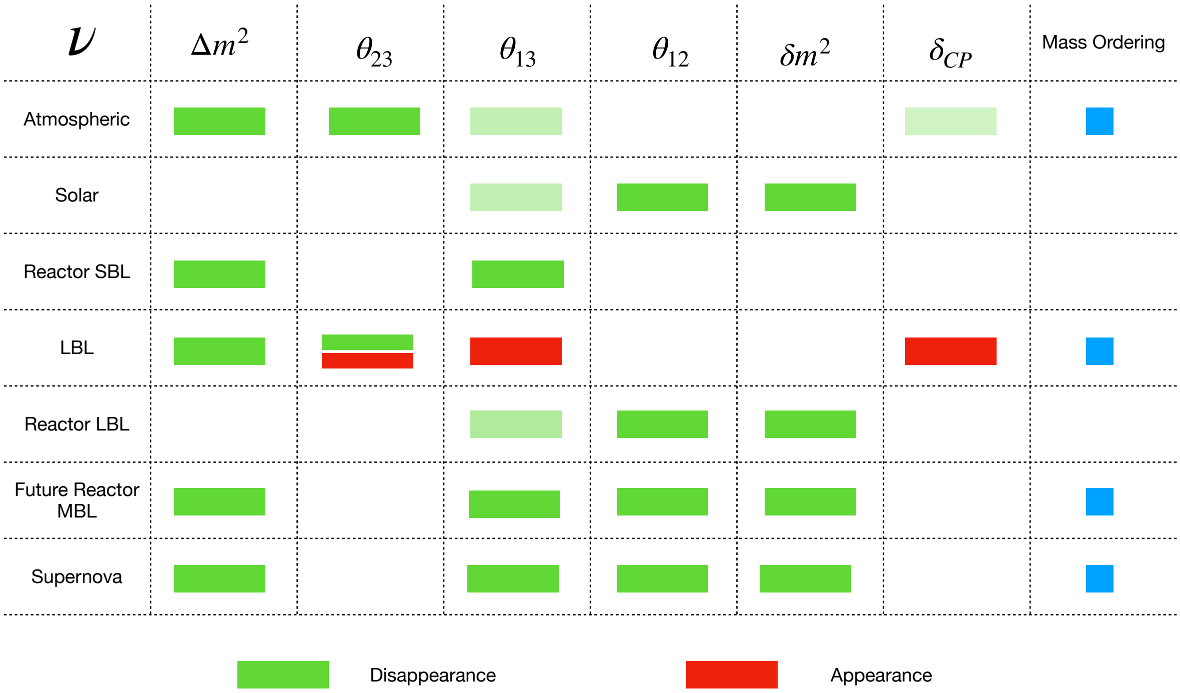


**Figure (3.3) :** Schematic table of the various neutrino oscillations experiment categories. A green or red box means that the experiment is sensitive to the correspondent parameter. If there is only a subleading sensitivity, the color is opaque. Green is for disappearance, red for appearance experiments. The blue squares indicate sensitivity to the mass ordering.

## 3.3 Phenomenology of Neutrino Oscillations

We show in Figure (3.3) the neutrino oscillation parameters that each class of experiments is sensitive to. Even a quick glance at Figure (3.3) allows you to convince yourself that only a combined analysis of the data can explore the whole neutrino oscillation parameter space. In many cases, the small ratio $\delta m^2/\Delta m^2 \sim 3 \times 10^{-2}$, reduces the analysis of a given class of experiments to an effective two-generation oscillation problem, to a first approximation. For instance, solar neutrino oscillations depend mainly on the "solar" parameters $(\delta m^2, \theta_{12})$, atmospheric neutrino oscillations on the "atmospheric" parameters $(\Delta m^2, \theta_{23})$, short-baseline reactor neutrino experiments (Reactor SBL) are sensitive to $(\Delta m^2, \theta_{13})$ and long-baseline accelerator experiments are mainly sensitive to $(\Delta m^2, \theta_{23}, \theta_{13}, \delta)$.

### 3.3.1 Solar and long-baseline reactor neutrinos

The Sun produces electron neutrinos with energies $E_\nu \sim 1$ MeV in fusion reactions. Because of the relatively low energy, the absorption in solar matter can be neglected and the Sun is virtually transparent to them. To detect solar neutrinos, we need large underground detectors to suppress the cosmic rays background. The theoretical neutrino flux is shown in Figure (3.4). The pioneering solar neutrino experiment was the Homestake experiment, the first to have found the solar neutrino deficit. Neutrinos were detected using the inverse inverse $\beta$-decay $\nu_e +^{37}\mathrm{Cl} \to^{37}\mathrm{Ar} + e^-$ with a threshold of 0.814 MeV. Homestake detected intermediate and high-energy neutrinos with the

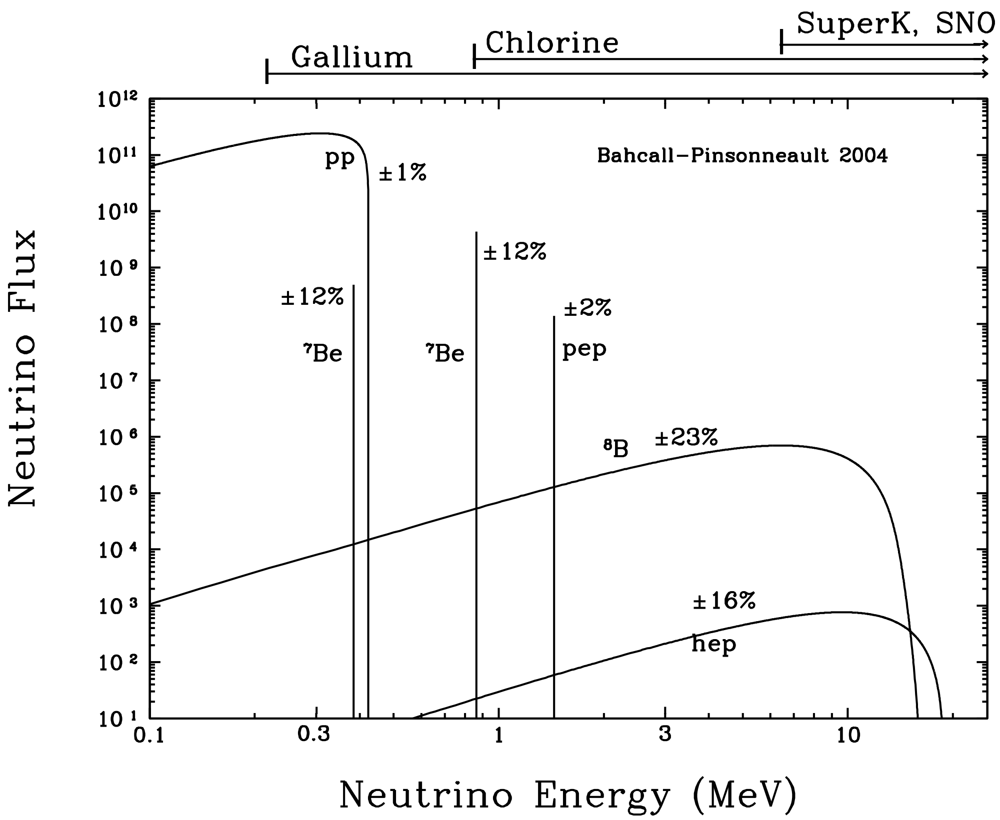


**Figure (3.4) :** Solar neutrinos.

main contribution coming from high-energy $^8$B neutrinos, as shown Figure (3.4). The gallium radiochemical GALLEX/GNO and SAGE experiments have measured pp chain neutrinos, with a threshold of 0.233 MeV, through the reaction $\nu_e +^{71} \text{Ga} \to^{71} \text{Ge} + e^-$. Figure (3.4) shows how the low threshold allows the cumulative measurement of solar neutrinos from all sources. Gallium experiments measured a flux about half of that predicted by the SSM, with an error that proves the deficit at more than $5\sigma$. Super-Kamiokande and SNO measured the $^8$B spectrum, with a threshold of about 5 MeV. The Super-Kamiokande used a water Cherenkov detector measuring the energy and angular distribution of solar neutrinos through their elastic scattering on electrons. SNO was a heavy-water Cherenkov detector that measured the angular and energy spectrum of solar neutrinos through the following reactions

$$\begin{aligned} &\text{CC} : \nu_e + d \to p + p + e^- \\ &\text{NC} : \nu_\alpha + d \to p + n + \nu_\alpha \\ &\text{ES} : \nu_\alpha + e^- \to \nu_\alpha + e^- \; . \end{aligned} \tag{3.2}$$

By exploiting all three processes (3.2), the SNO experiment was able to confirm the solar neutrino deficit in a model independent manner. Today we know that the solar neutrino deficit is explained by the so-called Large Mixing Angle Solution, shown in Figure (3.6). For the LMA solution, there is no resonance for neutrinos with low energies ($E_\nu \lesssim 2$ MeV) for which the survival probability

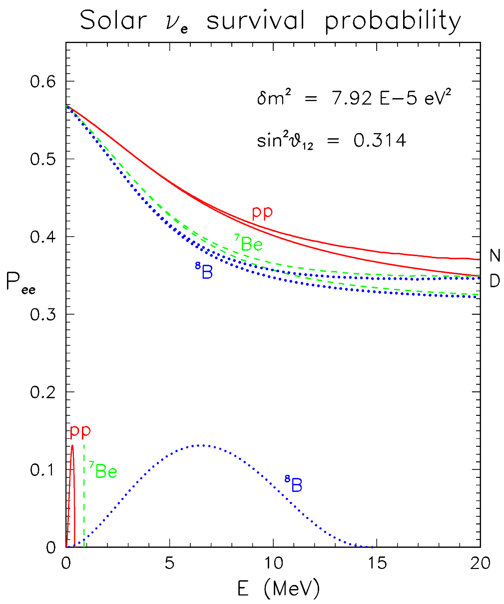


**Figure (3.5) :** Energy profile of the solar survival probability for different energies. Also shown are the corresponding solar neutrino energy spectra, in arbitrary scale.

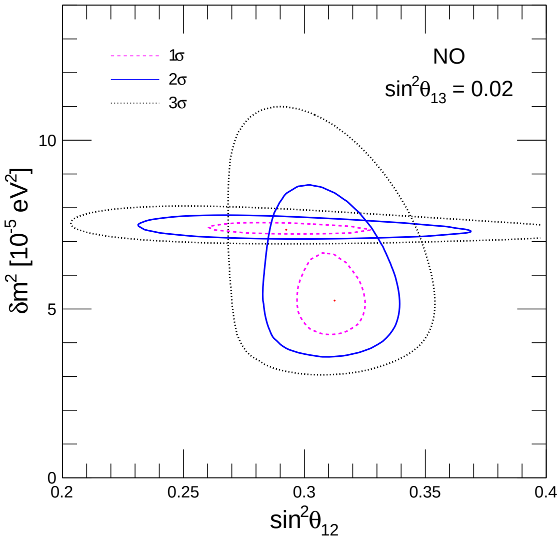


**Figure (3.6) :** Allowed regions from Solar and KamLAND data, in the $((\sin^\theta_{12}, \delta m^2))$ plane, for fixed $\sin^2\theta_{13} = 0.02$

is equal to its average value in vacuum, $P(\nu_e \to \nu_e) = 1 - 1/2\sin^2 2\theta$, while for $E_\nu \gtrsim 2$ MeV the resonance is crossed adiabatically. The MSW effect is also important when solar neutrinos cross the earth, causing the so-called Day/Night effect, depending on neutrinos crossing or not the Earth on their way to the detector. Even if there are many analytically accurate approximations in different energy and density ranges, both for the Sun and the Earth propagation, in the end the calculation must be performed numerically, as shown for instance in Figure (3.5).

The solar neutrino parameters, i.e. $(\delta m^2, \sin^2\theta_{12})$, and to a lesser degree $\sin^2\theta_{13}$, are also explored by LBL reactor neutrino experiments, in particular KamLAND. The result of the KamLAND analysis is also shown in Figure (3.6). The combined analysis of Solar+KamLAND data gives

$$\sin^2\theta_{12} = 0.303 \pm 0.013\ , \quad \delta m^2 = 7.36 \pm 0.15\ . \tag{3.3}$$

### 3.3.2 Atmospheric neutrinos

Through interactions with nuclei in the air, primary cosmic rays produce cascades of particles, and, among those products, atmospheric neutrinos. A typical scheme for the production processes of atmospheric neutrinos is as follows:

$$\begin{aligned} p(n, \alpha, \dots) + \mathrm{Nuc}_{\mathrm{Air}} \to & \pi^\pm(K^\pm) + \dots \\ & \pi^\pm(K^\pm) \to \mu^\pm + \nu_\mu(\bar\nu_\mu) \\ & \qquad\qquad \mu^\pm \to e^\pm + \nu_e(\bar\nu_e) + \bar\nu_\mu(\nu_\mu)\ . \end{aligned} \tag{3.4}$$

The energy spectrum of cosmic rays follows a power law distribution $d\phi/dE \propto E^{-(\gamma+1)}$, with good approximation. Experimentally, the observed terrestrial spectrum is characterized by $\gamma \simeq 1.7$. In turn, the energy spectrum of atmospheric neutrinos follows the spectrum of primary

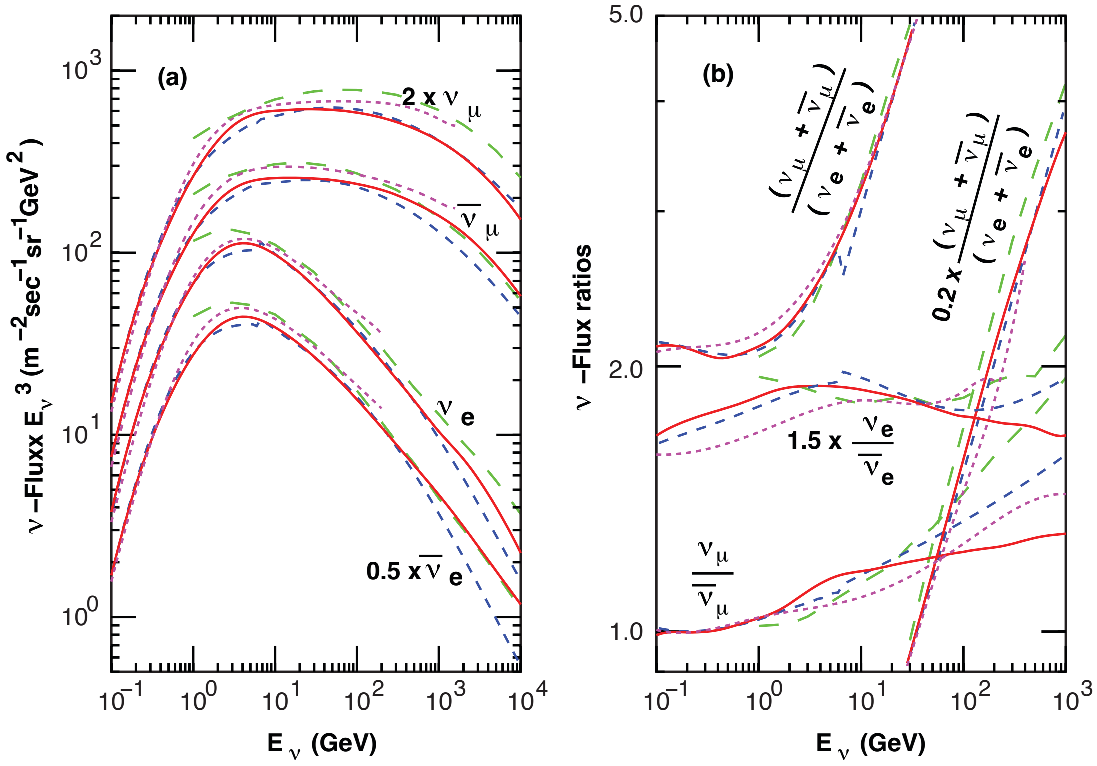


**Figure (3.7) :** Examples of atmospheric neutrino fluxes, from the theoretical calculation [5].

cosmic rays up to energies of the order of 100 GeV, while at higher energies, $\gamma$ increases by one unit. The energy at which the slope of the spectrum changes depends on the zenith angle $\theta$, mainly through the angular factor coming from the decay of pions, which has a typical behavior of $\sim \sec\theta$. The increase in the slope of the energy spectrum is a result of the fact that, at low energies, all secondary particles have time to decay. Hence, the neutrino spectrum reproduces that of the primary cosmic rays. As the energy increases, fewer and fewer secondary particles have time to decay.

Consider the ratio

$$r = \frac{\nu_\mu + \bar{\nu}_\mu}{\nu_e + \bar{\nu}_e}\,, \tag{3.5}$$

which is particularly relevant in neutrino oscillation research. For cosmic rays with energies around GeV, practically all secondary particles decay (including muons from the decay of pions, which are the main source of $\nu_e$ and a relevant source of $\nu_\mu$). In this case, the neutrino production scheme exemplified in (3.4) suggests that the ratio of $\nu_\mu$ to $\nu_e$ should be $\sim 2$. Additionally, since in primary cosmic rays, protons are in excess compared to neutrons, $\pi^+$ are slightly in excess compared to $\pi^-$, and one can expect $\bar{\nu}_e/\nu_e \sim \mu^-/\mu^+ < 1$. Figure (3.7) shows the result of a numerical calculation.

In atmospheric neutrino experiments as Super-Kamiokande (SK), neutrino fluxes of are detected through neutrino–nucleon collisions

$$\nu_\ell + \mathcal{N} \to \ell^- + \mathcal{X}\,, \quad \overline{\nu}_\ell + \mathcal{N} \to \ell^+ + \mathcal{X}\,. \tag{3.6}$$

Being a water Cherenkov detector, SK cannot distinguish $\ell^-$ from $\ell^+$, so does not distinguishes $\nu_\ell$ form $\overline{\nu}_\ell$.

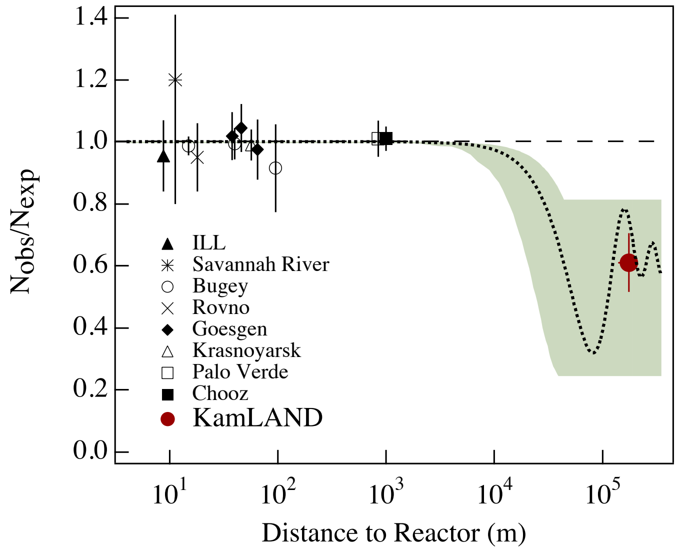


**Figure (3.8) :** Ratio of measured to expected flux from reactor experiments. The solid dot is the KamLAND point plotted at a flux-weighted average distance. Figure taken from [6].

### 3.3.3 Terrestrial neutrinos: Reactors and Accelerators Neutrinos

We mentioned the KamLAND experiment, in connection with solar neutrinos. It was an experiment measuring reactor antineutrinos coming from a distance between 80 km and 800 km, with an average of about 180 km. In combination with solar neutrinos, KamLAND data gave a first hint in favor of a nonzero $\theta_{13}$. The other SBL reactor experiments Double CHOOZ, RENO and more importantly, Daya Bay, have measured the mixing angle $\theta_{13}$ with great accuracy, $\sin^2\theta_{13} = 0.0223 \pm 0.006$, but also $\Delta m^2$ with an accuracy comparable to the one of the LBL accelerator experiments. Figure (3.8) shows the ratio of measured to expected $\overline{\nu}_e$ flux from reactor experiments. When the distance between the reactor core and the detector is $\gtrsim 1$ km (SBL), a deficit of the flux is a signal of oscillations governed by $\theta_{13}$.

As for reactors, also in the case of accelerator experiments the baseline can be long or short. All the SBL accelerator experiments did not find any indication of neutrino oscillations, with the exception of the LSND experiment, which found a signal in the $\overline{\nu}_\mu \to \overline{\nu}_e$ channel and a weaker one in the $\nu_\mu \to \nu_e$, pointing to possible $\nu_\mu$ and $\overline{\nu}_\mu$ to $\nu_s$ oscillations. A following project, MicroBooNE, found no evidence for a sterile neutrino, but with results still controversial. Currently, two LBL accelerator experiments are studying the $\overset{(-)}{\nu}_\mu \to \overset{(-)}{\nu}_e$ channel, T2K and NOvA. These experiments were optimized to measure $\theta_{13}$, but they give important information about the parameters $\Delta m^2, \theta_{13}, \theta_{23}$ and the CP phase $\delta$. For instance, Figure (3.10) shows the allowed regions in the planes $(\sin^2\theta_{13}, \delta)$ and $(\sin^2\theta_{23}, \Delta m^2_{32})$, from the latest T2K data [7].

### 3.3.4 Global Analysis of Neutrino Oscillation Data

To get bounds to all oscillation parameters in the 6-dimensional parameter space ($\Delta m^2$, $\delta m^2$, $\theta_{12}$, $\theta_{13}$,$\theta_{23}$, $\delta$), one should combine the analysis of all experiments. Obviously, one could perform the global combination from the beginning, both for normal and inverted ordering, but in this way, it is much more difficult to understand all the correlations between the parameters. To this end, it can

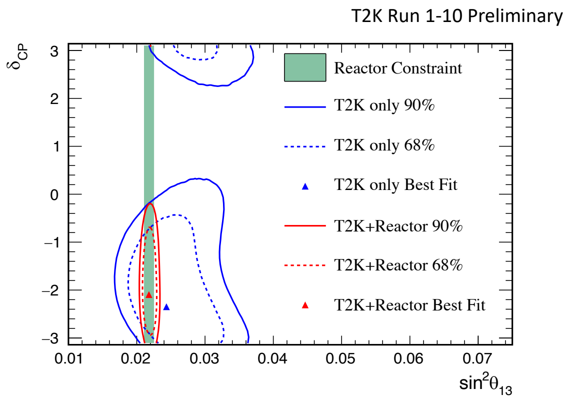


**Figure (3.9) :** T2K allowed region in the $(\sin^2 2\theta_{13}, \delta)$ plane for NO. Also shown, in green, the bounds on $\theta_{13}$ from SBL reactors.

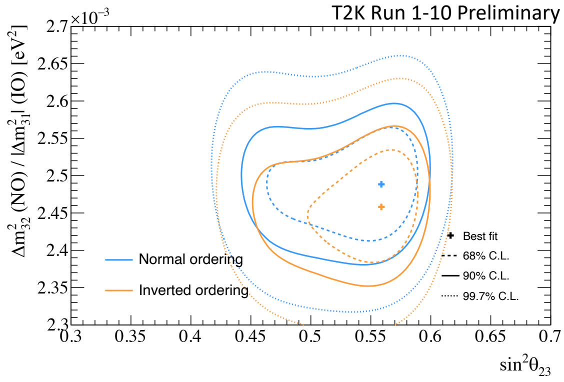


**Figure (3.10) :** T2K allowed region in the $(\sin^2 2\theta_{13}, \delta)$ plane for NO. Also shown, in green, the bounds on $\theta_{13}$ from SBL reactors.

help to combine data into three different steps:

- We start by combining solar, KamLAND, and LBL accelerator data (Figure (3.11)). Solar and KamLAND data are mainly sensitive to the solar parameters ($\delta m^2$, $\theta_{12}$), and, to a sub-leading order, to $\theta_{13}$. On the other hand, the solar parameters are a necessary input for the LBL analysis. LBL data, by means of the $\nu_\mu \to \nu_\mu$ disappearance and the $\nu_\mu \to \nu_e$ appearance channel, allow us to explore the parameters ($\Delta m^2$, $\theta_{23}$, $\theta_{13}$). These three datasets represent the minimal subsample of data sensitive to all the oscillation parameters.

- In the next step, we add the analysis of SBL reactor data (see Figure 3.12)), that improve the constraints on $(\Delta m^2, \theta_{13})$, and indirectly affect the parameters $(\theta_{23}, \delta)$ and the mass ordering, i.e. the sign of $\Delta m^2$. Through the correlations between the mass-mixing parameters, the preference for the mass ordering is reversed, and NO ordering is preferred at $\sim 1.5\sigma$.

- Finally, we add to the analysis the atmospheric data that are mainly sensitive to the "atmospheric" parameters $(\Delta m^2, \sin^2\theta_{23})$ but also, to a lesser degree, to the solar parameters and $\delta$ (Figure (3.13)). By combining all oscillation data, the sensitivity to the mass ordering can rich the $\sim 2\sigma$ level.

Figures (3.11), (3.12) and (3.13) show the bounds on each oscillation parameter, by marginalizing over all the others. Blue curves are for NO, red ones for IO. From solar and KamLAND data (3.11), IO is slightly preferred at level of $\sim 1\sigma$. The two parameters $\delta m^2$ and $\sin^2\theta_{12}$ are fairly well measured, with almost gaussian uncertainties, that, if $\sqrt{\Delta\chi^2}$ is shown on the $y$ axes, correspond to straight lines. There is no significant difference between the bounds in NO and IO. The mixing angles $\theta_{13}$ and $\theta_{23}$ are less accurately constrained, and there is a double minimum for both angles. For $\theta_{23}$, this is a consequence of octant ambiguity in the $\nu_\mu \to \nu_\mu$ disappearance searches at LBL accelerators. The bounds on the phase $\delta$ are weak, although it appears to be slightly favored around $\pi$ in NO, and around $3\pi/2$ in IO, while it is disfavored around $\pi/2$ in both cases.

Figure 3.12 shows the results of the analysis, with the inclusion of SBL reactor data, which are sensitive to $|\Delta m^2|$ and $\sin^2\theta_{13}$. The uncertainty on $\sin^2\theta_{13}$ is strongly decreased. The correlations between the oscillation parameters alter the preference for the $\theta_{23}$ octant. The independent measurements of $\Delta m^2$, through a synergy between the SBL and LBL data, changes also the preference

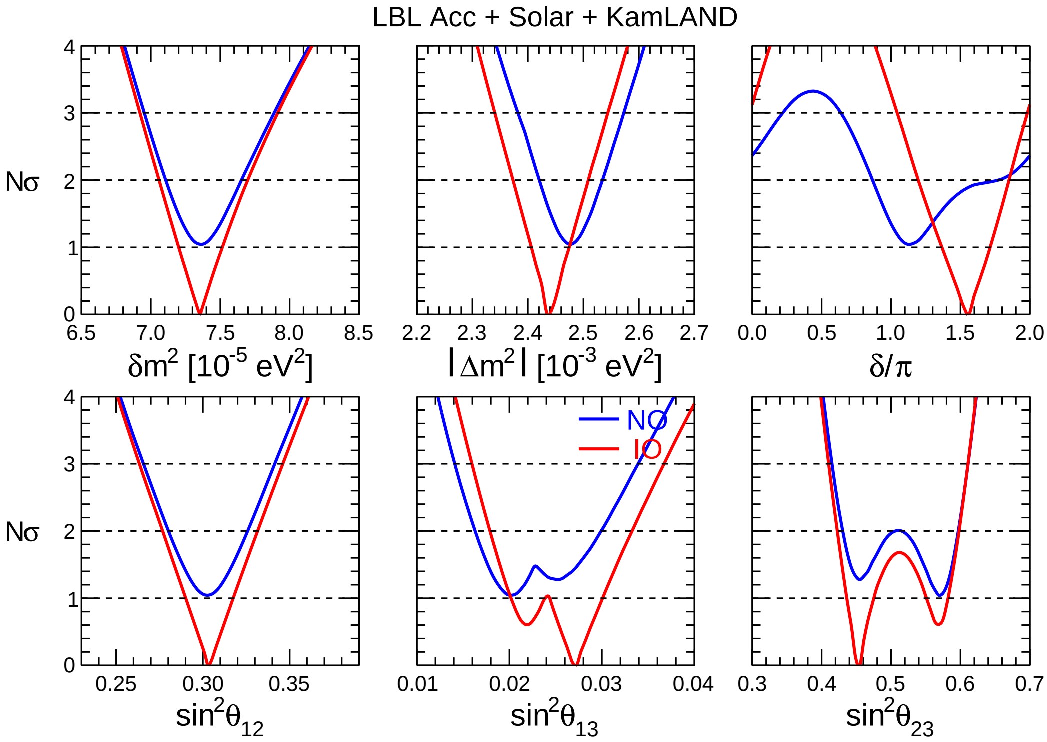


**Figure (3.11) :** Global analysis of long-baseline accelerator, solar and KamLAND $\nu$ data. Bounds on $\delta m^2$, $|\varDelta m^2|$, $\sin^2\theta_{ij}$, and $\delta$, for NO (blue) and IO (red), in terms of $N_\sigma = \sqrt{\varDelta\chi^2}$ from the global best fit. The offset between separate minima in IO and NO, $\varDelta\chi^2_{\mathrm{IO-NO}} = -1.1$, favors the IO case by $\sim 1.0\sigma$.

for the mass ordering, from IO to NO, with NO preferred at the level of $\sim 1.3\sigma$. Note that the best-fit value of $\varDelta m^2$ is increased with respect to Figure (3.11). The preference for $\delta \sim \pi$ ($\sim 3\pi/2$) in both mass orderings does not change. Figure (3.13) shows the effect of adding atmospheric $\nu$ data, which add further sensitivity to the atmospheric parameters, $\varDelta m^2$ (and to its sign), $\sin^2\theta_{23}$ and $\delta$. Atmospheric data analysis depends on all parameters in a complicated way, since the SK data span a large range of energies, and the information on neutrino and antineutrino oscillations is integrated. The atmospheric analysis takes as inputs $(\delta m^2,\ \theta_{12},\ \theta_{13})$ from the combination of solar, KamLAND and SBL reactor data. In particular, the inclusion of atmospheric data strengthens the preference for NO at a level of $\sim 2.5\sigma$), and flips the $\theta_{23}$ preference from the upper to the lower octant in NO (at $\sim 1.6\sigma$). The best-fit value of $\delta$ is slightly higher, and the $\delta = \pi$ is disfavored at $\sim 1.6\sigma$. The bounds on each single parameter, do not allow us to understand how different datasets combine or compete to set constraints on parameters. For these reasons, it is useful to look at the combined bounds in the planes $(\sin^2\theta_{13}, \sin^2\theta_{23})$, $(\sin^2\theta_{23}, |\varDelta m^2)$ and $(\sin^2\theta_{23}, \delta)$.

Figure (3.14) shows the covariance of the pair $(\sin^2\theta_{23},\ \sin^2\theta_{13})$ for increasingly rich data sets, in both NO (top) and IO (bottom). In each row, it is shown the $\varDelta\chi^2$, with respect to the corresponding mass ordering. We see that there is an octant ambiguity for $\theta_{23}$, with two nearly degenerate solutions at $1\sigma$. Maximal mixing is allowed at $\sim 2\sigma$. The dominant term in the LBL appearance probability is proportional to $\sin^2\theta_{23}\sin^2\theta_{13}$ and induces an anticorrelation between $\theta_{23}$ and $\theta_{13}$. Before including the results of the SBL reactors, the relatively large range for $\sin^2\theta_{13}$, does not select one of the two octants. In the central column, the SBL analysis, whose constraints on $\theta_{13}$ are shown with a $\pm 2\sigma$ error bars, tends to prefer the upper-octant solution, corresponding to a lower

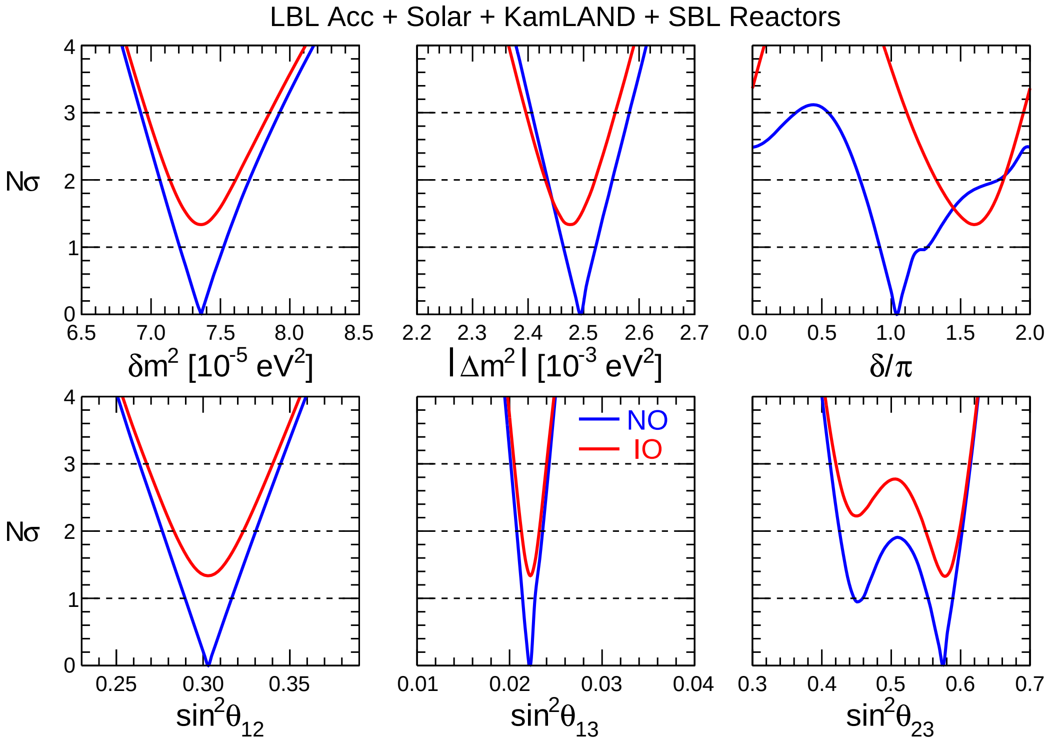


**Figure (3.12) :** As in Figure (3.11), but adding SBL data. The offset $\Delta\chi^2_{\mathrm{IO-NO}} = +1.8$ favors the NO case by $\sim 1.3\sigma$.

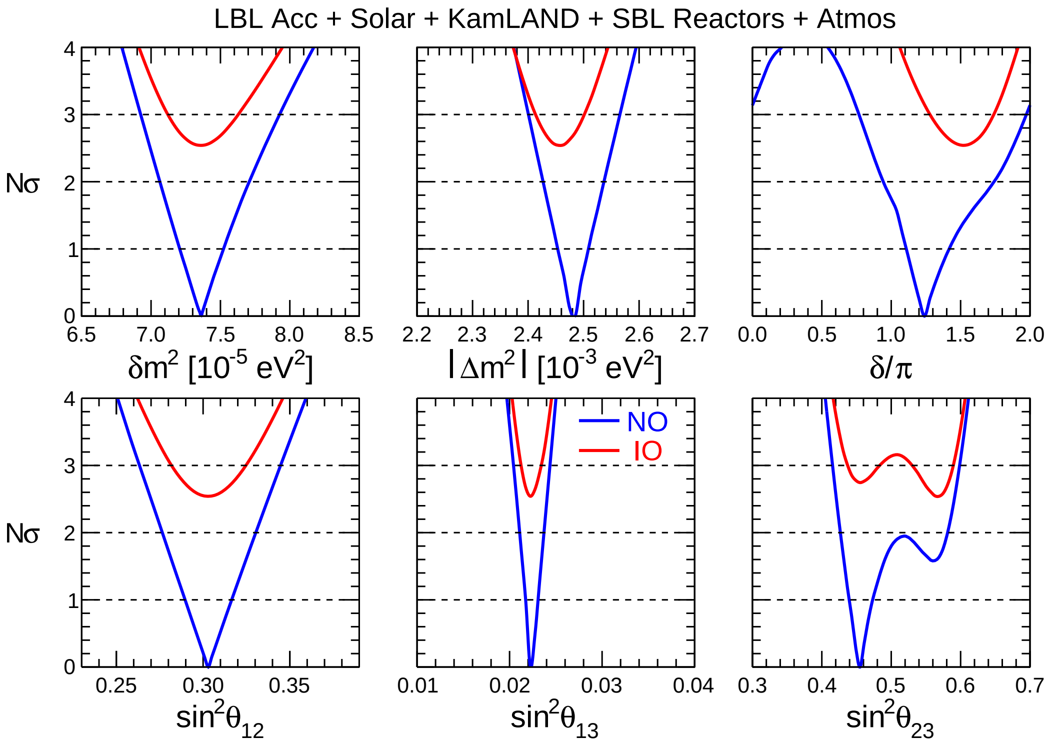


**Figure (3.13) :** As in Figure (3.12), but adding atmospheric $\nu$ data (i.e., with all oscillation data included). The offset $\Delta\chi^2_{\mathrm{IO-NO}} = +6.5$ favors the NO case by $\sim 2.5\sigma$.

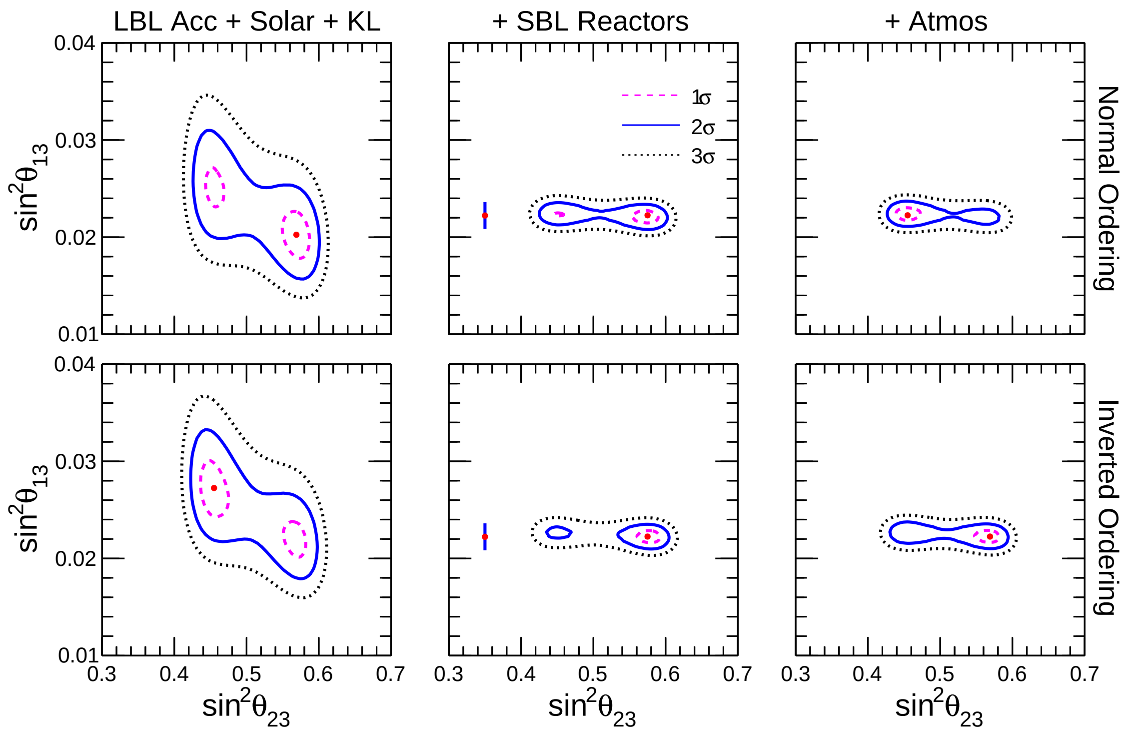


**Figure (3.14) :** Regions allowed in the plane $(\sin^2\theta_{23},\, \sin^2\theta_{13})$ for different dataset combinations: Solar + KamLAND + LBL accelerator data (left), + SBL reactor data (center), + Atmospheric data (right). Top and bottom panels refer, respectively, to NO and IO as taken separately, without any relative offset. The error bars in the middle panels show the $\pm 2\sigma$ range for $\theta_{13}$ arising from SBL reactor data only.

value of $\theta_{13}$, both for NO and IO. Therefore, the combination selects a more flattened region at lower $\theta_{13}$. The best-fit values of $\theta_{23}$ flips into the upper octant for IO, suggesting that there is still no robust indication for the $\theta_{23}$ octant. Combining all the data, there is virtually no improvement in the $\theta_{13}$ constraints, and the preferred octant in NO for $\theta_{23}$ flips into the first $\theta_{23}$ octant, confirming the instability of the $\theta_{23}$ solution. In particular, for both NO and IO, maximal mixing is allowed at $\sim 2\sigma$. Another interesting case, is that of the bounds in the plane $(\sin^2\theta_{23},\, |\Delta m^2|)$, shown in Figure (3.15). In this figure we put $|\Delta m^2|$, on the $y$ axes, so that both mass orderings can be represented in the same plot. The blue error bar in the second row represents the constraints on $\Delta m^2$, from SBL data alone. The SBL analysis favors relatively high values of $\Delta m^2$, as compared to LBL data. Therefore, in the combination LBL+SBL, there is a better agreement in NO that in IO. Additionally, relatively high values of $\theta_{23}$ are preferred, disfavoring $\theta_{23}$ maximal mixing. The overall preferences for NO and for nonmaximal of $\theta_{23}$ are corroborated by atmospheric data that, however, change in NO the preferred octant from the upper to the lower one. Even though SBL experiments are not directly sensitive to the mass ordering, i.e. to the sign of $\Delta m^2$, and to the mixing angle $\theta_{23}$, the correlations between the oscillation parameters make them capable of helping to constrain both the mass ordering and $\theta_{23}$, once they are combined with other datasets.

Finally, it is also very interesting to look at the bounds on $\delta$ in the plane $(\sin^2\theta_{23},\, \delta)$ of Figure (3.16). The octant ambiguity leads to two quasi-degenerate best fits, surrounded by allowed regions that merge at $2\sigma$ or $3\sigma$. The allowed regions for $\delta$ are larger in NO, and approximately correspond to the interval $[\pi, 2\pi]$, at $\sim 3\sigma$. In particular, CP-conserving case $\delta \simeq \pi$ is allowed

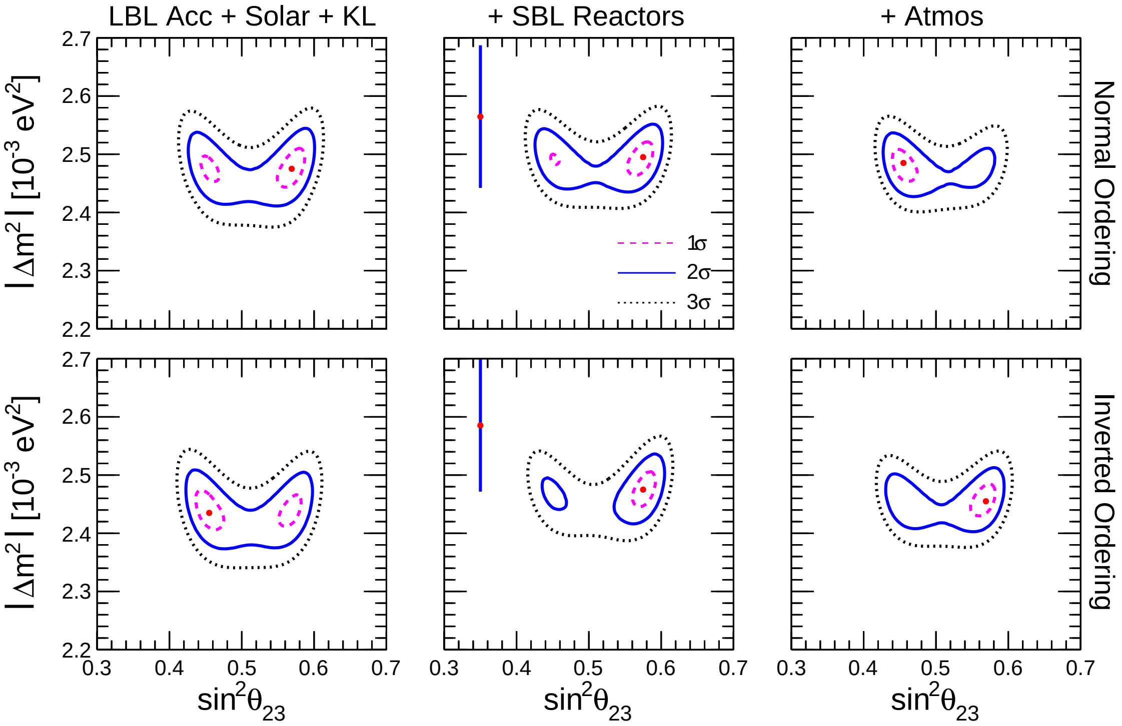


**Figure (3.15) :** As in Figure (3.14), but in the plane $(\sin^2\theta_{23},\ |\Delta m^2|)$. The error bars in the middle panels show the $\pm 2\sigma$ range for $|\Delta m^2|$, arising from SBL reactor data only.

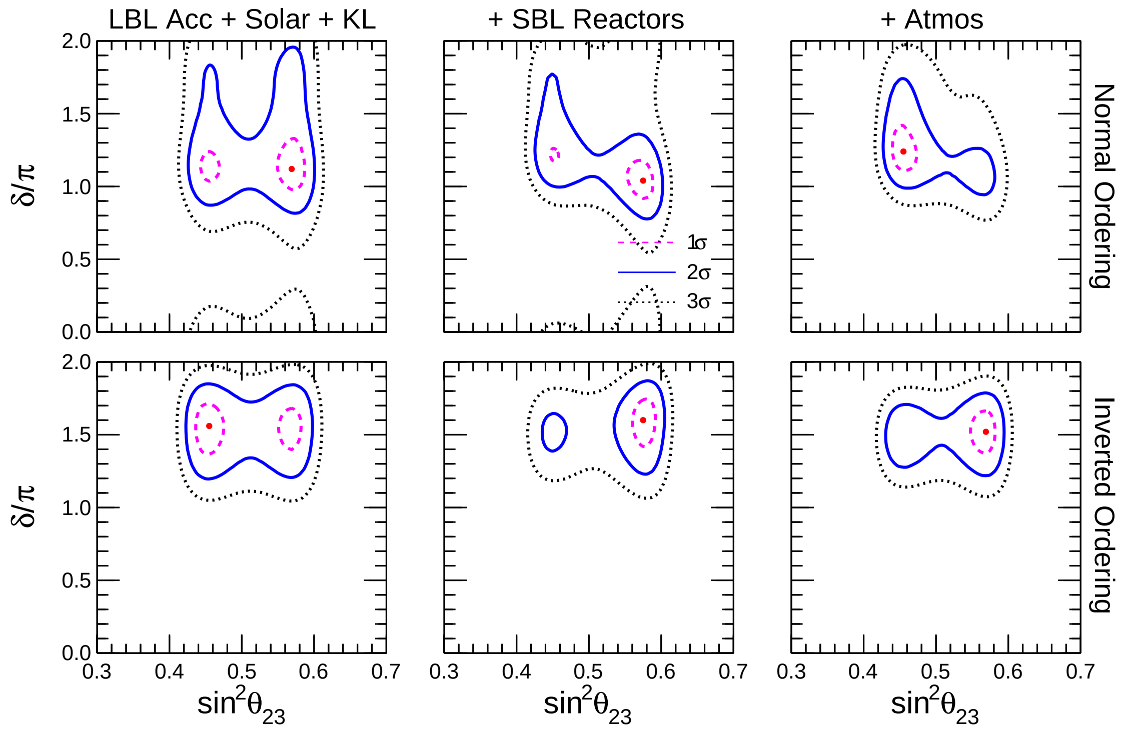


**Figure (3.16) :** As in Figure (3.15), but in the plane $(\sin^2\theta_{23},\ \delta)$.

at $2\sigma$. In IO there is rather stable preference for CP-violation, $\delta \simeq 3\pi/2$ in all data combina-

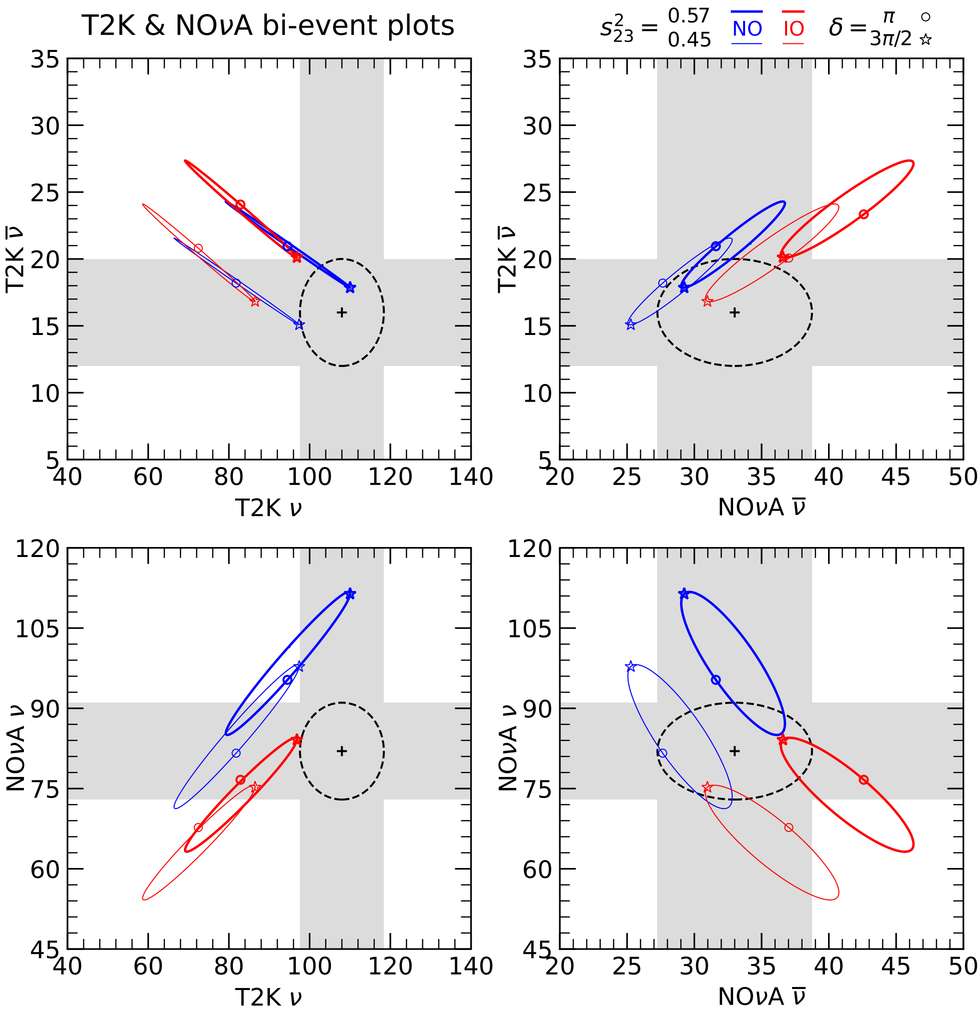


**Figure (3.17) :** Bi-event plots: Total number of $\nu$ and $\overline{\nu}$ appearance events for T2K and NOvA, in four possible combinations. The slanted ellipses represent the theoretical expectations for NO (blue) and IO (red), and for two representative values of $\sin^2\theta_{23}$: 0.45 (lower octant, thin ellipses) and 0.57 (upper octant, thick ellipses). The CP-conserving value $\delta = \pi$ and the CP-violating value $\delta = 3\pi/2$ are marked as a circle and a star, respectively. Each gray band represents one datum with its $\pm 1\sigma$ statistical error; the combination of any two data provides a (black dashed) $1\sigma$ error ellipse, whose center is marked by a cross.

tions, and $\delta \simeq \pi$ is excluded at $3\sigma$. The two parameters $\delta$ and $\theta_{23}$ appear to be uncorrelated in IO. A slight negative correlation between $\delta$ and $\sin^2\theta_{23}$ emerges when adding SBL reactor data. The anticorrelation between $\delta$ and $\sin^2\theta_{23}$ in NO moves the best fit of $\delta$ to slightly higher values, since atmospheric neutrino data prefer $\delta \sim 3\pi/2$ and the lower octant of $\theta_{23}$. The CP-conserving value $\delta = \pi$ is disfavored at 90% C.L. or, equivalently at $\sim 1.6\sigma$. The bounds on all oscillation parameters as well the percentage accuracy are reported in Table 2. In summary, current neutrino oscillation experiments, have measured the three mixing angles and the two squared-mass

**Table (2) :** Global $3\nu$ analysis of oscillation parameters: best-fit values and allowed ranges at $N_\sigma = 1$, 2 and 3, for either NO or IO, including all data. The latter column shows the formal "$1\sigma$ fractional accuracy" for each parameter, defined as 1/6 of the $3\sigma$ range, divided by the best-fit value and expressed in percent. We recall that $\Delta m^2 = m_3^2 - (m_1^2 + m_2^2)/2$ and that $\delta \in [0, 2\pi]$ (cyclic). The last row reports the difference between the $\chi^2$ minima in IO and NO.

| Parameter | Ordering | Best fit | $1\sigma$ range | $2\sigma$ range | $3\sigma$ range | "$1\sigma$" (%) |
|---|---|---|---|---|---|---|
| $\delta m^2/10^{-5}\ \mathrm{eV}^2$ | NO, IO | 7.36 | 7.21 – 7.52 | 7.06 – 7.71 | 6.93 – 7.93 | 2.3 |
| $\sin^2\theta_{12}/10^{-1}$ | NO, IO | 3.03 | 2.90 – 3.16 | 2.77 – 3.30 | 2.63 – 3.45 | 4.5 |
| $\|\Delta m^2\|/10^{-3}\ \mathrm{eV}^2$ | NO | 2.485 | 2.454 – 2.508 | 2.427 – 2.537 | 2.401 – 2.565 | 1.1 |
| | IO | 2.455 | 2.430 – 2.485 | 2.403 – 2.513 | 2.376 – 2.541 | 1.1 |
| $\sin^2\theta_{13}/10^{-2}$ | NO | 2.23 | 2.17 – 2.30 | 2.11 – 2.37 | 2.04 – 2.44 | 3.0 |
| | IO | 2.23 | 2.17 – 2.29 | 2.10 – 2.38 | 2.03 – 2.45 | 3.1 |
| $\sin^2\theta_{23}/10^{-1}$ | NO | 4.55 | 4.40 – 4.73 | 4.27 – 5.81 | 4.16 – 5.99 | 6.7 |
| | IO | 5.69 | 5.48 – 5.82 | 4.30 – 5.94 | 4.17 – 6.06 | 5.5 |
| $\delta/\pi$ | NO | 1.24 | 1.11 – 1.42 | 0.94 – 1.74 | 0.77 – 1.97 | 16 |
| | IO | 1.52 | 1.37 – 1.66 | 1.22 – 1.78 | 1.07 – 1.90 | 9 |
| $\Delta\chi^2_{\mathrm{IO-NO}}$ | IO$-$NO | +6.5 | | | | |

differences with an accuracy between $1\%$ and $5\%$. the best known parameter is the atmospheric $\Delta m^2$, with an accuracy of $1.1\%$. The determination of the octant of $\theta_{23}$ is still fragile. The worst known parameter is $\delta$, with uncertainties $\sim 10 - 15\%$, depending on the mass ordering. There is a preference at about $2.6\sigma$ for NO. The uncertainty on the CP phase comes mostly from a tension between the NOvA and T2K experiments. This tension can be exemplified by a bi-event plots where event rates at T2K and NOvA are compared. The plots in Figure (3.17) are a variation of the bi-probability plots representing the $\nu_\mu \to \nu_e$ and $\overline{\nu}_\mu \to \overline{\nu}_e$ appearance probabilities in LBL accelerator experiments, at fixed neutrino energy. If $\delta$ is continuously varied, the bi-probability plot produces ellipses and can help to understand parameter degeneracies. By averaging over energy weighted by fluxes and cross sections, the probabilities can be converted into total number of appearance events, and thus into bi-event plots, preserving elliptic shapes that can be compared with experimental data. Figure (3.17) shows four possible combinations of the $\nu$ and $\overline{\nu}$ appearance events: the blue and red ellipses represent the theoretical expectations for NO and IO, respectively, while the grey bands and the black ellipses represent the data with their $1\sigma$ statistical errors. The mixing angle $\theta_{23}$ is fixed in the lower octant (thin) or upper octant (thick). Two representative values of $\delta$ ($\pi$ and $3\pi/2$) are indicated on each ellipse. One can analyze the experiments, separately, as shown in the upper left and lower right plots. For T2K, the best agreement of theory and data is reached for NO, with a clear preference for $\delta = 3\pi/2$, and a slight preference for the upper octant of $\theta_{23}$. For NOvA, the situation is not so clear, since all the colored ellipses are close to the experimental one. The agreement is larger in NO, with a preference for $\delta = \pi/2$, with no significant distinction of the $\theta_{23}$ octants.

If one combines T2K and NOvA separately in the $\nu$ and $\overline{\nu}$ channels, as shown in the upper right panel and in the lower-left panel, the best agreement of data and theory is now reached for IO, with a clear preference for $\delta = 3\pi/2$. The preference for the $\theta_{23}$ octant changes in the $\nu$ and $\overline{\nu}$ channel. It is evident that the combination of T2K and NOvA data results in a tension with respect to the preferred $\delta$, mass ordering and octant of $\theta_{23}$.

# 4 Direct Measurements of Neutrino Masses

The absolute neutrino mass scale can be probed by non-oscillatory neutrino experiments. The most sensitive laboratory experiments to date have been focussed on tritium beta decay and on neutrinoless double beta decay. Beta decay experiments probe the so-called effective electron neutrino mass $m_\beta$,

$$m_\beta = \left[c_{13}^2 c_{12}^2 m_1^2 + c_{13}^2 s_{12}^2 m_2^2 + s_{13}^2 m_3^2\right]^{\frac{1}{2}} \ . \tag{4.1}$$

Current experiments provide upper limits in the range $m_\beta \lesssim$ few eV.

Neutrinoless double beta decay ($0\nu 2\beta$) experiments are instead sensitive to the so-called effective Majorana mass $m_{\beta\beta}$ (if neutrinos are Majorana fermions)

$$m_{\beta\beta} = \left|c_{13}^2 c_{12}^2 m_1 + c_{13}^2 s_{12}^2 m_2 e^{i\phi_2} + s_{13}^2 m_3 e^{i\phi_3}\right| \ , \tag{4.2}$$

where $\phi_2$ and $\phi_3$ are the two Majorana phases. All $0\nu 2\beta$ experiments placed only upper bounds on $m_{\beta\beta}$.

Astrophysical and cosmological observations have started to provide indirect upper limits on absolute neutrino masses, competitive with those from laboratory experiments. In particular, the combined analysis of high-precision data from Cosmic Microwave Background (CMB) anisotropies and Large Scale Structures (LSS) has already reached a sensitivity of $O(\mathrm{eV})$ for the sum of the neutrino masses $\Sigma = m_1 + m_2 + m_3$.

In beta decay experiments, a nucleus emits a beta particle (an electron or positron) and an antineutrino or neutrino, for instance

$${}^A_Z X \rightarrow {}^A_{Z+1} Y + e^- + \overline{\nu}_e \tag{4.3}$$

in which ${}^A_Z X$, the parent nucleus, decays in a ${}^A_{Z+1} Y$ daughter nucleus, emitting an electron and an antineutrino. The energy and momentum of the decay products can be measured to infer the neutrino mass, by looking at the distortions, induced by neutrino masses, in the electron energy spectrum. The final nucleus is much heavier than the leptons, and its kinetic energy ca be neglected. Therefore, the neutrino energy is $E_{\nu_e} = Q - T$, where $T$ is the kinetic energy of the electron and the $Q$-value is the total available energy. If neutrinos were massless, $Q$ would coincide with the maximal kinetic energy of the electron.

The differential reta for the beta decay can be written as

$$\frac{d\Gamma}{dE_e} = \frac{G_F^2 m_e^5}{2\pi^3} \cos^2\theta_C |M|^2 F(Z, E_e) E_e p_e E_{\nu_e} p_{\nu_e} \ , \tag{4.4}$$

where $\theta_C$ is the Cabibbo angle, $M$ is the nuclear matrix element, $F(E, Z)$ is the Fermi function which describes the Coulomb interaction between the emitted electron and the residual nucleus, $p_\alpha$ and $E_\alpha$ with $\alpha = e, \nu_e$ are the momentum and energy of the final leptons. The product $p_{\nu_e} E_{\nu_e}$ can be rewritten as[9]

$$p_{\nu_e} E_{\nu_e} = E_{\nu_e}\sqrt{E_{\nu_e}^2 - m_{\nu_e}^2} = (Q - T)\sqrt{(Q-T)^2 - m_{\nu_e}^2} \tag{4.5}$$

[9] Acually, a more accurate formula must take into account the excited energy levels of the electrons in the final atom.

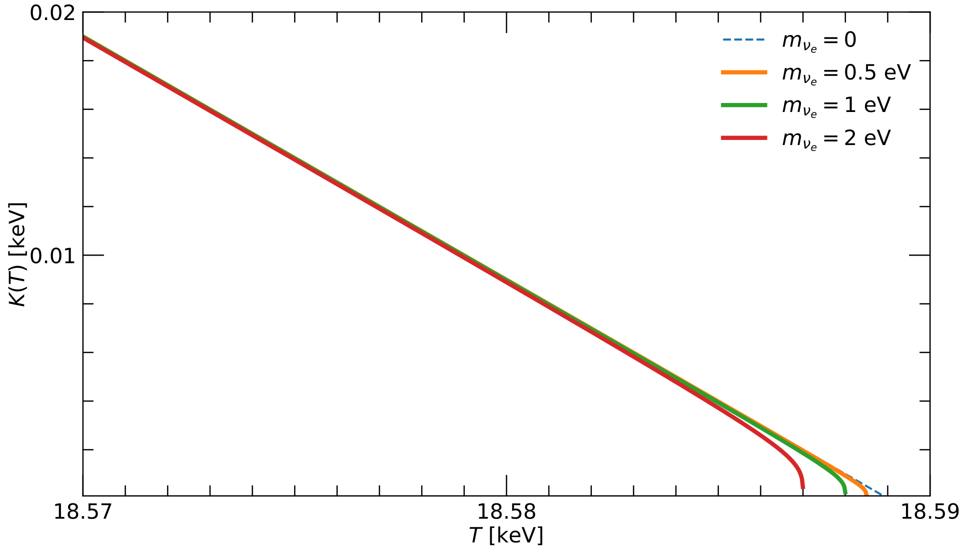


**Figure (4.1) :** Kurie plot for tritium beta decay.

The so-called Kurie function is defined in the following way, by factoring out all the terms that do not depend on neutrino momentum or energy

$$K(T) = \sqrt{\frac{d\Gamma/dT}{\frac{G_F^2 m_e^5}{2\pi^3}\cos^2\theta_C |M|^2 F(Z,E_e) E_e p_e}} = \sqrt{(Q-T)\sqrt{(Q-T)^2 - m_{\nu_e}^2}}\,, \tag{4.6}$$

where we have used $dT = d(E_e - m_e) = dE_e$. For massless neutrinos $K(T) = Q - T$, while, when $m_{\nu_e} \neq 0$, $K(T)$ is no more linear in $T$. An example of the distortions in the linearity of the Kurie plot is shown in Figure (4.1).

However, if the neutrino mixing is taken into account, the $K(T)$ becomes

$$K(T) = \sqrt{(Q-T)\sum_{i=1}^{3} |U_{ei}|^2 \sqrt{(Q-T)^2 - m_{\nu_i}^2}} \tag{4.7}$$

If $m_i \ll Q - T$ (for instance the KATRIN experiment $Q \sim 18.6$ keV, and therefore, at the electron spectrum endpoint, this condition is absolutely verified), then

$$\sqrt{(Q-T))^2 - m_{\nu_i}^2} = (Q-T)\sqrt{1 - \frac{m_i^2}{(Q-T)^2}} \sim (Q-T) - \frac{m_i^2}{2(Q-T)}\,, \tag{4.8}$$

so that

$$\begin{aligned} &\sum_{i=1}^{3} |U_{ei}|^2 \sqrt{(Q-T)^2 - m_{\nu_i}^2} \sim \sum_{i=1}^{3} |U_{ei}|^2 \left[(Q-T) - \frac{m_i^2}{2(Q-T)}\right] = \\ &= Q - T - \frac{\sum_{i=1}^{3} |U_{ei}|^2 m_i^2}{2(Q-T)^2} \sim \sqrt{(Q-T)^2 - m_\beta^2}\,, \end{aligned} \tag{4.9}$$

where we have introduced the “effective electron neutrino mass”, firstly defined in (4.13),

$$m_\beta^2 = \sqrt{\sum_{i=1}^{3} |U_{ei}|^2 m_i^2} = c_{12}^2 c_{13}^2 m_1^2 + s_{12}^2 c_{13}^2 m_2^2 + s_{13}^2 m_3^2 \,. \tag{4.10}$$

Note that $m_\beta$ depends on the three masses $m_i$ and the two mixing angles $\theta_{12}$ and $\theta_{13}$, but not on $\theta_{23}$ The KATRIN $\beta$-decay experiment has recently presented the result $m_\beta < 0.8$ eV [8], representing the first constraint on the effective $\beta$-decay mass in the sub-eV range.

Besides beta decay experiments, measuring the endpoint of the electron energy spectrum, another class of experiments probes the possible neutrinoless double beta decay $(0\nu\beta\beta)$ of some long lived nuclei like $^{76}$Ge, $^{136}$Xe, $^{130}$Te,

$${}^A_Z X \to {}^{A}_{Z+2}Y + 2\,e^- \,. \tag{4.11}$$

As pictorially shown in Figure (4.2), $(0\nu\beta\beta)$ is possible when neutrinos are Majorana particles, since it implies the existence of a vertex where two antineutrinos annihilate each other. The Feynman diagram corresponding to a double neutron decay that happens inside the nucleus is shown in Figure (4.3). The hal-life of a nucleus decaying though a neutrinoless double beta decay

$$\frac{1}{T_{1/2}^{0\nu\beta\beta}} = G|M_{\rm nucl}|^2 m_{\beta\beta} \,, \tag{4.12}$$

depends on the phase space $G$, the nuclear matrix element $M_{\rm nucl}$, and on $m_{\beta\beta}$,

$$m_{\beta\beta} = \left|\sum_i U_{ei}^2 m_i\right| = \left|c_{13}^2 c_{12}^2 m_1 + c_{13}^2 s_{12}^2 m_2 e^{i\phi_2} + s_{13}^2 m_3 e^{i\phi_3}\right| \,. \tag{4.13}$$

firstly introduced in (4.2). In particular, $m_{\beta\beta}$ depends on the absolute neutrino masses $m_i$ and the two mixing angles $\theta_{12}$ and $\theta_{13}$, like $m_\beta$, but also on the two majorana phases, $\phi_2$ and $\phi_3$. Figure (4.4) shows the current limits on the decaying half-life from current experiments. The corresponding bounds on $m_{\beta\beta}$ require the knowledge of the nuclear matrix elements, that are still affected by large theoretical uncertainties. Both $m_\beta$ and $m_{\beta\beta}$ depends on the oscillation parameters.

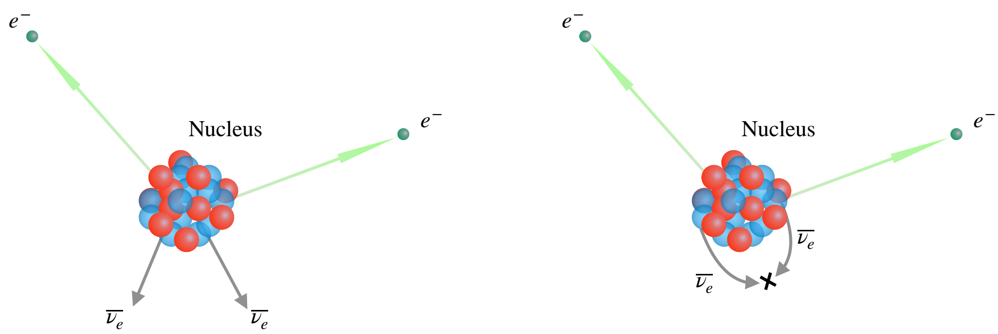


**Figure (4.2) :** On the left, neutrino double beta decay; on the right, neutrinoless double beta decay.

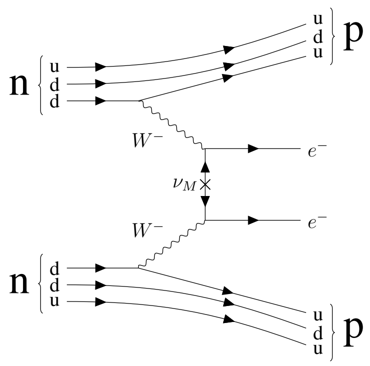


**Figure (4.3) :** Feynman diagram for the neutrinoless double beta decay.

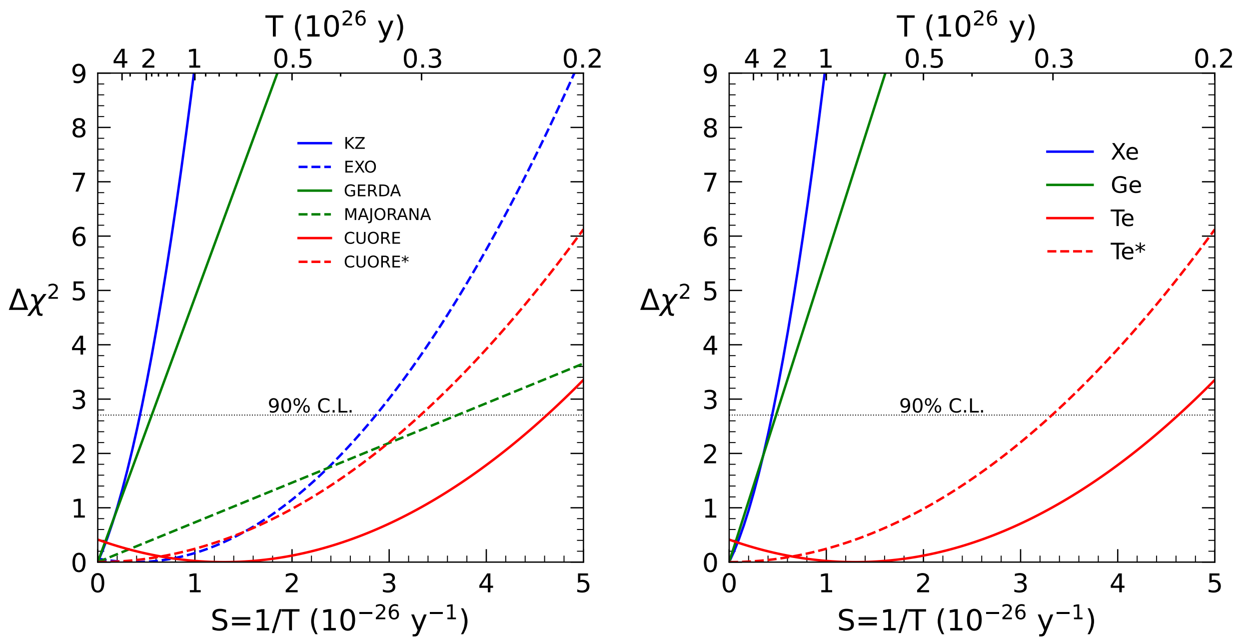


**Figure (4.4) :** $\Delta\chi^2$ functions in terms of the half-life $T$ (top abscissa) and of the signal strength $S = 1/T$ (bottom abscissa). Left and right panels: separate experiments and their combinations for the same isotope, respectively.

The accurate knowledge of the two squared mass differences $\delta m^2$ and $\Delta m^2$, makes it possible to eliminate two absolute masses from the expression of $m_\beta$ and $m_{\beta\beta}$, leaving us with only one unknown mass, for instance the smallest one, $m_1$. Since, as we will see in the following, cosmology and astrophysics constrain the sum of neutrino masses $\Sigma = m_1 + m_2 + m_3$, a second, more physically founded option, is to express $m_1$, $m_2$ and $m_3$ as functions of $\delta m^2$, $\Delta m^2$ and $\Sigma$, in both $m_\beta$ and $m_{\beta\beta}$.

# 5 Supernova Neutrinos

Supernova (SN) neutrinos are of great interest in astroparticle physics for several reasons. On one side, since they are produced during the core-collapse of the star, they can give information on the explosion mechanism. The knowledge of their energy spectrum, and its variation in time, would be very useful to understand better the explosion and the dynamics of the shock wave. From this point of view, neutrinos are a probe to study the interior of a newborn Supernova. On the other side, if the explosion mechanism is well understood, SN neutrinos will allow us to get another measurement of the mass-mixing oscillation parameters, not to mention the neutrino magnetic moment and other possible "nonstandard" $\nu$ properties (for instance, the violation of the Lorentz invariance). So far, 20 neutrino events were observed by the Kamiokande and IMB experiments, during the SN 1987A explosion. Besides the observation of the next galactic SN explosion, nowadays, experiments aim at measuring the diffuse SN neutrino flux, the relics of all past SN explosions. We estimate there are $\sim 10$ supernova explosions per second in the visible Universe, and $1-3$ galactic SN explosion per century. Given that oscillation parameters have been measured with percent accuracy, today, the most important piece of information we could have from a SN neutrino signal is on the mass ordering.

As Figure (5.1) shows, the timescale of the neutrino emission is of the order of about 10 sec, with different flux characteristics and hierarchies. The energy range is ~1-100 MeV with different mean energy hierarchies in the three phases: the neutrino burst, the accretion phase and the proto-neutron star cooling. During the gravitational collapse of the star, neutrinos carry away lepton number and energy. Electron neutrinos are produced by electron captures on nuclei and on free protons, in the first steps of the explosion. Then, they continue to be emitted, driving the evolution toward a deleptonized neutron star. Neutrinos and antineutrinos of all flavors carry out most of the gravitational binding energy of the nucleus and can transfer energy to the shock, thus triggering the explosion. Afterwards, neutrino interactions with the ejected matter affect the heavy element production. While propagating inside the exploding star, neutrino oscillations will change the neutrino spectra. After leaving the SN, neutrinos will undergo vacuum oscillations on their way to the Earth, and, possibly, matter oscillations inside the Earth, depending on the detector position. Matter effects on SN neutrinos have been widely studied to predict the energy spectra, taking into account the shock-wave evolution and stochastic matter fluctuations induced by turbulence (see

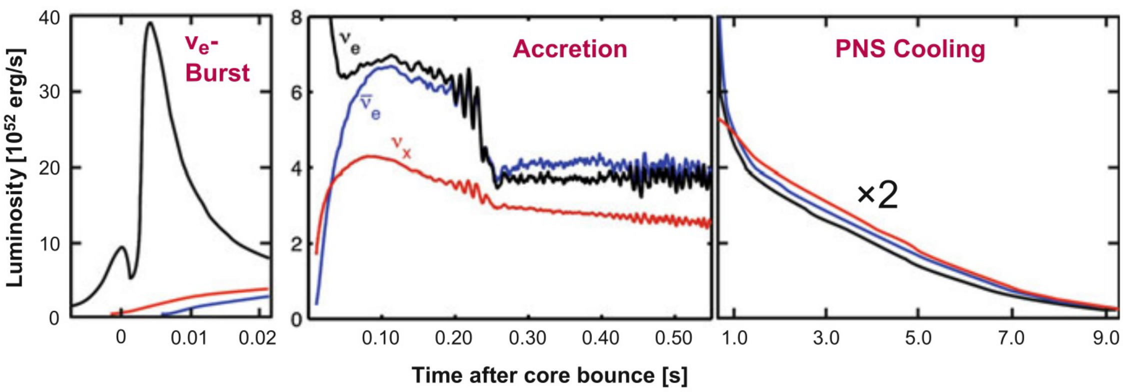


**Figure (5.1) :** Example of SN neutrino fluxes (from arXiv:1702.08825).

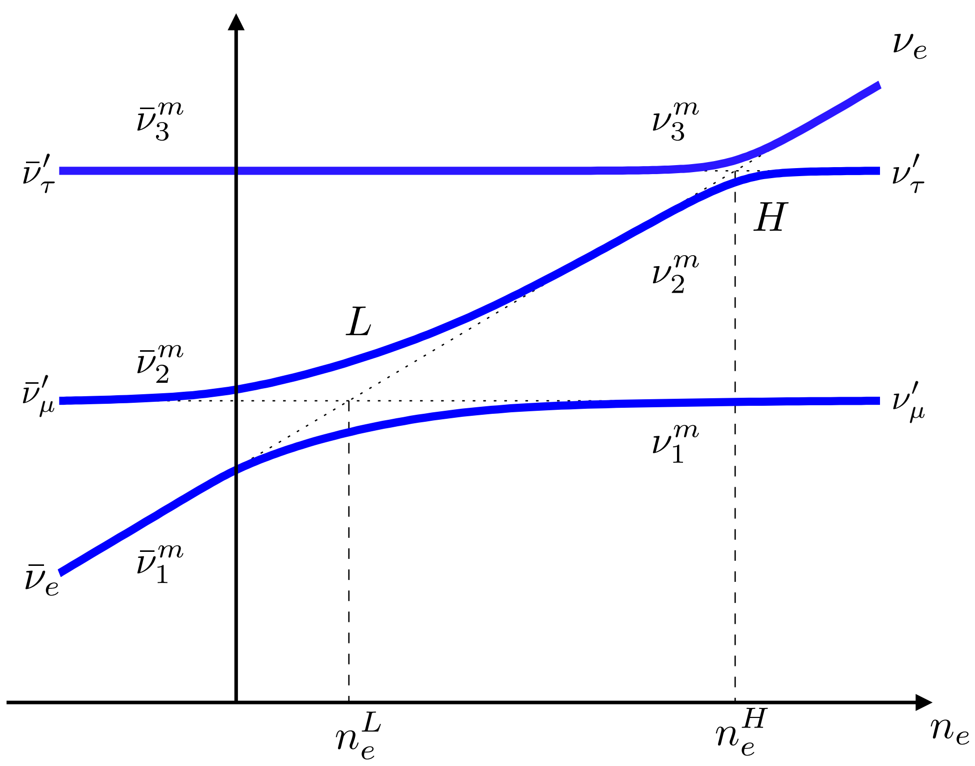


**Figure (5.2) :** Matter effects for SN neutrinos in NO. The evolution starts on the right. $(\nu'_\mu, \nu'_\tau)$ are linear combinations of $(\nu_\mu, \nu_\tau)$ which diagonalise the $2-3$ part of theHamiltonian

for instance [9] for a review). Neutrino streaming through the outer SN layers undergo ordinary MSW transitions, with two resonances, one governed by the atmospheric squared-mass difference (H) and the second by the solar squared-mass difference (L), when the distance from the center is larger than about $\sim 1000$ km. The dynamics can be approximately factorised into two generation neutrino oscillations with relevant parameters $(\Delta m^2, \theta_{13})$ or $(\delta m^2, \theta_{12})$. Let us recall that

$$\begin{aligned} \sin 2\theta_{\rm m} &= \frac{\sin 2\theta}{\sqrt{(\cos 2\theta_{12} - A_{CC}/\Delta m^2)^2 + \sin^2 2\theta_{12}}} \,, \\ \cos 2\theta_{\rm m} &= \frac{\cos 2\theta - A_{CC}/\Delta m^2}{\sqrt{(\cos 2\theta_{12} - A_{CC}/\Delta m^2)^2 + \sin^2 2\theta_{12}}} \,. \end{aligned} \tag{5.1}$$

In the limit $A_{CC} \to \infty$, at the production point the density is extremely large ($\sim 10^{12}$ gr/cm$^3$), one has $\theta_{\rm m} \to (0, \pi)$, depending on the squared mass difference considered. For antineutrinos, the potential changes its sign and we have

| | NormalOrdering | InvertedOrdering |
|---|---|---|
| $\nu$ | $(\theta_{\rm m13}, \theta_{\rm m12}) = (\pi/2, \pi/2)$ | $(\theta_{\rm m13}, \theta_{\rm m12}) = (0, \pi/2)$ |
| $\overline{\nu}$ | $(\theta_{\rm m13}, \theta_{\rm m12}) = (0, 0)$ | $(\theta_{\rm m13}, \theta_{\rm m12}) = (\pi/2, 0)$ |

because $\delta m^2 > 0$ and the sign of $\Delta m^2$ is +1 (-1) in NO (IO). For NO one has $(\nu_e \equiv \nu_{\rm m1},\ \overline{\nu}_e \equiv \overline{\nu}_{\rm m3})$ and for IO $(\nu_e \equiv \nu_{\rm m2},\ \overline{\nu}_e \equiv \overline{\nu}_{\rm m3})$, at the production point. Afterwards, given the small value of

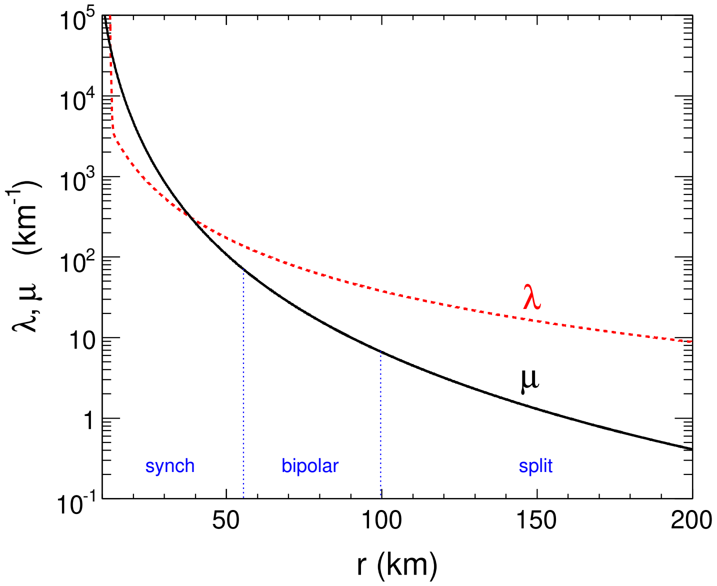


**Figure (5.3) :** Radial profiles of the neutrino self-interaction parameter $\mu(r)$ and of the matter-interaction parameter $\lambda(r)$. The approximative ranges where self-interaction effects are expected to produce mainly synchronization, bipolar oscillations and spectral split are also shown.

$\theta_{13}$, the evolution for NO is adiabatic, as schematically shown for in Figure 5.2, with decreasing electron density from right to left. In this plot $\nu'_\mu$ and $\nu'_\tau$ are linear combination of $\nu_\mu$ and $\nu_\tau$ that diagonalize the $2-3$ sector of the hamiltonian. The fluxes for the mass eigenstates at the SN surface ($F$) can be calculated as a function of the initial fluxes ($F^0$) and the transition probabilities at the resonances (rescaled by the distance$^{-2}$). For instance, one has

$$F_{\nu_1} = P_H P_L F^0_{\nu_{m3}} + (1-P_L)F^0_{\nu_{m1}} + P_L(1-P_H)F^0_{\nu_{m2}} \,, \tag{5.2}$$

where $P_L$ and $P_H$ are the transition probabilities, that are equal to zero for adiabatic propagation.

If we denote with $E$, the neutrino energy, $N_e(r)$ the electron number density at a distance $r$

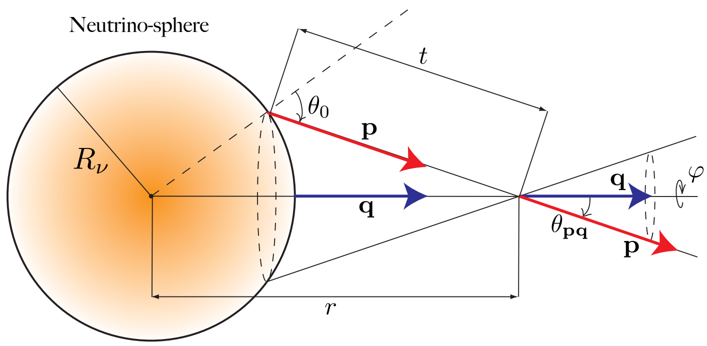


**Figure (5.4) :** Spherical simplified SN geometry: the bulb model. The single angle approximation is equivalent to consider $\theta_0 = \pi/4$ for all neutrinos.

from the SN center, than the two quantities

$$\omega = \frac{\Delta m^2}{2E} \, , \quad \lambda(r) = \sqrt{2}\, G_F\, N_e(r) \, , \tag{5.3}$$

are of the same order, $\omega \sim \lambda(r)$, when matter effects are important, (note that also $\lambda$ is a frequency). The parameter $\lambda$ is the interaction energy difference between $\nu_e$ and $\nu_{\mu,\tau}$ (see equation (2.36)). The radius $r$, for which $\omega \sim \lambda(r)$, is typically of the order of hundreds or thousands of kilometers. However, there is another interaction that must be considered, the neutrino interaction on the neutrino background itself. When the parameter $\mu$, defined aas

$$\mu(r) = \sqrt{2}\, G_F\, [N(r) + \overline{N}(r)] \tag{5.4}$$

where $N(r)$ and $\overline{N}(r)$ are the total neutrino and antineutrino number density, is larger or of the order of $\omega$, we can expect the neutrino self-interactions to be important. Self-interactions can induce "collective" flavor transition in which neutrinos of different energies can oscillate together. In this context, it is convenient to use the formalism of the density matrix to describe neutrino oscillations. The density matrix $\rho$ is defined as

$$\rho = \begin{pmatrix} \rho_{ee} & \rho_{ex} \\ \rho_{xe} & \rho_{xx} \end{pmatrix} = \begin{pmatrix} |\nu_e|^2 & \nu_e \nu_x^* \\ \nu_e^* \nu_x & |\nu_x|^2 \end{pmatrix} \, , \tag{5.5}$$

The diagonal entries of $\rho$ are the occupation numbers for the corresponding flavor and diagonal terms are related to te oscillations. Actually $\rho = \rho(\vec{p}, \vec{r}, t) = \rho_{\vec{p},\vec{r},t}$ and depends on the radius, the momentum and changes with time. With $\overline{\rho}_{\vec{p},\vec{r},t}$ we denote the density matrix for antineutrinos. The differential equation governing the evolution of $\rho$ is

$$\partial_t \rho_{\vec{p},\vec{r},t} + \vec{v}_{\vec{p}} \cdot \nabla_{\vec{r}} \rho_{\vec{p},\vec{r},t} = -i[\Omega_{\vec{p},\vec{r},t}, \rho_{\vec{p},\vec{r},t}] \, , \tag{5.6}$$

where $\Omega = \Omega_{\text{vac}} + \Omega_{\text{MSW}} + \Omega_{\nu\nu}$ contains three terms depending, respectively, on $\omega$, $\lambda$ and $\mu$:

$$\begin{aligned} \Omega_{\text{vac}} &= \frac{1}{2E} U M_{\text{diag}} U^\dagger, \\ \Omega_{\text{MSW}} &= \sqrt{2}\, G_F\, N_e(r) \text{diag}(1,0,0) \, , \\ \Omega_{\nu\nu} &= \sqrt{2} G_F \int \frac{d^3 q}{(2\pi)^3} (\rho_{\vec{p},\vec{r},t} - \overline{\rho}_{\vec{q},\vec{r},t})(1 - \vec{v}_{\vec{q}} \cdot \vec{v}_{\vec{p}}) \, . \end{aligned} \tag{5.7}$$

The last term makes the differential equation nonlinear and contains a term dependent on the neutrino-neutrino scattering angle. The angular term averages to zero for an isotropic neutrino distribution. In the case of a SN, instead, this cannot be true and neutrinos propagating in different directions feel different interactions. As a first step to tackle the problem, one can use a simplified model, the so-called bulb model, depicted in Figure (5.4). If we average out the angle between $\vec{p}$ and $\vec{q}$ in the third term of (5.7), or we fix the angle between $\vec{p}$ and $\vec{q}$ to be $\pi/4$, then we obtain the "single-angle" approximation. The effect of the collective oscillations is to create spectral splits and swaps in the original spectra. An example is shown in Figure (5.5): the spectral split effect on the neutrino spectrum (left panel) and the corresponding swap of $\nu_e$ and $\nu_x$ fluxes above $E_c \simeq 7$ MeV. In the right panel, the antineutrino spectra are nearly completely swapped with respect to the initial ones. The multi-angle calculation, see Figure (5.6), shows the same qualitative

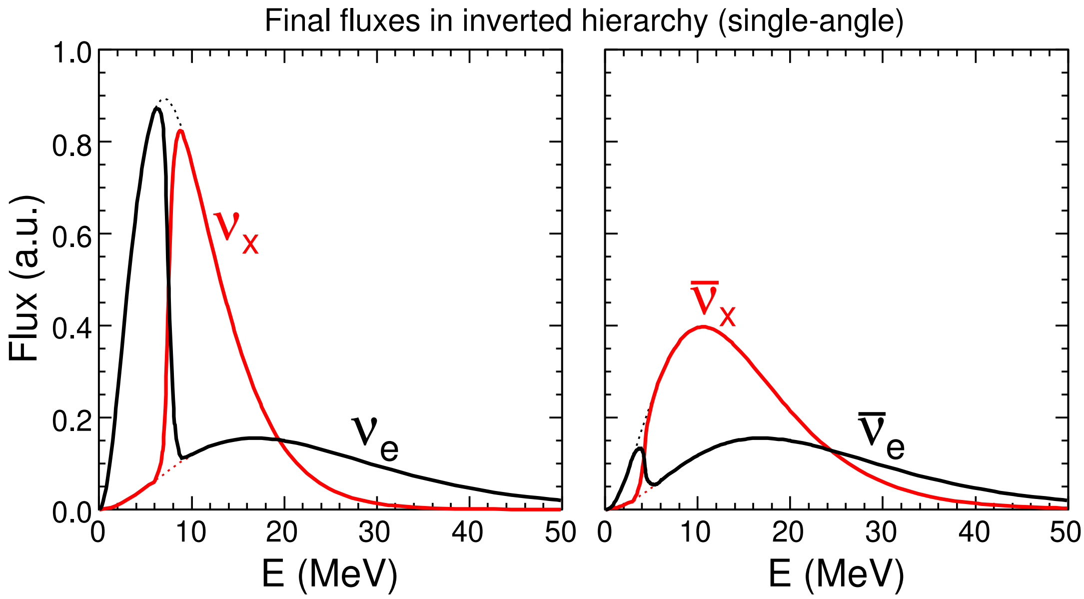


**Figure (5.5) :** Single-angle simulation in inverted hierarchy: Final fluxes (at $r = 200$ km, in arbitrary units) for different neutrino species as a function of energy. Initial fluxes are shown as dotted lines to guide the eye.

behavior with respect to the splits and swaps of the spectra, but less pronounced. The spectra of Figures (5.5) and (5.6) are computed for inverted mass ordering and, for the particular set of input parameters for the calculation, are absent in normal ordering. Actually, the spectral splits form in the last part of the collective oscillation regime, as shown in Figure (5.3), after the synchronization and bipolar regimes. The synchronization and bipolar oscillations owe their name to the fact that neutrinos of all energies oscillate synchronously, and that there is an analogy with the motion of a spherical pendulum. For some time, it was believed that these effects could be a clear signature for the inverted ordering of the neutrino mass spectrum, although nonspherical symmetry, more realistic anisotropic initial neutrino spectra and inhomogeneities of the neutrinosphere could have complicated the outcome of the simulations. It was soon realized, however, that for the three-neutrino case, depending on the relative luminosities of the different flavors, multiple spectral splits can arise, both for neutrinos and antineutrinos, also for normal ordering. Finally, very recently, it has been realized that there is another kind of self-induced oscillations, called fast oscillations, in opposition to the collective "slow" oscillations we have talked about until now. When neutrinos are emitted half isotropically, like in the bulb model, it is impossible to have an angular crossing of the spectra. An angular crossings of the neutrino spectra can lead to new instabilities, on extremely short time scales, even without neutrino mixing. These fast oscillations can develop on a scale length of 1 m or so, due to conversions of the kind $\nu_e(\vec{p}) + \nu_x(\vec{q}) \to \nu_x(\vec{p}) + \nu_e(\vec{q})$ and $\nu_e(\vec{p}) + \overline{\nu_e}(\vec{q}) \to \nu_x(\vec{p}) + \overline{\nu}_x(\vec{q})$ and equalize the neutrino spectra, so that the subsequent oscillations are ineffective. At the moment, a complete understanding of all these oscillation regimes is far from been achieved, and an intense theoretical effort is underway.

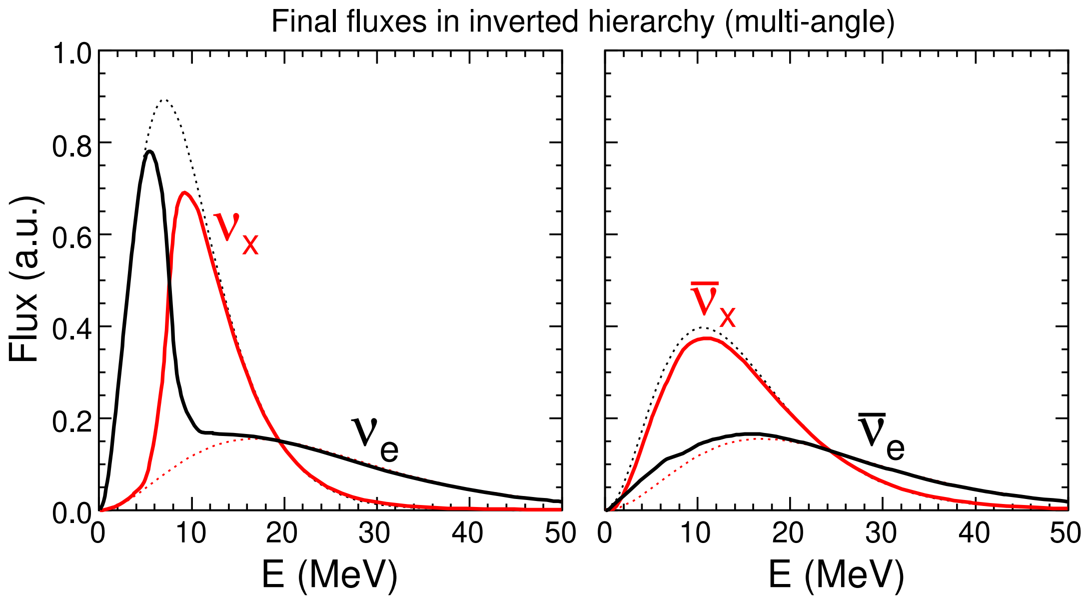


**Figure (5.6) :** Multi-angle simulation in inverted hierarchy: Final fluxes (at $r = 200$ km, in arbitrary units) for different neutrino species as a function of energy. Initial fluxes are shown as dotted lines to guide the eye.

# 6 Neutrinos in Cosmology

Neutrino physics if of fundamental importance to understand the evolution of the early Universe, in particular with respect to the contribution to the total energy density, to the CNB, to the Big Bang Nucleosynthesis and to formation and evolution of large scale structures (LSS). In turn, cosmological observations can aid in studying the properties of neutrinos. The isotropy and homogeneity of the early Universe implies that, on large scales, the metric is $g_{\mu\nu} = \mathrm{diag}(1, -a(t), -a(t), -a(t))$, the Friedmann- Robertson-Walker (FRW) metric. Here $a(t)$ is the scale factor, an adimensional parameter depending on the Hubble constant $H$:

$$H = \frac{\dot{a}(t)}{a(t)} \,. \tag{6.1}$$

The scale factor $a(t)$ determines the physical distance $D(t)$ in term s of the comoving coordinate $r$: $D(t) = ra(t)$. As a function of the redshift $z$, we have $a(t) = a(t_0)/(1 + z_0)$ or $z = (a(t_0) - a(t))/a(t)$. The Universe evolution can be studied by solving the Einstein equations in the FRW metric:

$$\begin{aligned} H^2 = \left(\frac{\dot{a}}{a}\right)^2 &= \frac{8}{3}\pi G\rho \, - \frac{k}{a^2} + \frac{\Lambda}{3}, \\ H^2 + \dot{H} = \frac{\ddot{a}}{a} &= \frac{4}{3}\pi G(\rho + 3p) + \frac{\Lambda}{3} \,, \end{aligned} \tag{6.2}$$

where $k$ is the curvature, $\Lambda$ the cosmological constant, $\rho$ the energy density and $p$ is the pressure. In the following, we will neglect the $k$ and $\Lambda$ terms, since we will discuss very early times, when the Universe is radiation dominated. By combining the two equations (6.2) with the definition of $H$, one obtains

$$\dot{\rho} = -3H(\rho + p) \,. \tag{6.3}$$

If we assume that pressure and density are related by an equation of state $p = \rho w$, with constant $w$, then we obtain

$$\rho \propto a^{-3(1+w)} \,. \tag{6.4}$$

If we separate the total density energy in the contributions from matter, vacuum and radiation, $\rho = \rho_m + \rho_v + \rho_r$, with $\Lambda = 8\pi G\rho_v$, from the first equation (6.2) one obtains

$$\begin{array}{llll} p = \rho/3 & \rho_r \propto a^{-4} \propto t^{-2} & a \propto t^{1/2} & \text{radiation era} \\ p = 0 & \rho_r \propto a^{-3} \propto t^{-2} & a \propto t^{2/3} & \text{matter era} \\ p = -\rho & \rho_v = \text{constant} & a \propto e^{\sqrt{\Lambda/3}t} & \text{vacuum era} \,. \end{array} \tag{6.5}$$

It is reasonable to expect that the matter density scales with the volume ($\rho_m \propto a^{-3}$), while the extra $a^{-1}$ for radiation comes from the redshift. $\rho_v \propto a^{-4}$ is true not only for photons but for all relativistic particles. For a radiation dominated Universe, the first equation of (6.2) gives

$$\rho_r = \frac{3}{32\pi G\, t^2} \,. \tag{6.6}$$

The energy density for relativistic neutrinos can be calculated from the Fermi-Dirac distribution

$$f_\nu(\vec{p}) = \frac{1}{e^{(E-\mu)/T} + 1} \,, \tag{6.7}$$

where $E$ is the neutrino energy, $T$ its temperature and $\mu$ the chemical potential. In the relativistic limit, $E \sim p$ and $T \gg m_\nu$, one obtains

$$\begin{aligned} n_\nu &= \frac{g_\nu}{(2\pi)^2}\int f_\nu(\vec{p})d^3p = \frac{3\zeta(3)}{4\pi^2}g_\nu T^3 \ , \\ \rho_\nu &= \frac{g_\nu}{(2\pi)^2}\int E f_\nu(\vec{p})d^3p = \frac{7\pi^2}{240}g_\nu T^4 \ , \\ p_\nu &= \frac{g_\nu}{(2\pi)^2}\int f_\nu(\vec{p})d^3p \sim \frac{\rho_\nu}{3} \ , \end{aligned} \tag{6.8}$$

where $g_\nu$ is the number of spin states (only one for strictly massless neutrinos). By performing an analogous calculation for bosons, one finds in the end

$$\rho_{\text{bos. + ferm.}} = \frac{g_*\pi^2}{30}T^4 \ , \tag{6.9}$$

where the effective number of degrees of freedom $g_*$ is

$$g_* = \sum_{\text{bos.}} g_b + \frac{7}{8}\sum_{\text{ferm.}} g_f \ , \tag{6.10}$$

in the radiation dominated epoch. By combining (6.9) and (6.6) one finds

$$t = \sqrt{\frac{45}{16 g_* G\pi^3}}\frac{1}{T^2} \sim \frac{0.301}{\sqrt{g_*}}\frac{M_{\text{Planck}}}{T^2} \sim 2.42 g_*^{-1/2}\left(\frac{T}{\text{MeV}}\right)^{-2} \ \text{sec} \ , \tag{6.11}$$

where $M_{\text{Plank}} = 1/\sqrt{G} \sim 1.2 \times 10^{19}$ GeV is the Plank mass. From the evolution equations (6.2) one has for the Hubble constant

$$H = \frac{\dot{a}}{a} = \frac{1}{2t} \sim 1.66\sqrt{g_*}\frac{T^2}{M_{\text{Planck}}} \ . \tag{6.12}$$

The effective number of degrees of freedom is a decreasing function of the time and so decreases when temperature drops. A particle decouples from the thermal bath when its interaction rate $\Gamma$ becomes smaller than the rate of change of temperature, $|\dot{T}_\gamma|/T_\gamma$. When this condition is satisfied, the interactions are not so fast to maintain the particle in equilibrium with the plasma: the particle decouples. For an instantaneous decoupling $T_\gamma \sim a^{-1}$ and $\dot{T}_\gamma/T_\gamma \sim -H$. Therefore, at the decoupling $\Gamma \sim H$. This condition means also that the mean free path ($\sim \Gamma^{-1}$) is of the same order as the horizon ($\sim H^{-1}$). After the decoupling, the number of decoupled particles in the comoving volume stays constant, so that the number density scales as $a^{-3}$. It can be demonstrated that if the particle is relativistic at the decoupling, then the momentum distribution retains its initial form (a Fermi-Dirac for neutrinos), with the temperature scaling with $a^{-1}$. At high temperature, $T$ larger that all the SM masses, all particles are in thermal equilibrium and $g_* \sim 106.75 = 28 + 7/8 \times 90$. When $T \sim \Lambda_{QCD} \sim 200$ MeV, and $t \sim 7 \times 10^{-6}$ sec, $g_* \sim 18 + 7/8 \times 50 \sim 61.75$, because only photons, gluons, the quarks $u$, $d$, $s$, electrons, muons, neutrinos and their antiparticles remain. When the expansion cools the Universe down to a few MeV, only photons, electrons positrons, neutrinos and antineutrinos are in thermal equilibrium, so that $g_* = 2 + 7/8 \times 10 = 10.75$. The reactions that keep neutrinos in equilibrium are $\nu + \overline{\nu} \leftrightarrow e^+ + e^-$ and elastic scattering on electrons. We have

$$\Gamma = n_\nu \langle \sigma v \rangle \sim a^{-3} G_F^2 T_\gamma^2 \sim G_F^2 T_\gamma^5 \ , \tag{6.13}$$

where $v \sim 1$ and we used that $a \sim t^{1/2}$, $t \sim T^{-2}$ and therefore $a \sim T^{-1}$. The equation (6.13) in combination with (6.11) gives for neutrinos

$$\boxed{T_{\rm decoupling} \sim (M_{\rm Planck} G_F^2)^{-1/3} \sim 1{\rm MeV}\ .} \tag{6.14}$$

Below $T^0 \sim 1$ MeV neutrinos are decoupled from the plasma ($T$ is the photon temperature) and their temperature falls as $T_\nu = T^0(1+z)$. However, at a temperature of about $m_e/3 \sim 0.2$ MeV, electrons and positrons too become nonrelativistic and annihilate. Their entropy is transferred to the photons, the only remaining relativistic particles. Entropy conservation ($g_*^3 T_\gamma \sim {\rm const}$) implies that the number of relativistic interacting particles in a comoving volume is constant when $g_*$ is constant, and that

$$T_\gamma = T_\gamma^0 \left(\frac{2}{g_*}\right)^{1/3} (1+z)\ . \tag{6.15}$$

At $T \sim 0.2$ MeV, $g_*$ goes from $2+7/8\times 4 = 11/2$ to 2, since 4 d.o.f. for $e^\pm$ are lost. Consequently, the ratio between photon and neutrino temperatures at $T \sim 0.2$ MeV is

$$\frac{T_\nu^0}{T_\gamma^0} = \left(\frac{2}{g_*}\right)^{1/3} = \left(\frac{2}{11/2}\right)^{1/3} = \left(\frac{4}{11}\right)^{1/3} \sim 0.714\ . \tag{6.16}$$

Therefore, the neutrino temperature today is

$$\boxed{T_\nu^0 = \left(\frac{4}{11}\right)^{1/3} T_\gamma^0 = \left(\frac{4}{11}\right)^{1/3} 2.725\ {\rm K} = 1.945\ {\rm K}\ .} \tag{6.17}$$

Given the neutrino temperature today, their density, see the first of (6.8), is

$$n_\nu = \frac{3\zeta(3)}{4\pi^2} g_\nu T^3 \sim 1.34\ {\rm K}^3 \sim 1.34 \frac{{\rm K}^3}{{\rm cm}^{-3}} {\rm cm}^{-3} \sim 1.34 \times 4.367^3\ {\rm cm}^{-3} \sim 112\ , \tag{6.18}$$

neutrinos and antineutrinos for each species, as we already knew (section 3.2).

Massive neutrinos can significantly contribute to the energy density of the Universe. This contribution can be evaluated by adding up the mass times the number density, for each neutrino and antineutrino. Plugging in the value of the critical density ($\rho_c \sim 5 \times 10^3$ eV cm$^{-3}$) one finds

$$\boxed{\Omega_\nu h^2 = \frac{\sum m_\nu}{93.14}\ ,} \tag{6.19}$$

where $\Omega_\nu$ is the neutrino energy density and $h = H_0/(100\ {\rm km\ s^{-1}\ Mpc^{-1}})$.

Cosmological data, and in particular the cosmic wave background, the BBN, and the formation of the LSS, are sensitive to the number of relativistic degrees of freedom, since the Universe evolution is influenced by the relativistic number of degrees of freedom that determines the value of $g_*$ as a function of the temperature. If we assume that the only relativistic degrees of freedom, besides photons, are neutrinos, then the "effective number of neutrino species" is 3. The precise value is 3.046, where the small deviation from 3 comes from the fact that the neutrino decoupling is not instantaneous, and that they are not completely decoupled when the temperature falls to 0.2 MeV. The present measurements give the constraint $N \sim 3 \pm 0.2$, depending on the cosmological model and on the data that are combined. A summary is shown in Figure (6.1). As we have seen,

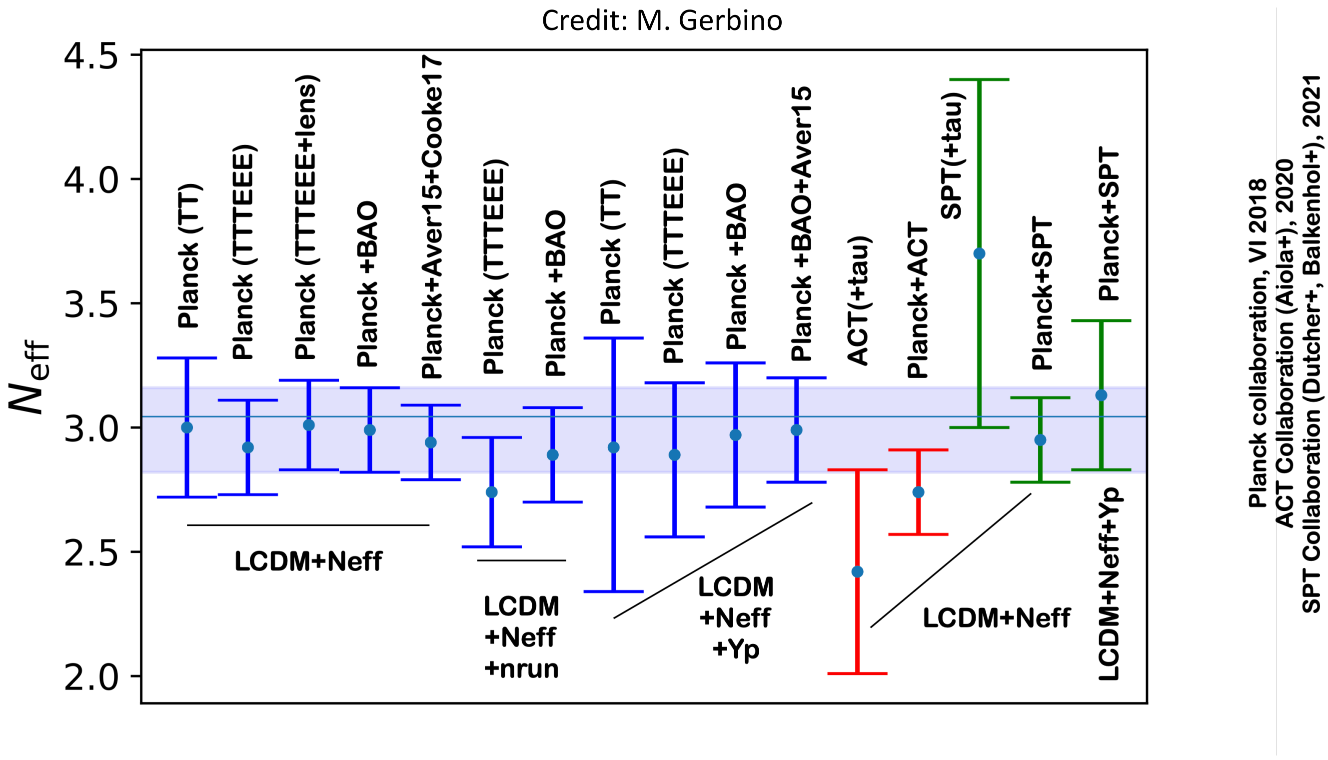


**Figure (6.1) :** Solar neutrinos

neutrino contribute to the overall energy density of the universe. They also play a relevant role in large scale structure formation. Neutrinos suppress the growth of fluctuations on scales below the horizon when they become nonrelativistic. Massive neutrinos with masses $\lesssim 1$ eV produce a significant suppression in the clustering on small cosmological scales. The relevant parameter constrained by cosmological data is the sum of neutrino masses $\Sigma = m_1 + m_2 + m_3$. Current experimental precision gives very poor sensitivity to the details of the mass spectrum and on the mass ordering. Current limits on $\Sigma$ depends on the details of the cosmological model, because of the many degeneracies among the cosmological parameters. Interesting information and synergies arise when cosmological data constraints are combined with results from neutrinoless double beta decay and beta decay, also sensitive to absolute masses, and when, finally, they are combined with the analysis of oscillation data.

## 6.1 Combination of oscillation and nonoscillation experiments

As we have seen, beta decay and neutrinoless beta decay experiments are sensitive to the neutrino absolute masses, through the observables $m_\beta$ and $m_{\beta\beta}$, that we rewrite here for clarity

$$\begin{aligned} m_\beta &= \left[c_{13}^2 c_{12}^2 m_1^2 + c_{13}^2 s_{12}^2 m_2^2 + s_{13}^2 m_3^2\right]^{\frac{1}{2}} , \\ m_{\beta\beta} &= \left|c_{13}^2 c_{12}^2 m_1 + c_{13}^2 s_{12}^2 m_2 e^{i\phi_2} + s_{13}^2 m_3 e^{i\phi_3}\right| , \end{aligned} \tag{6.20}$$

while cosmological and astrophysical data constrain the sum of neutrino masses $\Sigma$. However, these three observables contain the mixing angles and, implicitly the mass squared differences, that are constrained by the oscillation experiments and so they are not independent of each other.

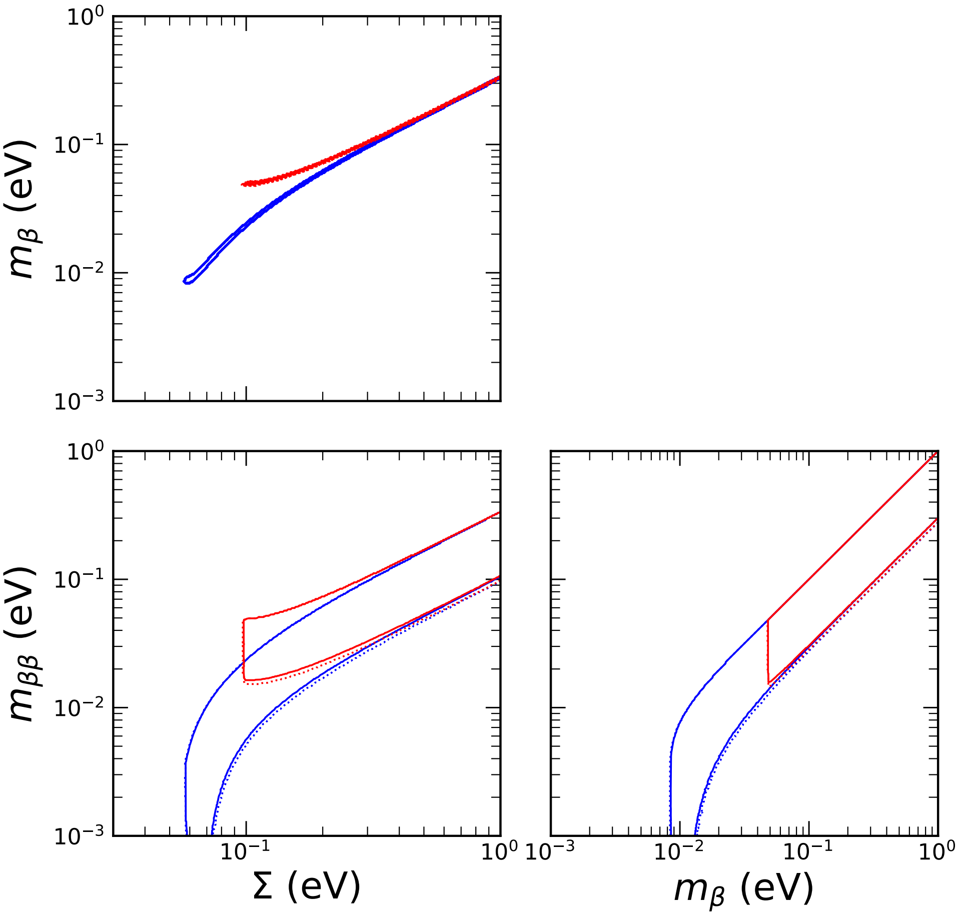


**Figure (6.2) :** Oscillation bounds on the nonoscillation observables ($\Sigma$, $m_\beta$, $m_{\beta\beta}$), in each of the three planes charted by a pair of such observables. Bounds are shown as contours at $2\sigma$ (solid) and $3\sigma$ (dotted) for NO (blue) and IO (red) taken separately. Majorana phases are marginalized away. Note that we take $\Delta\chi^2_{\mathrm{IO-NO}} = 0$ in this figure.

For instance, in NO, one can write the three equations

$$
\begin{aligned}
m_2 &= \sqrt{m_1^2 + \delta m^2}\ , \\
m_3 &= \sqrt{m_1^2 + \delta m^2/2 + \Delta m^2}\ , \\
\Sigma &= m_1 + m_2 + m_3 = m_1 + \sqrt{m_1^2 + \delta m^2} + \sqrt{m_1^2 + \delta m^2/2 + \Delta m^2}\ .
\end{aligned}
\tag{6.21}
$$

By fixing a value for $\Sigma$, and solving the third equation of (6.21), one can derive $m_2$ and $m_3$ as a function of $\Sigma$. Moreover, experimental errors on the squared mass differences can be propagated to $\Sigma$. We prefer to use the sum of neutrino mass, as an independent variable, since $m_1$ is unobservable and cosmological data directly constrain $\Sigma$. The two parameters $m_\beta$ and $m_{\beta\beta}$ depend on the neutrino masses and so are correlated to $\Sigma$.

The correlations between the three absolute-mass-related observables $(\Sigma, m_\beta, m_{\beta\beta})$ are shown in Figure (6.2), where all the experimental measurements on neutrino oscillation parameters have been used. The blue (red) contours show the allowed region at $2\sigma$ for NO (IO), in each of the three projected planes of the space ($\Sigma$, $m_\beta$, $m_{\beta\beta}$). The spread of the bands on $m_{\beta\beta}$ bounds comes mostly from the unknown majorana phases. You will immediately notice two things:

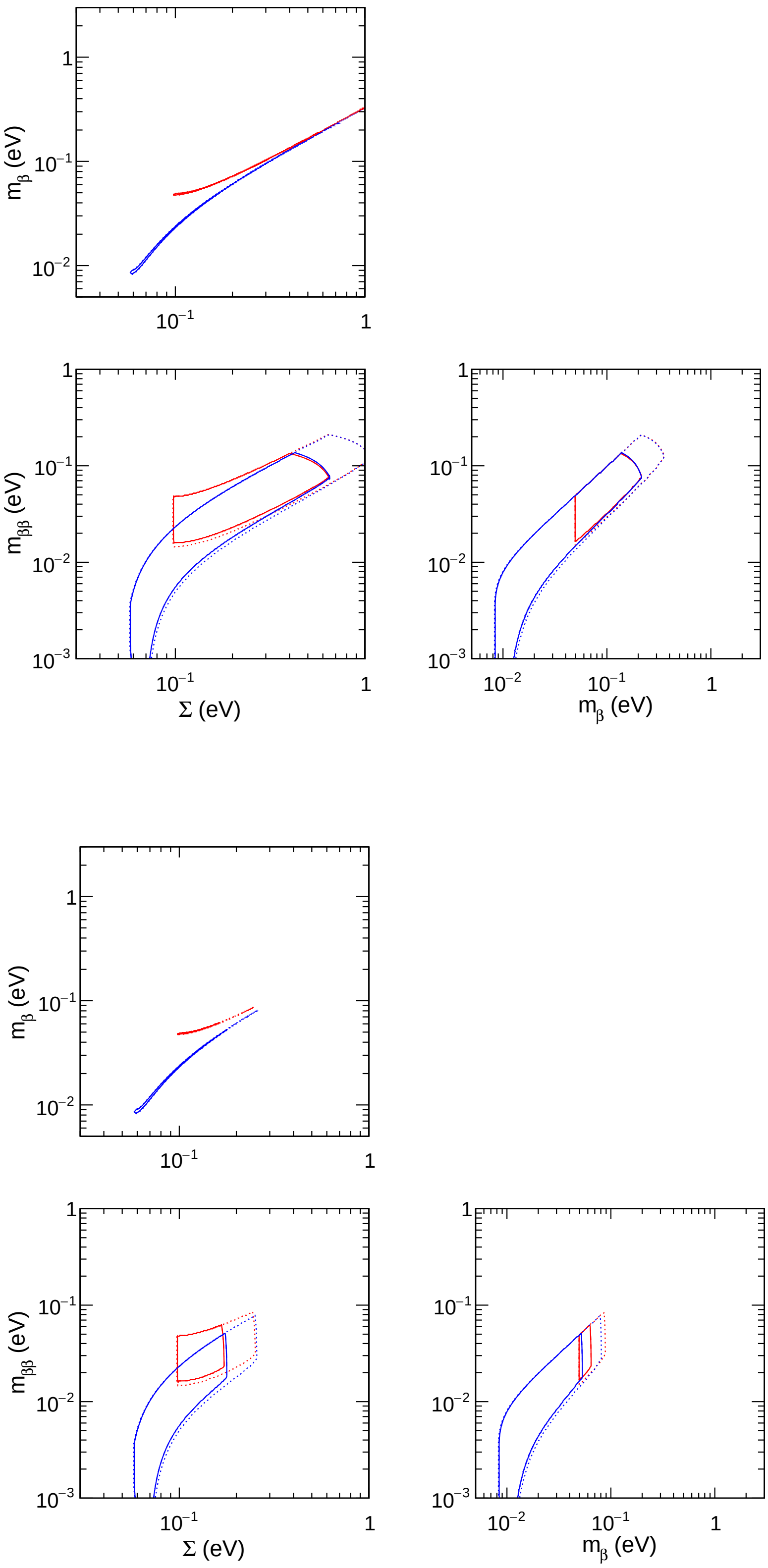


Figure (6.3) : Example of a combined $3\nu$ analysis of oscillation and nonoscillation data, with different cosmological datasets (from [10]).

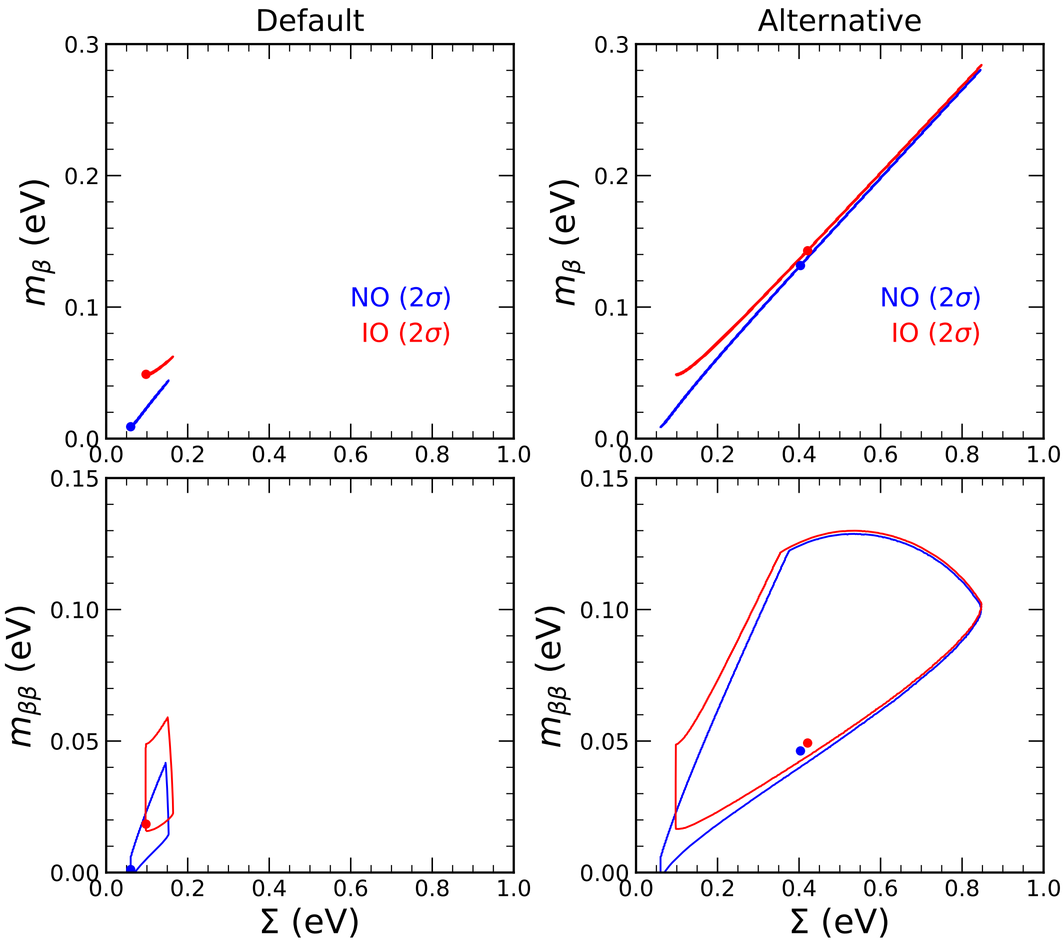


**Figure (6.4) :** Constraints at $2\sigma$ placed by current oscillation data and nonoscillation data from [11]. The dots mark the best fits.

- The minimum allowed value for $\Sigma$ is different in the two orderings, and is smaller in NO than in IO;
- The minimum allowed value for $m_{\beta\beta}$ is zero in NO and larger than zero in IO.

The first thing is a consequence of the fact that in IO there are two massive and one light neutrino states, so that when $m_3 \to 0$ (see Figure (3.1)), $\Sigma \to \sqrt{\Delta m^2 - \delta m^2} + \sqrt{\Delta m^2 - \delta m^2} \sim 2\sqrt{\Delta m^2} \sim 2 \times 0.05$ eV. In NO, instead, when $m_1 \to 0$, $\Sigma \to \sqrt{\delta m^2} + \sqrt{\Delta m^2 + \delta m^2} \sim \sqrt{\Delta m^2} \sim 0.05$ eV. It is worthwhile to note that when, in the future, cosmological data will be sensitive to values of $\Sigma$ in the $0.05 - 0.1$ eV range, strong constraints will be derived on the mass ordering. About the second point, this is a consequence of the cancellations than can take place between the two complex addenda in (6.20): in IO, $m_1$ refers to a neutrino state of the massive doublet, while in NO is the lightest state that can also be massless. Figure (6.3) shows two examples of the combined analysis. Depending on the cosmological data used, the bound on $\Sigma$ can be so strong to begin to test the $\sim 0.1$ eV region. The latest analysis is shown in Figure (6.4), with a

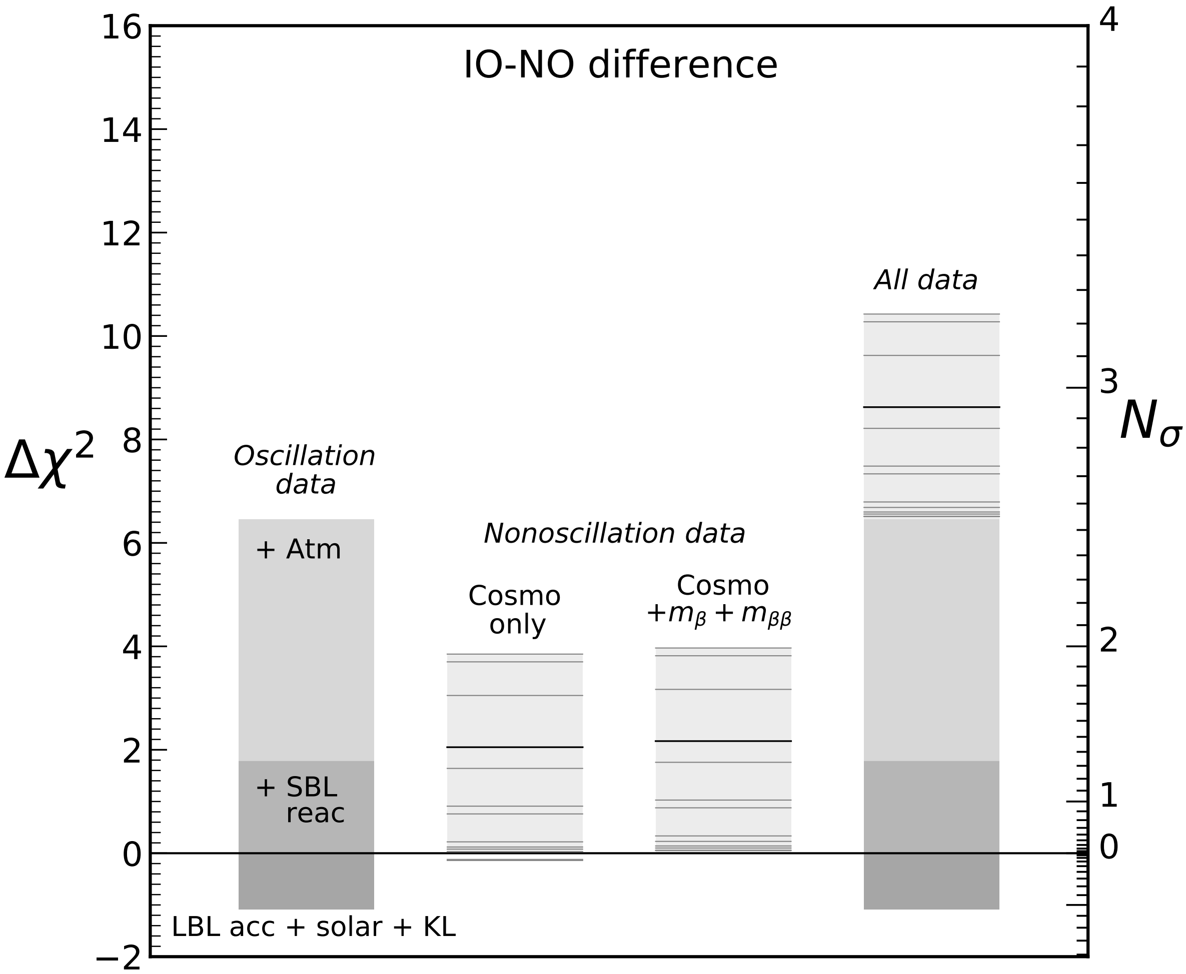


**Figure (6.5) :** Breakdown of contributions to the IO-NO $\chi^2$ difference from oscillation and nonoscillation data (from [10]).

linear scale on all parameters, since we are starting to probe the region where the two mass orderings can be discriminated. In the default case, on the left, the cosmological bounds on $\Sigma$ dominate the constraints on $m_\beta$ and $m_{\beta\beta}$, because $\Sigma < 0.15$ at $2\sigma$ from cosmology alone. In the alternative case, the minimum for $\Sigma$ is not at the smallest allowed value, but is reached for $\Sigma \sim 0.5$ from cosmology alone, and there is an interplay between cosmological and $0\nu\beta\beta$ data. In the default case, the KATRIN experiment (probing $m_\beta > 0.2$ eV) is not expected to find any signal, while planned $0\nu\beta\beta$ experiments are expected to probe at least the region covered by both NO and IO ($m_{\beta\beta} > 0.02$ eV). In the less constraining case, on the right, $\beta$ decay and $0\nu\beta\beta$ decay searches could be able to find some interesting signal.

Finally, Figure (6.5) shows the present information on the mass ordering, by merging the information coming from the analysis of oscillation and nonoscillation The histogram displays how each class of experiments contributes to the $\mathit{\Delta}\chi^2_{\mathrm{IO-NO}}$. On the left, the contributions from oscillation data, LBL accelerator, solar and KamLAND, SBL reactor and atmospheric data are reported. The second bin shows the range spanned by all the cosmological datasets considered in [10], from the fit to cosmological data only. The third bin shows the slight change induced by adding current constraints on $m_\beta$ and $m_{\beta\beta}$. The last bin on the right shows the global combination that results in a preference for NO in the range $\sim 2.5$–$3.2\sigma$.

# Appendices

# A Dirac matrices

Dirac's matrices are four-dimensional matrices that satisfy

$$\{\gamma^\mu, \gamma^\nu\} = 2g^{\mu\nu} \;\text{ and }\; \gamma^0\gamma^{\mu\dagger}\gamma^0 = \gamma^\mu \, . \tag{A.1}$$

The anticommutation relations imply ${\gamma^0}^2 = -{\gamma^i}^2 = \mathbb{1}_{4\times 4}$. It is also easy to verify that $\gamma^0$ is real and ${\gamma^0}^\dagger = \gamma^0$, and so it is also symmetric. The other Dirac matrices satisfy ${\gamma^i}^\dagger = -\gamma^i$. By defining $\gamma_\mu = g_{\mu\nu}\gamma^\nu$, for the four matrices we can write $\gamma^{\mu\dagger} = \gamma_\mu$. The chirality matrix $\gamma_5$ is defined by

$$\gamma_5 = \gamma^5 \equiv i\gamma^0\gamma^1\gamma^2\gamma^3 \, , \tag{A.2}$$

and it anticommutes with all $\gamma$'s and its square is $\mathbb{1}$:

$$\{\gamma^5, \gamma^\mu\} = 0 \quad {\gamma_5}^2 = \mathbb{1} \tag{A.3}$$

The Dirac matrices are not uniquely determined, but there are an infinity of possible choices connected by a similarity transformation by means of a unitary matrix.

## A.1 The standard Pauli-Dirac representation

The standard representation of the Dirac matrices in $2\times 2$ block diagonal form is the following

$$\gamma^0 = \begin{pmatrix} \mathbb{1} & 0 \\ 0 & -\mathbb{1} \end{pmatrix} \qquad \gamma^i = \begin{pmatrix} 0 & \sigma_i \\ -\sigma_i & 0 \end{pmatrix} \qquad \gamma_5 =, \begin{pmatrix} 0 & \mathbb{1} \\ \mathbb{1} & 0 \end{pmatrix} \, , \tag{A.4}$$

where $\sigma_i$ are the Pauli matrices

$$\sigma_1 = \begin{pmatrix} 0 & 1 \\ 1 & 0 \end{pmatrix} \qquad \sigma_2 = \begin{pmatrix} 0 & -i \\ i & 0 \end{pmatrix} \qquad \sigma_3 = \begin{pmatrix} 1 & 0 \\ 0 & -1 \end{pmatrix} \, . \tag{A.5}$$

Note that in the standard representation the $\gamma_0$ matrix is diagonal while $\gamma_5$ is not. In particular, writing the Dirac spinor $\psi$ as $\psi = (\phi, \chi)^T$

$$\gamma_5 \begin{pmatrix} \phi \\ \chi \end{pmatrix} = \begin{pmatrix} \chi \\ \phi \end{pmatrix} \, . \tag{A.6}$$

## A.2 The Weyl representation

In the Wey representation, the Dirac matrices are

$$\gamma^0 = \begin{pmatrix} 0 & -\mathbb{1} \\ -\mathbb{1} & 0 \end{pmatrix} \qquad \gamma^i = \begin{pmatrix} 0 & \sigma_i \\ -\sigma_i & 0 \end{pmatrix} \qquad \gamma_5 = \begin{pmatrix} \mathbb{1} & 0 \\ 0 & -\mathbb{1} \end{pmatrix} \, , \tag{A.7}$$

so that, with respect to the standard representation, $\gamma^0$ and $\gamma^5$ are switched and there is a minus sign in the definition of the $\gamma^0$ while the $\gamma^i$ are unchanged.[10] Now we have that

$$\gamma_5 \begin{pmatrix} \phi \\ \chi \end{pmatrix} = \begin{pmatrix} \phi \\ -\chi \end{pmatrix} \tag{A.8}$$

[10] There is also another convention in which $\gamma^0$ and $\gamma^5$ are switched and the $\gamma^i$ change sign: this amounts to invert the role of $\phi$ and $\chi$ in (A.8) and (A.9).

and

$$\frac{1+\gamma_5}{2}\begin{pmatrix}\phi\\ \chi\end{pmatrix}=\begin{pmatrix}\mathbb{1} & 0\\ 0 & 0\end{pmatrix}\begin{pmatrix}\phi\\ \chi\end{pmatrix}=\begin{pmatrix}\phi\\ 0\end{pmatrix}\ ,$$
$$\frac{1-\gamma_5}{2}\begin{pmatrix}\phi\\ \chi\end{pmatrix}=\begin{pmatrix}0 & 0\\ 0 & \mathbb{1}\end{pmatrix}\begin{pmatrix}\phi\\ \chi\end{pmatrix}=\begin{pmatrix}0\\ \chi\end{pmatrix}\ .$$

# B Chirality

The Weyl representation is particularly useful for the discussion of the Chirality, which is the quantum number associated to the eigenvalues and eigenvectors of $\gamma^5$. Since $\gamma_5^2=\mathbb{1}$, the eigenvalues are $\pm 1$. This is trivial in the Weyl representation where $\gamma_5=\mathrm{diag}(1,1-1-1)$. The properties that we will illustrate here are valid in every representation, but they are self-evident in the Weyl representation. Let call $\psi_R$ and $\psi_L$ the eigenvalues of $\gamma_5$ corresponding to the the eigenvalues $+1$ and $-1$ respectively

$$\gamma_5\psi_R=+1\psi_R \qquad \gamma_5\psi_L=-1\psi_L\ . \tag{B.1}$$

$\psi_R$ and $\psi_L$ are the chirality eigenstates and they can be projected from the projectors $P_R$ and $P_L$ defined by the relations

$$\psi_R=P_R\psi=\frac{1+\gamma_5}{2}\psi \qquad \psi_L=P_L\psi=\frac{1-\gamma_5}{2}\psi\ . \tag{B.2}$$

They satisfy the relations:

$$P_L^2=P_L \qquad P_R^2=P_R \qquad P_LP_R=P_RP_L=0 \qquad P_L+P_R=\mathbb{1}\ , \tag{B.3}$$

and are indeed well defined projectors. Since $\gamma_5$ is real and symmetric, the chirality projectors are hermitian. Moreover, the anticommutation relation $\{\gamma_\mu,\gamma_5\}$ implies

$$P_L\gamma_0=\gamma_0P_R \qquad P_R\gamma_0=\gamma_0P_L\ . \tag{B.4}$$

These properties are useful to demonstrate that

$$\begin{aligned}\overline{\psi_R}&=\overline{P_R\psi}=(P_R\psi)^\dagger\gamma_0=\psi^\dagger P_R^\dagger\gamma_0=\psi^\dagger P_R\gamma_0=\psi^\dagger\gamma_0P_L=\overline{\psi}P_L\ ,\\ \overline{\psi_L}&=\overline{P_L\psi}=(P_L\psi)^\dagger\gamma_0=\psi^\dagger P_L^\dagger\gamma_0=\psi^\dagger P_L\gamma_0=\psi^\dagger\gamma_0P_R=\overline{\psi}P_R\ .\end{aligned} \tag{B.5}$$

We see that $\overline{\psi_R}$ is left–handed and $\overline{\psi_L}$ is right–handed. This fact is self evident if we use the Weyl representation of the Dirac matrices where we explicitly have

$$\begin{aligned}&\overline{\psi_R}=(P_R\psi)^\dagger\gamma_0=\psi^\dagger\begin{pmatrix}\mathbb{1} & 0\\ 0 & 0\end{pmatrix}\begin{pmatrix}0 & -\mathbb{1}\\ -\mathbb{1} & 0\end{pmatrix}=\begin{pmatrix}\phi^\dagger & \chi^\dagger\end{pmatrix}\begin{pmatrix}\mathbb{1} & 0\\ 0 & 0\end{pmatrix}\begin{pmatrix}0 & -\mathbb{1}\\ -\mathbb{1} & 0\end{pmatrix}=\\ &\begin{pmatrix}\phi^\dagger & 0\end{pmatrix}\begin{pmatrix}0 & -\mathbb{1}\\ -\mathbb{1} & 0\end{pmatrix}=\begin{pmatrix}0 & -\phi^\dagger\end{pmatrix}\ ,\end{aligned} \tag{B.6}$$

so that $\overline{\psi_R}$ has lower (left) components. Analogously, for $\overline{\psi_R}$ we have

$$\begin{aligned}&\overline{\psi_L}=(P_L\psi)^\dagger\gamma_0=\psi^\dagger\begin{pmatrix}0 & 0\\ 0 & \mathbb{1}\end{pmatrix}\begin{pmatrix}0 & -\mathbb{1}\\ -\mathbb{1} & 0\end{pmatrix}=\begin{pmatrix}\phi^\dagger & \chi^\dagger\end{pmatrix}\begin{pmatrix}0 & 0\\ 0 & \mathbb{1}\end{pmatrix}\begin{pmatrix}0 & -\mathbb{1}\\ -\mathbb{1} & 0\end{pmatrix}=\\ &\begin{pmatrix}0 & \chi^\dagger\end{pmatrix}\begin{pmatrix}0 & -\mathbb{1}\\ -\mathbb{1} & 0\end{pmatrix}=\begin{pmatrix}-\chi^\dagger & 0\end{pmatrix}\ ,\end{aligned} \tag{B.7}$$

that has upper (right) components. The two fields $\psi_L$ and $\psi_R$ are called Weyl spinors. To be more explicit, we define a four–component Dirac spinor in term of two two–component spinors

$$\psi = \begin{pmatrix} \chi_R \\ \chi_L \end{pmatrix} , \tag{B.8}$$

so that in the Weyl representation

$$\begin{aligned} P_R\psi &= \begin{pmatrix} \mathbb{1} & 0 \\ 0 & 0 \end{pmatrix} \begin{pmatrix} \chi_R \\ \chi_L \end{pmatrix} = \begin{pmatrix} \chi_R \\ 0 \end{pmatrix} \\ P_L\psi &= \begin{pmatrix} 0 & 0 \\ 0 & \mathbb{1} \end{pmatrix} \begin{pmatrix} \chi_R \\ \chi_L \end{pmatrix} = \begin{pmatrix} 0 \\ \chi_L \end{pmatrix} . \end{aligned} \tag{B.9}$$

Therefore, the upper components correspond to a right–handed particle, while the lower components correspond to a left–handed one.[11] It is easy now to prove, or to convince ourselves just from (B.7) and (B.6), that the all the terms of the kind $\overline{\psi_L}\psi_L$ and $\psi_L\partial\!\!\!/\psi_R$ are equal to zero, and the Lagrangian for a free massless Dirac field, in terms of their chiral components, can be written as

$$\mathcal{L} = \overline{\psi_L} i\partial\!\!\!/\psi_L + \overline{\psi_R} i\partial\!\!\!/\psi_R - m(\overline{\psi_L}\psi_R + \overline{\psi_R}\psi_L) . \tag{B.10}$$

From (B.10), we can obtain the Euler–Lagrange equations in terms of the chiral fields

$$\begin{aligned} i\partial\psi_L &= m\psi_R , \\ i\partial\psi_R &= m\psi_L . \end{aligned} \tag{B.11}$$

Therefore, for massless particles the equations for the chiral fields decouple. Once again, it is worthwhile to stress that the Weyl representation is particularly useful because, in this representation, the Weyl spinors are simply the upper and the lower two–component parts of the four–dimensional Dirac spinor.

[11] With an abuse of notation, sometimes $\psi_R$ ($\psi_L$) is written instead of $\chi_R$ ($\chi_L$). The dimension of the spinor, four or two, shoud be clear from the context.

# C Mixing matrix

## C.1 Biunitary transformation

A general $N \times N$ complex matrix $M$ can be diagonalized through a biunitary transformation If $M$ is nondegenerate, $\det M \neq 0$, the matrix $A = MM^\dagger$ is Hermitian, and its eigenvalues are strictly positive. In fact

$$A^\dagger = (MM^\dagger)^\dagger = M^{\dagger\dagger} M^\dagger = A \,, \tag{C.1}$$

and

$$\begin{aligned} &\forall x^T = (x_1, x_2, \cdots, x_N) \in \mathbb{R} \,, x \neq 0 : \quad x^T A x = x^T M M^\dagger x = \sum_{ij} x_i M_{ij} (M^\dagger)_{ji} x_i = \\ &= \sum_{ij} M^*_{ij} M_{ij} x_i^2 = \sum_{ij} |M_{ij}| \, x_i^2 > 0 \,. \end{aligned} \tag{C.2}$$

A hermitian matrix $A$ can be diagonalized through a unitary transformation $U$

$$U^\dagger A U = A_{\text{diag}} \quad \text{with} \;\; UU^\dagger = U^\dagger U = I \,, \tag{C.3}$$

Now $A$ have strictly positive eigenvalues, since it is positive definite, and therefore we can define a new diagonal matrix $m_D$ with all positive elements $m_i$ on the diagonal, so that $A = m_D^2$. Therefore

$$\begin{aligned} U^\dagger A U = U^\dagger M M^\dagger U = A_{\text{diag}} = m_D^2 \Rightarrow MM^\dagger = U m_D^2 U^\dagger \to M(M^\dagger U m_D^{-1}) = \\ = U m_D \to MV = U m_D \Rightarrow M = U m_D V^{-1} \,, \end{aligned} \tag{C.4}$$

with $V = M^\dagger U m_D^{-1}$. We can verify that $V$ is unitary:

$$VV^\dagger = M^\dagger U m_D^{-1} m_D^{-1} U^\dagger M = M^\dagger U (U^\dagger A U)^{-1} U^\dagger M = M^\dagger (M^\dagger)^{-1} M^{-1} M = I \,. \tag{C.5}$$

We have thus demonstrated that a generic nonsingular complex matrix $M$ can be written as $M = U m_D V^\dagger$, by means of two unitary matrices, with $m_D$ a diagonal nonsingular matrix with positive eigenvalues.

## C.2 The unitary mixing matrix

Consider two unitary matrices $W_L^U$ and $W_L^D$. The product $U = W_L^{U\dagger} W_L^D$ is unitary ($U(N)$ is a group). An unitary $N \times N$ matrix $U$ has $N^2$ free parameters. In fact, $N$ of the $2N^2$ real parameters of $U$ can be eliminated by imposing the normalization of the $N$ rows or columns to 1, while $2 \times N(N-1)$ parameters can be eliminated by imposing the orthogonality of all pairs of rows or columns, giving $2N^2 - N - 2 * N(N-1)/2 = N^2$ real independent parameters. There are many possible general parametrizations for $U$, and, most commonly, the $N^2$ parameters are divided into $N(N-1)/2$ angles (corresponding to rotations of $SO(N)$, which is a subgroup of $U(N)$) and $N(N+1)/2$ phases. In the case of a three–dimensional mixing matrix there are three mixing angles and six phases.

# D Lorentz group and spinors

The group $SL(2,\mathbb{C})$, the group of complex two–dimensional matrices with determinant 1, is isomorphic to the Lorentz group $\mathcal{L} \equiv (1,3)$. The Weyl spinors transform under Lorentz transformations according to particular two–dimensional non–equivalent irreducible representations of the group $SL(2,\mathbb{C})$. The action of these two representations on the Weyl spinors encodes the way that the spin state of a particle transforms under a Lorentz transformation.

## D.1 The Lorentz group

The elements of the Lorentz group are real four–dimensional matrices that satisfy the condition

$$\Lambda^T \eta \Lambda = \eta \ , \tag{D.1}$$

which is a direct consequence of the relativistic interval conservation. The $\Lambda$ matrices satisfy the conditions

$$\det \Lambda = \pm 1 \ , \qquad |\Lambda^0{}_0| \geqslant 1 \ . \tag{D.2}$$

We will focus on a subgroup of the full Lorentz group, $\mathcal{L}_+^\uparrow \equiv SO(1,3)$, the proper orthochronous Lorentz group, for which the determinant is equal to 1 and $\Lambda^0{}_0 \geqslant 1$.

A generic $\Lambda \in \mathcal{L}_+^\uparrow$ can be written as

$$\Lambda^\mu{}_\nu = \left[ e^{-\frac{i}{2}\omega^{\rho\sigma} M_{\rho\sigma}} \right]^\mu{}_\nu \ , \tag{D.3}$$

where the 6 matrices $M_{\rho\sigma}$ form a basis of the $\mathfrak{so}(1,3)$ the algebra of $SO(1,3)$. The factor $i$ makes the M matrices hermitian. It can be verified that the explicit expression for the $M_{\rho\sigma}$ matrices is the following

$$(M_{\rho\sigma})^\mu{}_\nu = i(\eta_{\sigma\nu}\delta^\mu_\rho - \eta_{\rho\nu}\delta^\mu_\sigma) \ . \tag{D.4}$$

If we suitably define the matrices $M$ in the following way

$$M = \begin{pmatrix} 0 & -K_1 & -K_2 & -K_3 \\ K_1 & 0 & J_3 & -J_2 \\ K_2 & -J_3 & 0 & J_1 \\ K_3 & J_2 & -J_1 & 0 \end{pmatrix} \ , \tag{D.5}$$

then we obtain (with a somewhat tedious calculation) the following commutation relations which define the algebra

$$\begin{aligned} [J_i, J_j] &= i\epsilon_{ijk} J_k \\ [K_i, J_j] &= i\epsilon_{ijk} K_k \\ [K_i, K_j] &= -i\epsilon_{ijk} J_k \ . \end{aligned}$$

The first of the (D.6) implies that $SO(3)$ is a subgroup of $\mathcal{L}_+^\uparrow$ and that similarly the algebra $\mathfrak{so}(3)$ is a subalgebra of $\mathfrak{so}(1,3)$, while the second of the (D.6) implies that $\vec{K}$ behaves like a vector under rotations. In order to classify the irreducible non-unitary finite-dimensional representations of $\mathcal{L}_+^\uparrow$ we change the basis of the algebra by introducing the generators $S_i$ and $T_i$ defined as:

$$\begin{aligned} S_i &= \frac{1}{2}(J_i + iK_i) \\ T_i &= \frac{1}{2}(J_i - iK_i) \ , \end{aligned} \tag{D.6}$$

for which the commutation relations become

$$\begin{aligned}[S_i, S_j] &= i\epsilon_{ijk} S_k \\ [T_i, T_j] &= i\epsilon_{ijk} T_k \\ [S_i, T_j] &= 0 \ .\end{aligned} \tag{D.7}$$

We thus discover that the $\mathfrak{so}(1,3)$ algebra is the direct sum of two identical commuting $\mathfrak{su}(2)$ algebras. Note, however, that the algebra has been complexified:

$$\mathfrak{so}(1,3)_{\mathbb{C}} = \mathfrak{su}(2) \oplus \mathfrak{su}(2) \ . \tag{D.8}$$

On the other side, it can be proven that there is a two–to–one homomorphism between $SL(2,\mathbb{C})$ and the $SO(1,3)$ and that their algebras are isomorphic $\mathfrak{so}(1,3)_{\mathbb{R}} \simeq \mathfrak{so}(1,3)_{\mathbb{C}}$. The homomorphism of $SL(2,\mathbb{C})$ onto $SO(1,3)^+$ can be expressed through the relations algebra is homomorphic and not isomorphic to as can be explicitly shown by

$$\Lambda^{\mu}{}_{\nu}(M) = \frac{1}{2}\mathrm{Tr}\,[\overline{\sigma}^{\mu} M \sigma_{\nu} M^{+}] \ , \tag{D.9}$$

where $\sigma^{\mu} = (1, \vec{\sigma}) = (\sigma_0, \vec{\sigma})$ and $\overline{\sigma}^{\mu} = (\sigma_0, -\vec{\sigma})$, and

$$M(\Lambda) = \pm \frac{1}{[\det\{\Lambda^{\mu}{}_{\nu}\sigma_{\mu}\overline{\sigma}^{\nu}\}]^{\frac{1}{2}}} \Lambda^{\mu}{}_{\nu}\sigma_{\mu}\overline{\sigma}^{\nu} \ . \tag{D.10}$$

The meaning of the sign $\pm$ in the (D.10) is that the correspondence $\Lambda \leftrightarrow \pm M$ defines a two-valued representation of the restricted Lorentz group and leads to the identification

$$\mathcal{L}_{+}^{\uparrow} \simeq SL(2,\mathbb{C})/\mathbb{Z}_2 \ , \tag{D.11}$$

so that $SL(2,\mathbb{C})$ is $\mathcal{L}_{+}^{\uparrow}$ universal covering group.

The representations of $SO(1,3)$ can be classified by means of two numbers $n$ and $m$, integers or semi-integers, indicating the representation with (n,m), identifying the total spin (third projection) with $J_3 = S_3 + T_3$ and the size of the representation with $(2n+1)(2m+1)$. Parity acts on the generators as follows $J_i \to J_i$ and $K_i \to -K_i$. Consequently, the two $\mathfrak{su}(2)$ algebras are exchanged under parity, ie $S_i \to T_i$ and $T_i \to S_i$. If we consider the two fundamental $\mathfrak{su}(2) \oplus \mathfrak{su}(2)$ representations $(1/2, 0)$ and $(0, 1/2)$, called respectively the left-handed and right-handed spinor representation, they have no definite parity, since they go into each other under parity. To have a representation that has definite parity, it will be necessary to introduce the Dirac spinor that transforms with $(1/2, 0) \oplus (0, 1/2)$. The left– and right handed representations, from the point of view of the group $SL(2,\mathbb{C})$, correspond to the self–representation $D(M) = M$ and to the conjugate one, $D(M) = M^*$.

Looking back at the definition (D.5) we can summarize the transformation properties of le to the right–handed spinors:

$$\begin{aligned}\psi_L &= e^{\frac{1}{2}(i\boldsymbol{\theta}\cdot\boldsymbol{\sigma} - \boldsymbol{\beta}\cdot\boldsymbol{\sigma})}\psi_L \\ \psi_R &= e^{\frac{1}{2}(i\boldsymbol{\theta}\cdot\boldsymbol{\sigma} + \boldsymbol{\beta}\cdot\boldsymbol{\sigma})}\psi_R \ ,\end{aligned} \tag{D.12}$$

since $\psi_L$ transforms with $(1/2, 0)$ and the corresponding generators are $S_i = 1/2(J_i + iK)$ so that there is a -1 in front of $\beta$ in (D.12) from the $i^2$ factor, while $\psi_R$ transforms with $(0, 1/2)$ and the corresponding generators are $T_i = 1/2(J_i - iK)$ and there is a +1 in front of $\beta$.

# E Neutrino Oscillation Formulas

Here some useful formulas for neutrino oscillations are collected.

- Vacuum oscillation probability for one mass scale dominance, when $\Delta m^2 \gg \delta m^2$ and $\Delta m^2/4E \sim 1$:

$$\begin{aligned} P(\nu_\alpha \to \nu_\alpha) &= 1 - 4|U_\alpha 3|^2(1-|U_\alpha 3|^2)\sin^2\left(\frac{\Delta m^2 L}{4E}\right) , \\ P_{\nu_\alpha\to\nu_\beta} &= 4|U_\alpha 3|^2|U_\beta 3|^2\sin^2\left(\frac{\Delta m^2 L}{4E}\right) , \end{aligned} \tag{E.1}$$

  - same for neutrinos and antineutrinos
  - it does not depend on solar (12) parameters
  - independent on $\delta$ and on the mass ordering

- $\Delta m^2$ vacuum averaged $\nu_e$ survival probability:

$$P(\nu_e \to \nu_e) = \sin^4\theta_{13} + \cos^4\theta_{13}\left(1 - \sin^2\theta_{12}\sin^2\left(\tfrac{\delta m^2 L}{4E}\right)\right) , \tag{E.2}$$

  - same for neutrinos and antineutrinos
  - it does not depend on the mass ordering
  - independent on $\delta$

- $P(\nu_\mu \to \nu_e)$ in constant matter (NO):

$$\begin{aligned} &P(\nu_\mu \to \nu_e) = A\sin^2\theta_{13} + B\sin 2\theta_{12}\sin 2\theta_{13}\cos\left(\delta + \cos\left(\frac{\delta m^2 L}{4E}\right)\right) + C , \\ &\text{with} \\ &A = \left(\frac{\Delta m^2}{\Delta m^2 - A_{CC}}\right)^2 \sin^2\theta_{23}\sin^2\left(\frac{A_{CC}-\Delta m^2}{4E}L\right) , \\ &B = \left(\frac{\Delta m^2}{\Delta m^2 - A_{CC}}\right)\frac{\delta m^2}{A_{CC}}\sin\theta_{23}\sin 2\theta_{12}\sin\left(\frac{A_{CC}L}{4E}\right)\sin\left(\frac{A_{CC}-\Delta m^2}{4E}L\right) , \\ &C = \left(\frac{\delta m^2}{A_{CC}}\right)^2\cos^2\theta_{23}\sin^2 2\theta_{12}\sin^2\left(\frac{A_{CC}L}{4E}\right) . \end{aligned} \tag{E.3}$$

  It can be proven that

  - $P(\nu_\mu \to \nu_e) = P(\nu_e \to \nu_\mu|\delta \to -\delta)$
  - NO→ when $\Delta m^2 \to -\Delta m^2$
  - $P(\overline{\nu_\mu} \to \overline{\nu_e}) = P(\nu_\mu \to \nu_e|\delta \to -\delta, A_{CC} \to -A_{CC})$.

# References


[1] C. P. Burgess and G. D. Moore. *The standard model: A primer*. Cambridge University Press, 2006.

[2] P. Langacker. *The Standard Model and Beyond*. Taylor & Francis, 2017.

[3] C. Giunti and C. W. Kim. *Fundamentals of Neutrino Physics and Astrophysics*. 2007.

[4] E. Vitagliano, I. Tamborra, and G. Raffelt. “Grand Unified Neutrino Spectrum at Earth: Sources and Spectral Components”. In: *Rev. Mod. Phys.* 92 (2020), p. 45006.

[5] M. Honda, T. Kajita, K. Kasahara, and S. Midorikawa. “A New calculation of the atmospheric neutrino flux in a 3-dimensional scheme”. In: *Phys. Rev. D* 70 (2004), p. 043008.

[6] K. Eguchi et al. “First results from KamLAND: Evidence for reactor anti-neutrino disappearance”. In: *Phys. Rev. Lett.* 90 (2003), p. 021802.

[7] P. Dunne. “Latest Neutrino Oscillation Results from T2K”. 29th International Conference on Neutrino Physics and Astrophysics (Neutrino 2020). 2020.

[8] M. Aker et al. “Direct neutrino-mass measurement with sub-electronvolt sensitivity”. In: *Nature Phys.* 18.2 (2022), pp. 160–166.

[9] A. Mirizzi, I. Tamborra, H.-T. Janka, N. Saviano, K. Scholberg, R. Bollig, L. Hudepohl, and S. Chakraborty. “Supernova Neutrinos: Production, Oscillations and Detection”. In: *Riv. Nuovo Cim.* 39.1-2 (2016), pp. 1–112.

[10] F. Capozzi, E. Lisi, A. Marrone, and A. Palazzo. “Current unknowns in the three neutrino framework”. In: *Prog. Part. Nucl. Phys.* 102 (2018), pp. 48–72.

[11] F. Capozzi, E. Di Valentino, E. Lisi, A. Marrone, A. Melchiorri, and A. Palazzo. “Unfinished fabric of the three neutrino paradigm”. In: *Phys. Rev. D* 104.8 (2021), p. 083031.